Technical Report No. 137

4853-12-T

THE MICHIGAN AUTOMATIC DIRECTION FINDER

by

D. L. Mills

Approved By: B F Barton

B. F. Barton

for

COOLEY ELECTRONICS LABORATORY

Department of Electrical Engineering
The University of Michigan
Ann Arbor

Contract No. DA 36-039 sc-89227
Signal Corps, Department of the Army
Department of the Army Project No. 3A 99-06-001-01

February 1964

TABLE OF CONTENTS

LIST OF ILLUSTRATIONS

ABSTRACT

This report describes the theoretical basis and practical instrumentation of the Michigan Automatic Direction Finder (MADFI). The MADFI is an integrated data collection, processing, and display system for determination of bearing statistics of signals in the high-frequency radio spectrum and is intended as a research tool in the study of propagation phenomena and direction-finding techniques. Signal processing includes narrowband postdetection filtering and a type of linearly-weighted time averaging which improves the bearing estimates in the presence of multipath and noise processes. The MADFI is equipped with several types of readout suitable for telemetry transmission and computer processing of bearing statistics.

FOREWORD

The effort described in this report represents significant contributions by a number of individuals, each of whom has made his addition by expanding or specializing the body of theory inherited from his predecessors and leaving in turn a more profuse collection of reports, memos, and notations. Such a collection has made possible this report on the Michigan Automatic Direction Finder (MADFI). In this vein, I would like to acknowledge the invaluable assistance received through notes left by D. S. Heim and W. J. Lindsay, former Project Engineers on projects involving direction-finding research, and in particular to L. W. Orr, whose unpublished notes furnished the basis for a sizeable amount of this report. I also wish to credit R. E. Lillie, G. Ziedins, and K. E. Burkhalter, engineers who developed much of the hardware of the MADFI, and in particular, G. A. Hellwarth, whose technical advice "unstuck many an ornery circuit."

1. INTRODUCTION

The effort narrated in this report is a continuation of that initiated by W. J. Lindsay and D. S. Heim and described in Reference 7. The effort is directed toward the realization of a semi-automatic direction finder (df) suitable for collection of bearing statistics of signals in the high-frequency radio spectrum. Of considerable importance is the introduction of signal processing which simulates the behavior of a trained operator in stabilizing an indication distorted by multipath processes. As a result of this effort the Michigan Automatic Direction Finder (MADFI) was constructed. The MADFI is an integrated data collection, processing, and display system for determination of bearing statistics of radio signals in the 2-30-mcs range. The system consists of a modified AN/TRD-4A Tactical Direction Finder Set, laboratory-constructed analog and digital computing-type components, and a variety of display devices.

It is the purpose of this report to describe the theoretical basis and practical instrumentation of the MADFI. Since others have in some areas developed and published the theory (cf. References) responsible for the realization of some of the components, only those developments pertinent to the operation of the MADFI as a system are included. Accompanying these developments are descriptions of the AN/TRD-4A modifications and the additional laboratory-constructed equipment.

Due to time restrictions on this effort the MADFI has not undergone extensive field tests. For this reason little operational experience has been gained with the system, although preliminary tests indicate a significant improvement in the MADFI performance over that of the unmodified AN/TRD-4A equipment.

2. MICHIGAN AUTOMATIC DIRECTION FINDER SYSTEM DESCRIPTION

The MADFI consists of three basic subsystems: (1) The receiving system, which includes the antennas, goniometer, receiver and detector; (2) The processing system, which includes the filtering, computing, and synchronizing elements; and (3) The display and recording system, which includes the cathode-ray and digital displays, a pen recorder, and a paper punch. The three subsystems will be described in detail in Sections 3 through 5. The sections immediately following describe the organization of these subsystems as a whole.

2.1 AN/TRD-4A DF Set

The AN/TRD-4A, around which the system is designed, is a spinning-goniometer type direction finder utilizing a four-element Adcock antenna and a cathode-ray tube display. Its antenna, classified as a medium aperture system, may be of two dimensions: one for 2-10 mcs, the other for 10-30 mcs. Techniques of the MADFI are by no means restricted to this particular df set, however, and any df set which produces a sine wave signal of amplitude and phase corresponding to the amplitude and bearing of the incident signal is suitable for MADFI-type processing. Examples of these types of df sets include doppler and other commutated-antenna systems as well as spinning-antenna systems. The twin-channel system is applicable with some slight changes.

The reader is directed to pertinent publications concerning the operational characteristics of the AN/TRD-4A, including the R-390/URR Radio Receiving Set, and is presumed familiar with them (References 8 and 9). However, the casual reader will find an essential description of the operation of these components in this report.

2.2 MADFI

Figure 1 will be helpful in describing the system operation of the MADFI. As seen, there are two modes of operation: (1) The manual mode, which is that of the essentially unmodified AN/TRD-4A, and (2) The automatic mode, which includes the processing and display equipment of the MADFI. The two modes are selected by a single switch, enabling rapid comparisons.

The bulk of the antenna, goniometer, and receiving components of the MADFI is adopted with few changes from the corresponding AN/TRD-4A components. The two most significant changes involve the addition of a sense antenna at the center of the Adcock array and a redesigned receiver detector. These components will be described further in Section 3.

The processing system includes the narrowband filter and bearing computer. These elements, which will be described in Section 4, help to reduce bearing error due to multipath processes. A synchronizing generator utilizing a code wheel coupled to the goniometer rotor is used with the bearing computer and digital display elements. Meters monitor important signal levels.

The display and recording system, described in detail in Section 5, includes both analog and digital real-time displays together with corresponding analog and digital peripheral recording devices. The real-time displays consist of the AN/TRD-4A cathode-ray indicator

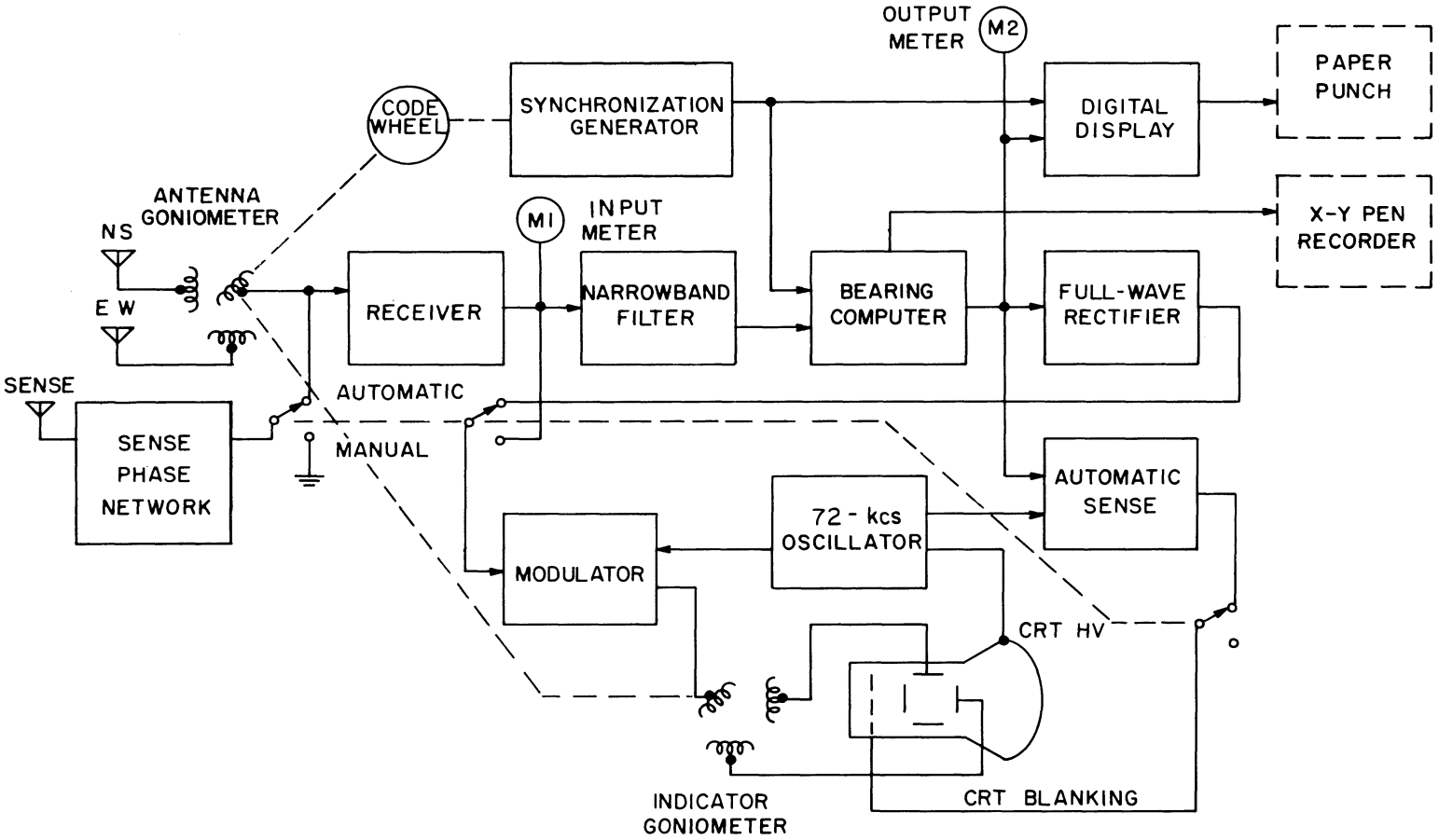

Fig. 1 MADFI System Block Diagram

and a three-digit decimal display reading directly in degrees. An automatic sense circuit eliminates the 180^{o}-bearing ambiguity inherent in the AN/TRD-4A. The peripheral recording devices consist of an eight-channel paper tape punch and a pen recorder. (The full-wave rectifier, modulator, 72-kcs oscillator, indicator goniometer, and cathode-ray tube elements of Figure 1 are all part of the modified AN/TRD-4A indicator.)

A photograph of the MADFI equipment is shown in Figure 2. Four of the five antenna elements, (not shown) the goniometer, the receiver, and the cathode-ray display are part of the AN/TRD-4A; the rest of the components are laboratory-constructed or modified to varying degrees. Except for the antennas the entire system is contained in two equipment racks. One five-foot rack contains the modified AN/TRD-4A DF Set and the processing and real-time display equipment. A smaller three-foot rack contains the peripheral recording devices. Except for the original AN/TRD-4A components and the Moseley pen recorder, the entire system is constructed with solid-state modularized circuitry.

Most of the component modules are visible in the two racks illustrated in Figure 2, the analog rack and the digital rack. Meters and test jacks are provided for system adjustment and servicing, and testing circuitry is in some instances an integral part of the equipment.

The patch panel shown in Figure 2 is provided so that individual processing, display, and recording elements may be interconnected for demonstration and evaluation procedures. Its connections are shown in Figure 3. Standard phone jacks are provided with a normally-closed contact which is disconnected when a simple patch cord is inserted. These contacts are wired so that when all patch cords are removed the system is interconnected as in Figure 1.

To allow the greatest flexibility when the MADFI components are interconnected in other than the normal manner shown in Figure 1, or when external devices are connected, the patch panel voltage and impedance levels are standardized. All circuits are designed to be linear to twice the operating level of 1-volt rms and to maintain an indicated bearing accuracy of $\pm 1/2^{o}$ under extreme conditions of circuit loading.

Records made with this equipment may be processed by either analog or digital general-purpose computers and may be used to evaluate system performance, to aid in refining processing techniques, and to study ionospheric propagation phenomena. Together with a remote-controlled df receiver, (Reference 1) and a telemetering link, the MADFI is suitable for installation at an unattended field site.

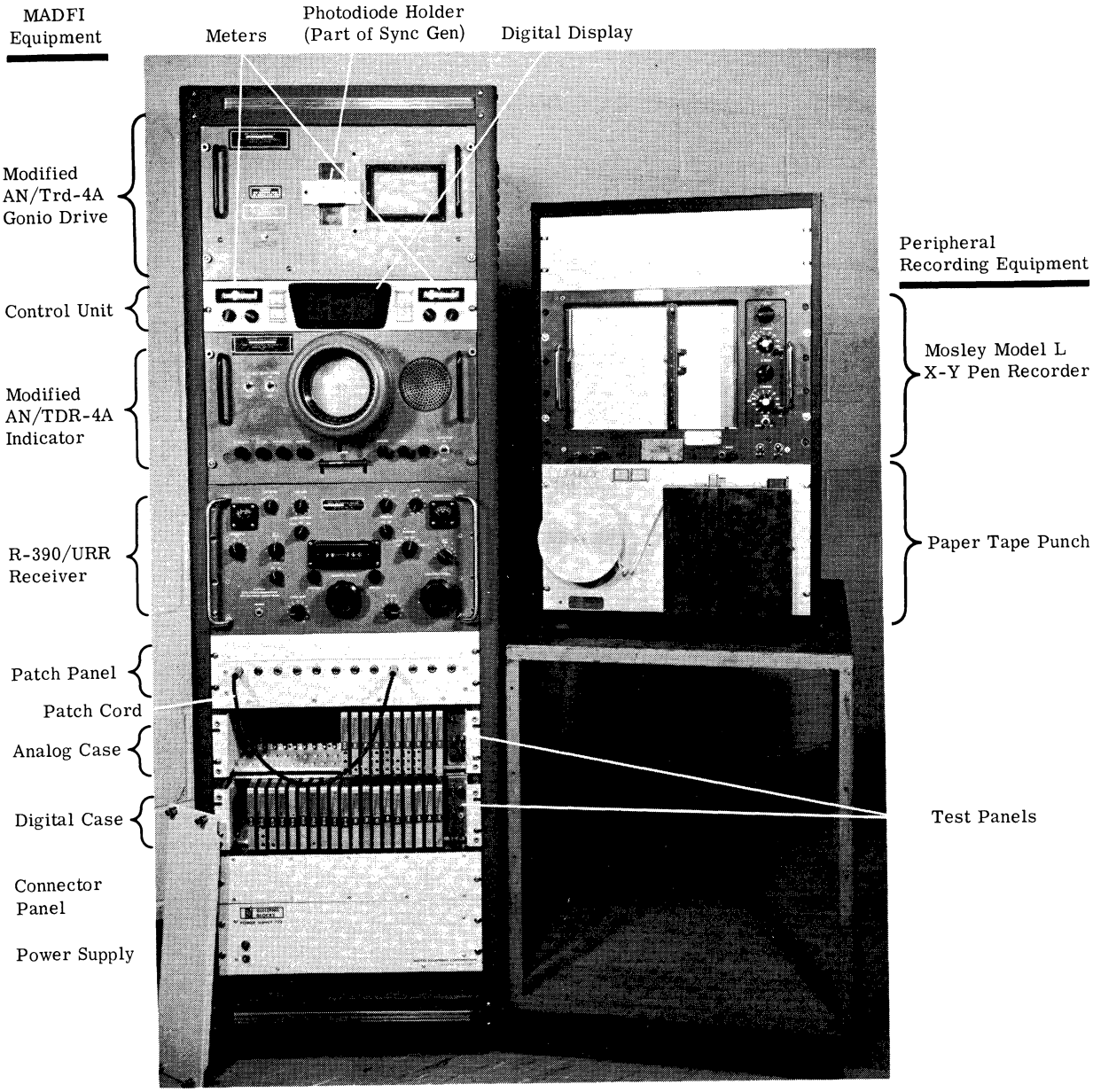

FIG. 2. MADFI PHYSICAL LAYOUT — FRONT VIEW
(Case Covers Removed)

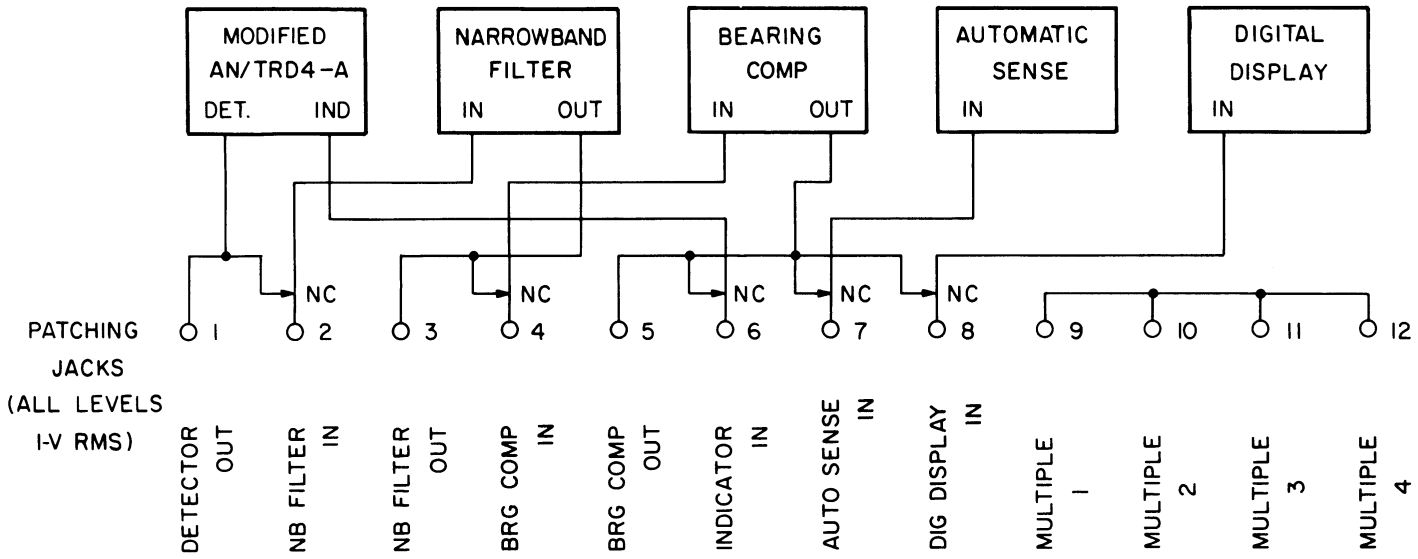

Fig. 3 Patch Panel Connections

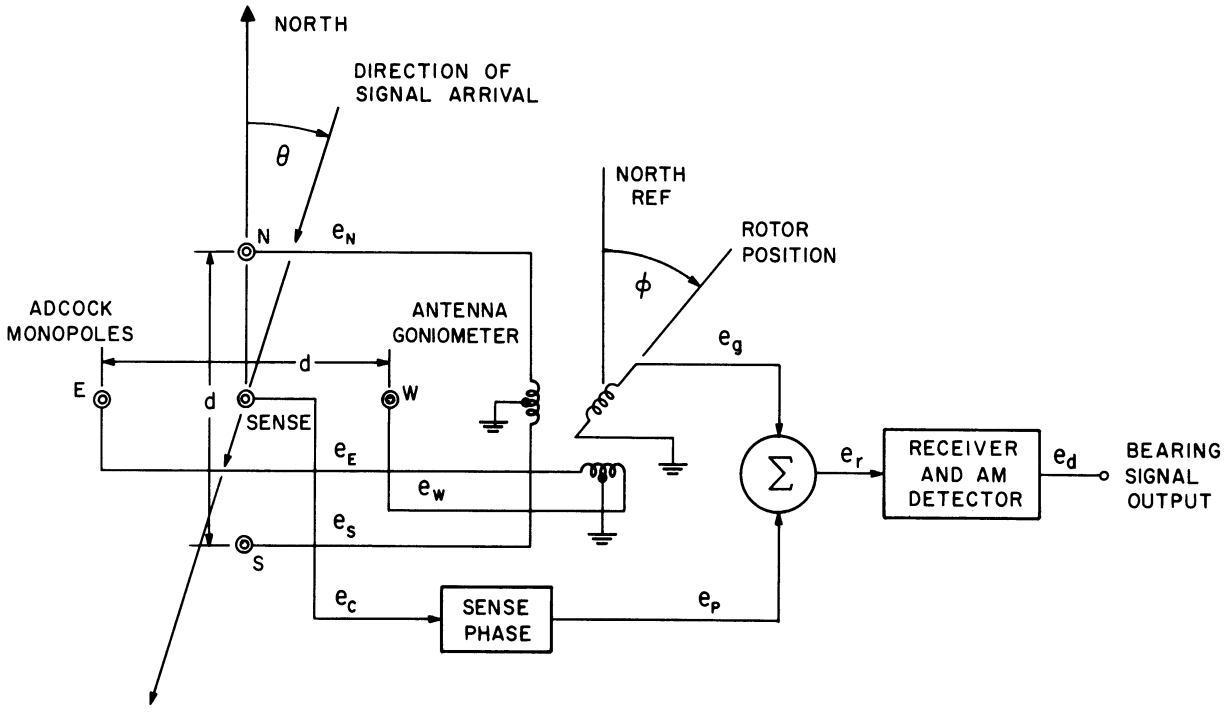

Fig. 4 Receiving System

3. RECEIVING SYSTEM

The receiving system used in the MADFI is diagrammed in Figure 4. The antennas consist of a four-element Adcock array together with a fifth centrally-located element used as a sense antenna. The antenna goniometer and sense-phase network act upon the element voltages to produce an amplitude-modulated signal e_r which is amplified and detected by the receiver. Phase information contained in the detector output voltage e_d is used in the processing and display systems to reconstruct the direction of signal arrival θ. The following analysis indicates how this is done and how the dimensions of the antenna system and adjustments of the sense-phase network affect the system accuracy.

3.1 Operation of Antennas and Goniometers

The central sense element will be assumed the reference element of the antenna array. Relative to a cw signal of frequency ω_c arriving from bearing θ relative to true north, the voltage induced in the central element is

$$e_c = A_c \cos \omega_c t, \tag{3.1}$$

while the differential voltages induced in the north-south and east-west pairs of elements are

$$e_N - e_S = 2A_c \sin\left(\frac{\pi d}{\lambda} \cos \theta\right) \sin \omega_c t,$$

and

$$e_E - e_W = 2A_c \sin\left(\frac{\pi d}{\lambda} \sin \theta\right) \sin \omega_c t. \tag{3.2}$$

If the goniometer rotor angular position φ is measured as in Figure 4, then the rotor voltage is

$$e_g = K[(e_N - e_S) \cos \varphi + (e_E - e_W) \sin \varphi], \tag{3.3}$$

where K is the transmission coefficient of the goniometer.[1] This voltage passes through a null where

$$\tan \varphi = -\frac{e_N - e_S}{e_E - e_W} = -\frac{\sin\left(\frac{\pi d}{\lambda} \cos \theta\right)}{\sin\left(\frac{\pi d}{\lambda} \sin \theta\right)}, \tag{3.4}$$

[1] C. E. Lindahl has analyzed K and other losses in the antenna system. See Reference 5.

which occurs twice in every revolution of the rotor. Thus the angle φ at null may be used as an indication of the bearing θ if $\frac{\pi d}{\lambda}$ is sufficiently small; for in that case

$$\tan \theta \cong \tan (\varphi \pm \pi/2). \tag{3.5}$$

The error $\Delta\theta$ in $\varphi = \theta + \Delta\theta$ is a function of the wavelength and the geometry of the antenna system, and is called the octantal error. A plot of $\Delta\theta$ as a function of d/λ is shown in Fig. 5, which indicates that for values of d/λ less than about 1/3 (the maximum value permitted in the MADFI) the octantal error is less than 3^{o}.[2]

The unmodified AN/TRD-4A operates in the fashion described above, the null points indicated in Eq. (3.5) becoming the tips of the propeller-like pattern displayed on the cathode-ray indicator. The $\pm\pi/2$ ambiguity apparent in Eq. (3.5) is resolved in the MADFI equipment by summing the rotor voltage and a voltage of appropriate phase and amplitude derived from the sense antenna. Letting the transfer constant of the sense-phase network be $\alpha e^{j\beta}$, this voltage is

$$e_p = \alpha A_c \cos (\omega_c t + \beta). \tag{3.6}$$

The goniometer rotor is spinning at a frequency ω_g. If the octantal error is neglected, then the rotor voltage is, from Eq. (3.3),

$$e_g = 2KA_c \frac{\pi d}{\lambda} \cos (\omega_g t - \theta) \sin \omega_c t. \tag{3.7}$$

3.2 Operation of Receiver and Detector

The voltage e_p and e_g are summed in the input circuitry of the receiver:

$$e_r = \alpha A_c \cos (\omega_c t + \beta) + 2KA_c \frac{\pi d}{\lambda} \cos (\omega_g t - \theta) \sin \omega_c t. \tag{3.8}$$

The results of this analysis will not be affected if the amplitude dependence in Eq. (3.8) is dropped by setting $\alpha A_c = 1$ and $\frac{2KA_c \pi d}{\lambda} = m$, so that e_r becomes proportional to

$$e_r' = \cos (\omega_c t + \beta) + m \cos (\omega_g t - \theta) \sin \omega_c t. \tag{3.9}$$

[2] C. E. Lindahl has demonstrated an antenna design that permits an error of less than 1^{o} for values of d/λ as high as unity. See Reference 6.

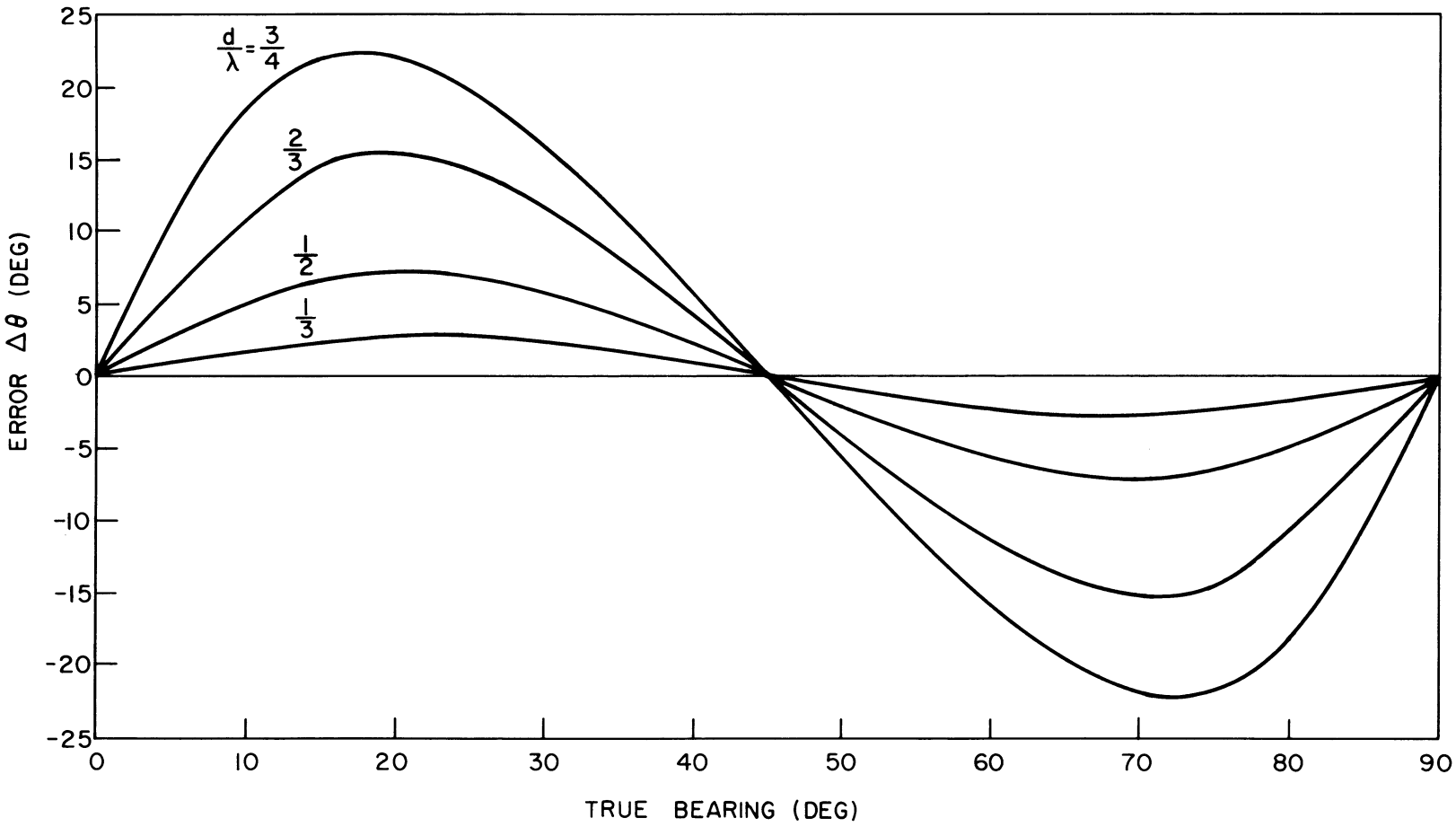

Fig. 5 Adcock Antenna Octantal Error Curves

Following the receiver and a conventional envelope detector, the signal becomes proportional to

$$e'_d = \left[1 + 2m \sin\beta \sin(\omega_g t - \theta) + m^2 \sin^2(\omega_g t - \theta)\right]^{1/2}. \tag{3.10}$$

It is evident that if β, the phase shift introduced by the sense phase network, is set equal to $\pi/2$, Eq. (3.10) may be further simplified. In this case, the detector voltage becomes proportional to

$$e'_d = 1 + m \sin(\omega_g t - \theta). \tag{3.11}$$

If β may not be adjusted to exactly $\pi/2$, then, since Eq. (3.10) is in the form $(1 + x)^{1/2}$, it may be expanded in a Maclaurin series. The expansion is valid for values of α and β chosen such that $|x| < 1$. The result, after some rearrangement of terms, is

$$e'_d = 1 + m \sin\beta \sin(\omega_g t - \theta) + \frac{m^2}{2} \cos^2\beta \sin^2(\omega_g t - \theta) + \ldots, \tag{3.12}$$

where the implicit terms are all at third and higher harmonics of $\sin(\omega_g t - \theta)$. If the second and higher harmonics of $\sin(\omega_g t - \theta)$ in Eq. (3.12) are removed by a low-pass filter following the detector, then Eq. (3.12) becomes

$$e'_d = 1 + m \sin\beta \sin(\omega_g t - \theta), \tag{3.13}$$

which is similar in form to Eq. (3.11). If the d-c term in either Eqs. (3.11) or (3.13) is removed by a high-pass filter and the goniometer rotor position φ noted at the time of a positive-going zero crossing, then it is clear that either Eqs. (3.11) or (3.13) will yield an unambiguous bearing indication $\varphi = \theta$. Furthermore, this indication does not vary over a range of the sense-phase network adjustments.

In the MADFI equipment, the narrowband filter included in the processing system functions as both the high- and the low-pass filters. The display system extracts the bearing indication from the resultant signal in the manner described above.

3.3 Receiving System Instrumentation

The MADFI receiving system consists of the AN/TRD-4A antenna and receiver components together with a sense antenna, sense-phase network, and the redesigned receiver detector.

The sense antenna, located at the center of the AN/TRD-4A Adcock array, is constructed and connected in the same fashion as the other four array elements. The other antenna and

goniometer components of the AN/TRD-4A remain unchanged, except that the manual sense provision of the AN/TRD-4A is disabled in the automatic or MADFI mode.

In the R390/URR receiver used with the AN/TRD-4A there is a 90^{o}-phase difference between the balanced antenna input and the unbalanced antenna input which is maintained up to about 10 mcs. Accordingly, if the goniometer is connected to the balanced input and the sense antenna is connected to the unbalanced input, then no sense-phase control is required over these frequencies. Above 10 mcs, however, phase equalization is required such as is provided by the simple delay line shown in Fig. 6, which consists of switch-selected lengths of coaxial cable. The increments, selectable at $1/2^{o}$ per mcs, are adequate at frequencies up to 30 mc.

The R390/URR receiver is not modified in any way. Predetection bandwidths of less than 2 kcs are desirable but cannot be obtained with the receiver i-f selectivity because of the excessively nonuniform phase characteristics introduced. An outboard i-f filter having phase characteristics uniform within 1^{o} over a 500-cps bandwidth has been constructed, but is not incorporated in the MADFI due to the critical tuning problems associated with its use (Reference 4). No attempt has been made to utilize either the automatic gain control or the envelope detector circuitry of the receiver, and output to the external detector is at the i-f frequency of 455 kcs.

The detector circuitry of the AN/TRD-4A is incorporated in the indicator chassis and consists of an i-f amplifier followed by a nonlinear detector. Considerable redesigning of these circuits was necessary in order to obtain linear operation over the dynamic ranges encountered under typical operating conditions. The redesigned detector, shown in Fig. 7, includes a phase-corrected high-pass filter to attenuate low-frequency transients generated by fluctuating carrier amplitudes. The low source-impedance amplifier included is capable of a 40-v output into the processing system.

4. PROCESSING SYSTEM

The heart of the MADFI is its processing system, including the narrowband postdetection filter, the bearing computer, and the synchronizing generator. The narrowband filter is used to remove modulation products and noise from the bearing signal. The bearing computer is used to improve the bearing accuracy under conditions of severe multipath distortion.

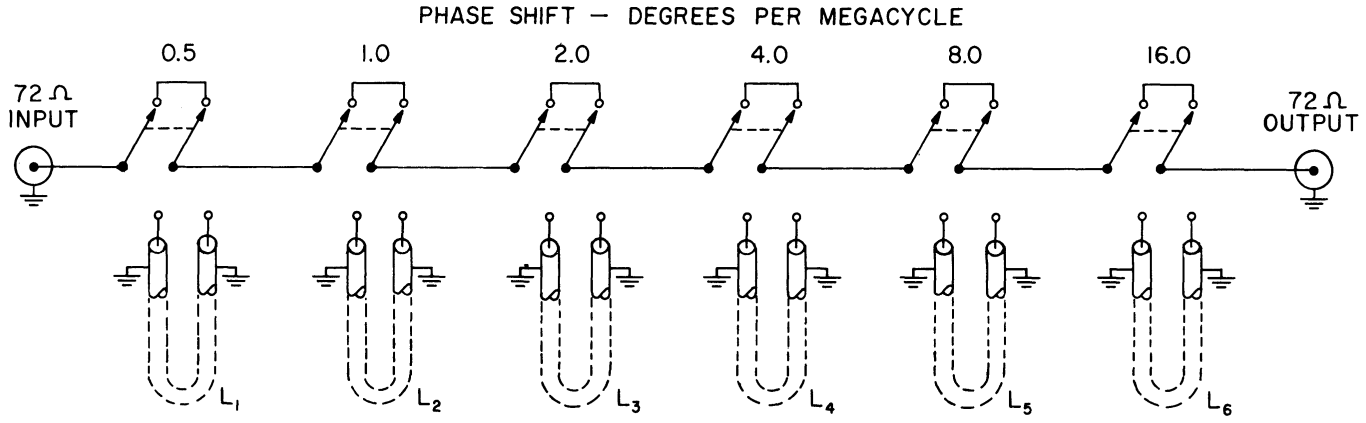

L_1 = 11"
L_2 = 1'10"
L_3 = 3'8"
L_4 = 7'4"
L_5 = 14'8"
L_6 = 29'4"

} LENGTHS OF RG/59U

Fig. 6 Phase Equalization Network

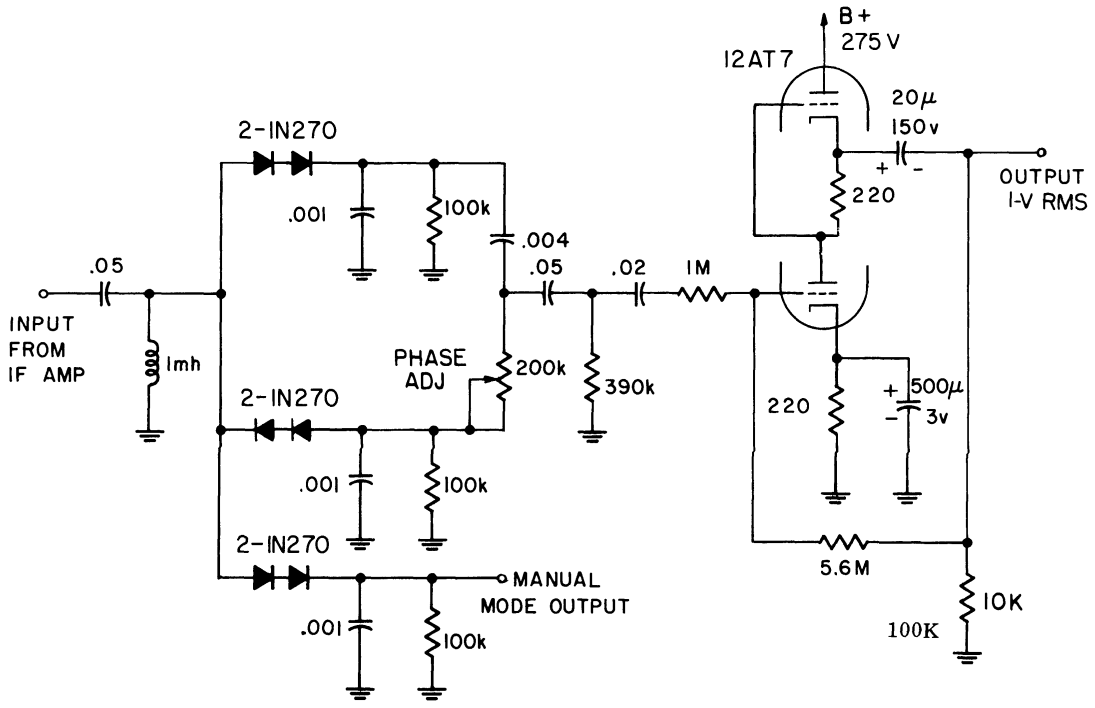

Fig. 7 AN/TRD-4A Detector Modifications

The synchronizing generator supplies special signals to the bearing computer and display circuits. Since it is believed that the processing system offers significant performance features, its theory of operation will be expanded in considerable detail below.

4.1 Narrowband Filter Operation

A narrowband filter of center frequency ω_g is necessary following the detector for the reasons explained in Section 3.2. The filter also removes any modulation products outside its passband which may accompany the incoming signal. Busignies and Dishal (Ref. 2) have shown that in addition a signal-to-noise performance improvement is possible through the use of filters of this type. The improvement is a function of the ratio of the predetection to the postdetection bandwidth:

$$(\text{signal-to-noise improvement}) = \left(\frac{\text{i-f bandwidth}}{\text{narrowband filter bandwidth}}\right)^{1/4}, \qquad (4.1)$$

which corresponds to an increase in signal-to-noise performance of 5 db per decade of bandwidth narrowing.

The input to the narrowband filter is the detector output voltage e_d described by Eq. (3.13). After passage through the filter, the bearing signal becomes

$$e_d = A \sin(\omega_g t - \theta), \qquad (4.2)$$

where A represents the various multiplicative factors implicit in the development.

4.2 Narrowband Filter Instrumentation

The principal requirement of the narrowband filter, other than a good selectivity characteristic, is a high degree of linearity. This requirement is necessary for proper operation of the bearing computer and display circuits under conditions of extreme fading. A linear phase characteristic is also highly desirable so that variations in goniometer spin-frequency ω_g will not affect the bearing accuracy.

The MADFI filter, which satisfies these requirements, is diagrammed in Fig. 8. This filter does not employ iron-core inductors, thus avoiding their inherent nonlinearities. The two filter sections shown have a bandwidth of about 30 cps. Using the formula of Busignies and Dishal (4.1) and noting that the prediction bandwidth of the system is 2 kcs, we see that this order of selectivity allows an increase of about 8 db in the signal-to-noise ratio.

The amplitude limiter shown between the filter sections is included as an operational convenience. Its limiting threshold is set somewhat above normal operating system level in

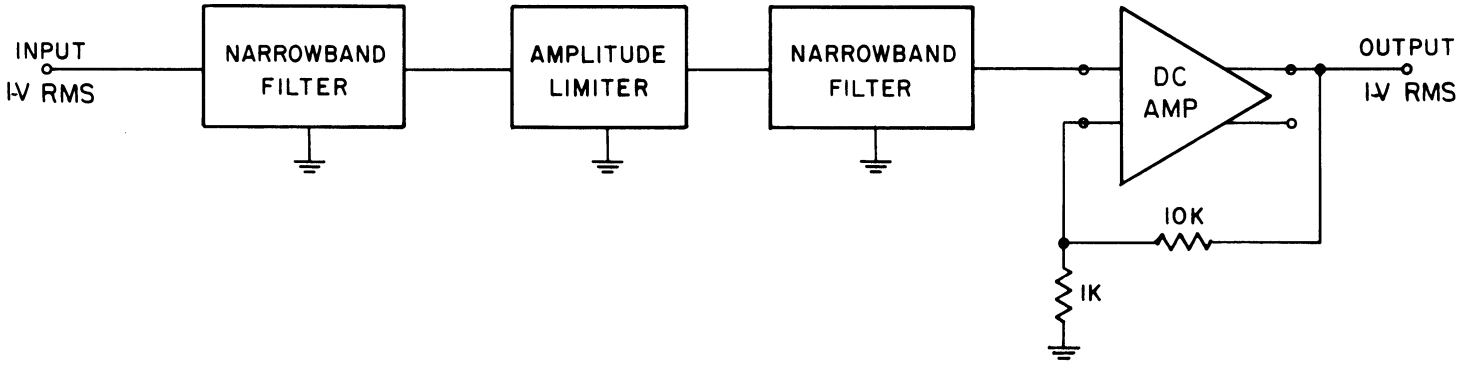

Fig. 8 Narrowband Filter (Simplified)

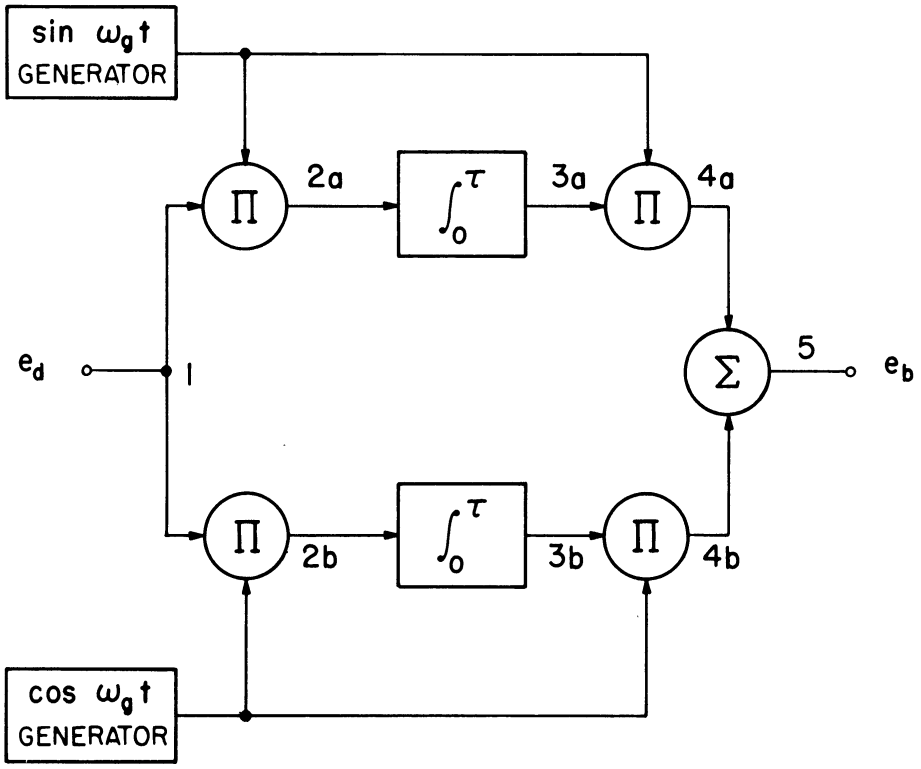

Fig. 9 Model Bearing Computer

order that overloading of the remainder of the processing system by occasional large peaks in signal amplitude can be avoided.

4.3 Bearing Computer Operation

In the preceding analysis the tacit assumption of a stationary amplitude and phase of the incident signal has been maintained. Under conditions of severe multipath distortion, this assumption must be abandoned, since signal amplitude variations of as much as 30 db and phase variations of a full 360^{o} are quite common in practice.

The amplitude and phase variations of the incident signal may be represented through a time dependence of the A and θ parameters of Eq. (4.2):

$$e_d = A(t) \sin [\omega_g t - \theta(t)]. \tag{4.3}$$

Now it is assumed that a good estimate of the true bearing $\bar{\theta}$ may be obtained from the expected value of θ. If this is correct, then a better estimate can be made by taking A into account. If it is agreed that for a multipath process the θ's obtained with correspondingly large A's are 'better' than those obtained with correspondingly small A's, then an obvious type of weighted average computation would use the expected value of the product of θ and some monotonic function of A, say f(A). An initial choice for f(A) is a linear relation of the form

$$\tan \bar{\theta} = \frac{E (A \sin \theta)}{E (A \cos \theta)}. \tag{4.4}$$

This process, called linearly-weighted time averaging, is carried out in the bearing computer. No claim is made as to its accuracy, but it appears to be a good initial choice from the impressive results seen on the display devices.

Since the practical details of the MADFI bearing computer somewhat obscure its intended function, the operation of an ideal bearing computer will be outlined in the following section. Following this outline the operation of the actual system implemented in the MADFI will be described. The operation of the MADFI system, however, does not depart from that of the ideal system except in those details as will be explained.

4.3.1 Model Bearing Computer

The ideal bearing computer is diagrammed in Fig. 9. The input to this system is normally the output from the narrowband filter e_d described by Eq. (4.3). In this system two sinusoidal generators phase-synchronized to the goniometer spin-frequency produce outputs of $\sin \omega_g t$ and $\cos \omega_g t$. Voltage e_d is applied to two linear four-quadrant multipliers as shown in Figure 9. The outputs from these multipliers at positions (2) are

$$e_{2a} = A \sin(\omega_g t - \theta) \sin \omega_g t = \frac{A}{2} \cos \theta + \frac{A}{2} \cos(2\omega_g t - \theta), \tag{4.5a}$$

$$e_{2b} = A \sin(\omega_g t - \theta) \cos \omega_g t = -\frac{A}{2} \sin \theta + \frac{A}{2} \sin(2\omega_g t - \theta). \tag{4.5b}$$

The two integrators are permitted to operate on these voltages for an interval of time T. If their outputs are both zero at the beginning of the integration interval, the voltages at time T are

$$e_{3a} = 1/2 \int_0^T A \cos \theta \, dt - 1/2 \int_0^T A \cos(2\omega_g t - \theta) \, dt, \tag{4.6a}$$

$$e_{3b} = -1/2 \int_0^T A \sin \theta \, dt + 1/2 \int_0^T A \sin(2\omega_g t - \theta) \, dt. \tag{4.6b}$$

Equations (4.6) cannot be integrated analytically without a knowledge of the functions A(t) and $\theta(t)$. Nevertheless, the first term in Eq. (4.6a) has the form of a weighted-average value of $\cos \theta$ indicated by $\overline{A \cos \theta}$ multiplied by T. The second term in Eq. (4.6a) will be small compared to the first term provided that T is large compared to $2\pi/\omega_g$. With a goniometer spin-frequency of 30 rps, $2\pi/\omega_g$ is only .034 sec. Since T can be made much greater than this, the error term can be made small. Similar reasoning applies to Eq. (4.6b) so that for long integration intervals, the following approximate equations are valid:

$$e_{3a} = 1/2 \int_0^T A \cos \theta \, dt = \frac{T}{2} \overline{A \cos \theta}, \tag{4.7a}$$

$$e_{3b} = -1/2 \int_0^T A \sin \theta \, dt = -\frac{T}{2} \overline{A \sin \theta}. \tag{4.7b}$$

These voltages are again multiplied by the sine and cosine generator voltages as indicated in Fig. 9, and the outputs at position (4) added to produce a voltage at position (5) given by

$$e_5 = \bar{A} \sin(\omega_g t - \bar{\theta}), \tag{4.8}$$

where

$$\bar{A} = \frac{T}{2} \left[\overline{A \sin \theta}^2 + \overline{A \cos \theta}^2 \right]^{1/2} \quad \text{and} \quad \tan \bar{\theta} = \overline{A \sin \theta} / \overline{A \cos \theta}.$$

If ideal integrators are used and if their inputs are both disconnected after the integration time T, the output voltage e_5 would clearly be a steady-state sine wave of amplitude $\bar{A}$ and phase angle $\bar{\theta}$.

If it is now assumed that the variations in A and θ are slow compared to ω_g, that is, that the fading process is not too rapid, then

$$\tan \bar{\theta} = \frac{\int_0^T A \sin \theta \, dt}{\int_0^T A \cos \theta \, dt} . \tag{4.9}$$

For long integration times T, this is equivalent to Eq. (4.4).

4.3.2 MADFI Bearing Computer

In order to realize in practice the system just discussed and to maintain the desired accuracy the following four conditions must be met:

(1) The sine and cosine generators must be of equal amplitude, have very low output distortion, and have a relative output phase of exactly 90°;

(2) To this is added a second problem of constructing four-quadrant multipliers which will give good accuracy over an appreciable dynamic range;

(3) The integrators must be stable and not subject to output drift over long periods of time and must be started together exactly in synchronism at the beginning of the integration interval;

(4) Should it be desired to vary the integration time T, integrator gains must be made to vary inversely with T so that the output multipliers will not be overloaded.

These problems are pointed out for the sake of clarity that, although providing the processing desired, the simplified bearing computer described in the previous section is in fact quite impractical. However, the simple bearing computer described serves as a model for the practical system used in the MADFI. The MADFI bearing computer differs only in the realization of some of the components of Fig. 9 and in the type of integration performed.

The MADFI bearing computer is shown in Fig. 10. The sine and cosine generators are replaced by square waves generated by the synchronizing generator which is, in turn, coupled to the goniometer rotor. The wave corresponding to the sine generator is the north-south (NS) signal, while the wave corresponding to the cosine generator is the east-west (EW) signal. Note that the fundamental components of these waves are in phase with the simplified generators. If the multipliers in Fig. 9 are replaced by simple choppers, or electronic switches, driven by the NS and EW generators, the waveforms at 2a and 2b are produced as shown in Fig. 11. This figure also shows the input voltage e_1 and the two chopper-drive square waves.

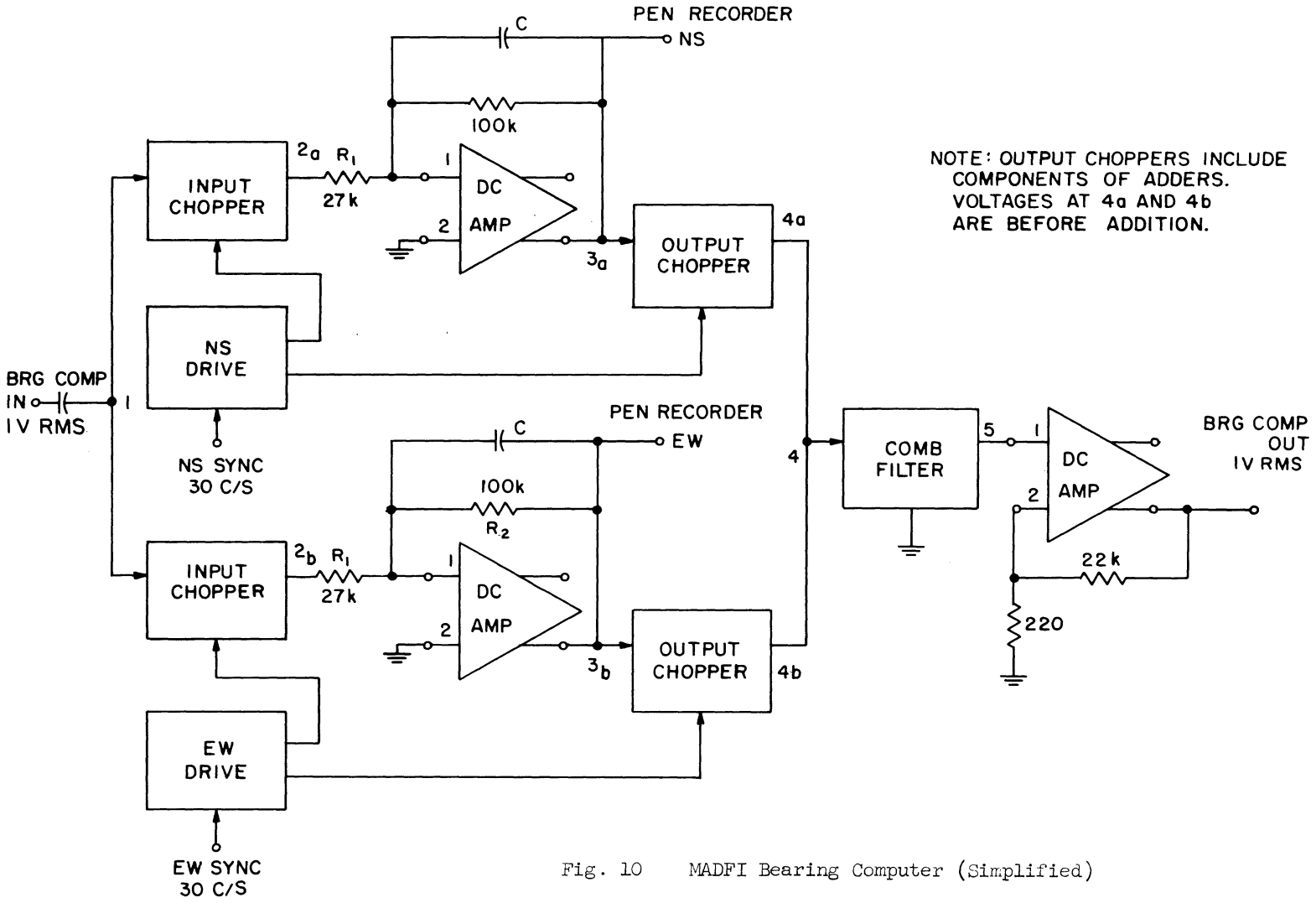

Fig. 10 MADFI Bearing Computer (Simplified)

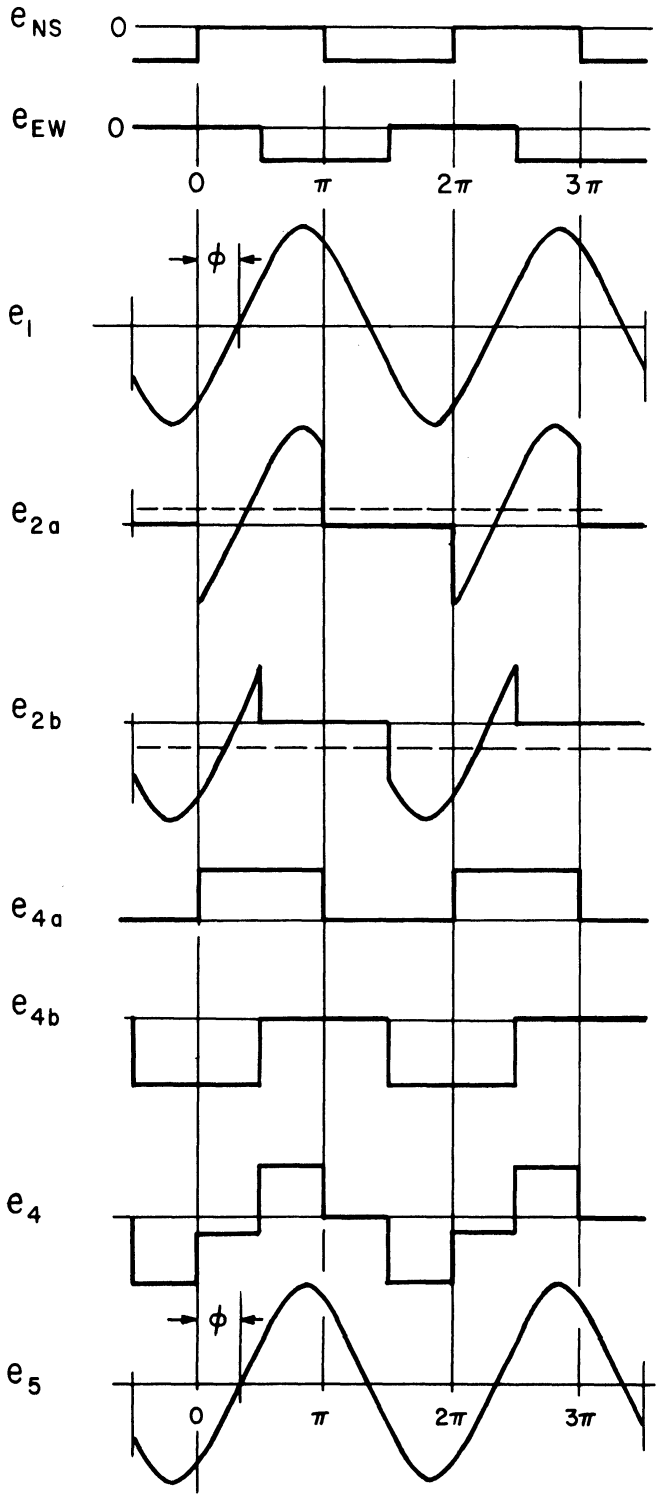

Fig. 11 MADFI Bearing Computer Waveforms

The input to the bearing computer is normally taken from the narrowband filter, and is given at (1) in Fig. 10 by

$$e_1 = A \sin (\omega_g t - \theta). \tag{4.10}$$

The choppers operate in such a way that the outputs (2) consist alternately of the input signal and then ground potential in synchronism with the system NS and EW signals as illustrated in Fig. 11. With the input voltage e_1, the chopper outputs are

$$e_{2a} = A \sin (\omega_g t - \theta) \left[\frac{1}{2} + \frac{2}{\pi} \sum_{k=0}^{\infty} \frac{(-1)^k}{2k+1} \sin (2k+1)\, \omega_g t \right], \tag{4.11a}$$

$$e_{2b} = A \sin (\omega_g t - \theta) \left[\frac{1}{2} + \frac{2}{\pi} \sum_{k=0}^{\infty} \frac{(-1)^k}{2k+1} \cos (2k+1)\, \omega_g t \right]. \tag{4.11b}$$

After some rearrangement and transformation,

$$e_{2a} = \frac{2}{\pi} A \sin (\omega_g t - \theta) \sin \omega_g t + \frac{1}{2} A \sin (\omega_g t - \theta)$$

$$+ \frac{2}{\pi} \sum_{k=1}^{\infty} \frac{(-1)^k}{2k+1} A \sin (\omega_g t - \theta) \sin (2k+1)\, \omega_g t, \tag{4.12a}$$

$$e_{2b} = -\frac{2}{\pi} A \sin (\omega_g t - \theta) \cos \omega_g t + \frac{1}{2} A \sin (\omega_g t - \theta)$$

$$+ \frac{2}{\pi} \sum_{k=1}^{\infty} \frac{(-1)^k}{2k+1} A \sin (\omega_g t - \theta) \cos (2k+1)\, \omega_g t. \tag{4.12b}$$

Comparing Eqs. (4.12 a, b) and (4.5 a, b) we see that the first terms of e_{2a} and e_{2b} are each equal to e_{2a} and e_{2b} of Eqs. (4.5 a, b) except for a multiplicative constant. The harmonics differ in amplitude and number, but are all at multiples of ω_g and attenuated significantly by the integration as in the previous case.

The transfer function of the integrators in Figure 10, where R_2 is typically 3-10 times R_1, may be written (dropping obvious subscripts):

$$\frac{e_3}{e_2} = \frac{1}{R_1 C \left(p + \dfrac{1}{R_2 C} \right)} = \frac{K}{p + a}, \tag{4.13}$$

where $K = \frac{1}{R_1 C}$ and $a = \frac{1}{R_2 C}$. In differential-equation form,

$$\frac{de_3}{dt} + ae_3 = K e_2. \tag{4.14}$$

If $e_3(0) = 0$, the general solution of this first-order linear differential equation is

$$e_3(t) = \int_0^t e_2(\tau)\, e^{a(\tau - t)}\, d\tau. \tag{4.15}$$

Now e_3 can be found when e_2 is the output of the choppers given in Eqs. (4.12). Finally, when the first terms of Eqs. (4.12 a, b) are rearranged as in (4.5 a, b), an expression for the outputs of the integrators is developed:

$$e_{3a} = \frac{K}{\pi} \int_0^t A\, e^{a(\tau-t)} \cos\theta\, d\tau - \frac{K}{\pi} \int_0^t A\, e^{a(\tau-t)} \cos(2\omega_g \tau - \theta)\, d\tau$$

$$+ \frac{K}{2} \int_0^t A\, e^{a(\tau-t)} \sin(\omega_g \tau - \theta)\, dt + \frac{2K}{\pi} \sum_{k=1}^{\infty} \frac{(-1)^k}{2k+1} \int_0^t A\, e^{a(\tau-t)}$$

$$\sin(\omega_g \tau - \theta) \sin(2k+1)\, \omega_g \tau\, d\tau, \tag{4.16a}$$

$$e_{3b} = \frac{-K}{\pi} \int_0^t A\, e^{a(\tau-t)} \sin\theta\, d\tau - \frac{K}{\pi} \int_0^t A\, e^{a(\tau-t)} \sin(2\omega_g \tau - \theta)\, d\tau$$

$$+ \frac{K}{2} \int_0^t A\, e^{a(\tau-t)} \sin(\omega_g \tau - \theta)\, d\tau + \frac{2K}{\pi} \sum_{k=1}^{\infty} \frac{(-1)^k}{(2k+1)} \int_0^t A\, e^{a(\tau-t)}$$

$$+ \cos(\omega_g \tau - \theta) \sin(2k+1)\, \omega_g \tau\, d\tau. \tag{4.16b}$$

If we make the same assumptions as in Section 4.3.1, that the integration time T is long compared to the goniometer spin period $2\pi/\omega_g$ and steady-state conditions have been reached, all terms in Eqs. (4.16) containing integrands periodic in multiples of ω_g, may be neglected and equations similar to Eqs. (4.6 a, b) result:

$$e_{3a} = \frac{K}{\pi} \int_0^T A\, e^{a(t-T)} \cos\theta\, dt, \tag{4.17a}$$

$$e_{3b} = -\frac{K}{\pi} \int_0^T A\, e^{a(t-T)} \sin\theta \, dt. \tag{4.17b}$$

Next the integrator, output voltages (4.17) are multiplied by the chopper-drive waves as in Figure 10. (Note that the high-order terms contain only odd harmonics of ω_g.)

$$e_{4a} = \frac{K}{\pi^2} \sin\omega_g t \int_0^T A\, e^{(t-T)} \cos\theta \, dt + \ldots \tag{4.18a}$$

$$e_{4b} = -\frac{K}{\pi^2} \cos\omega_g t \int_0^T A\, e^{(t-T)} \sin\theta \, dt + \ldots . \tag{4.18b}$$

The voltages at position (4) are linearly added, after which the high-order odd harmonic terms are removed by the comb filter. Thus the voltage at position (5) is:

$$e_5 = \bar{A} \sin(\omega_g t - \bar{\theta}) \tag{4.19}$$

where

$$\bar{A} = \frac{K}{\pi^2} \left\{ \left[\int_0^T A\, e^{a(t-T)} \cos\theta \, dt \right]^2 + \left[\int_0^T A\, e^{a(t-T)} \sin\theta \, dt \right]^2 \right\}^{1/2} \tag{4.20}$$

and

$$\tan\bar{\theta} = \frac{\int_0^T A\, e^{a(t-T)} \sin\theta \, dt}{\int_0^T A\, e^{a(t-T)} \cos\theta \, dt}. \tag{4.21}$$

Except for the $e^{a(t-T)}$ factors under the integrands, Eq. (4.21) is identical to Eq. (4.8). Thus the MADFI bearing computer does, in fact, perform substantially the same processing as the simple bearing computer described in Section 4.2.

4.4 MADFI Bearing Computer Instrumentation

Realization of the MADFI bearing computer components indicated in Fig. 10 is for the most part straightforward. The chopper and d-c amplifiers are designed for extremely low d-c offset and drift. The d-c amplifiers have an open loop gain of over 100 db but a closed loop d-c gain in the operational circuit shown of only about 3 db. It appears feasible to do away with these operational amplifiers by replacing them with simple RC circuits. They were included in the MADFI equipment for reasons of design flexibility and convenience.

The time constant of the feedback components of the operational amplifiers is selectable between 1/3 and 30 seconds. The exact values depend on the multipath process fading rate and are chosen experimentally for each operational situation. The integrated 'bias' in favor of a particular bearing may be reset at any time by a switch, which simultaneously shorts the feedback capacitors.

The comb filter contains three zeroes positioned to provide maximum attenuation of the most significant odd harmonic components of the goniometer spin-frequency ω_g and minimum attenuation of the fundamental component. A problem encountered during design was the change in incremental inductance of the iron-core inductors with changes in signal levels. Bearing errors of as much as a few degrees accrued at extremes in input signal levels, but were minimized by operating the inductors well below saturation levels.

4.5 Synchronizing Generator

The synchronizing generator provides the NS and EW signals to the bearing computer as required in the preceding sections. In addition it supplies special signals to the digital display, which will be described in Section 5.2. Figure 12 shows the three-output signal waveforms, which are periodic at multiples of the goniometer spin-frequency ω_g. Channel 1 (count) pulses occur at a repetition rate of about 5.3 kcs and are used in the digital display circuits. Channel 2 (NS) and 3 (EW) signals occur at a rate of about 30 cps and are used in the digital display and bearing computer circuits.

The waveforms shown in Figure 12 are generated by a photoelectric method involving a rotating code wheel coupled to the goniometer rotor. As indicated in Fig. 13, the rim of the transparent code wheel is divided into three tracks, one corresponding to each output channel. Each track consists of a series of strips of opaque material placed in the pattern indicated in Fig. 13. Three miniature lamps placed in the general area behind the strips and behind the outer web of the wheel provide illumination of three photosensitive diodes mounted outside the rim of the wheel. The output of each of the photodiode amplifiers corresponds to the presence or absence of opaque material in its respective track as the wheel revolves in the direction of the arrows and results in a square waveform as shown in Fig. 12. The circuit shown for supplying operating voltage to the lamps was chosen for mechanical convenience. The protective diodes shown prevent a multiple lamp burnout situation in event of a single lamp filament failure.

In this and other digital-type circuits used throughout the equipment, waveshape and driving levels are standardized for compatibility reasons. System waveshape characteristics

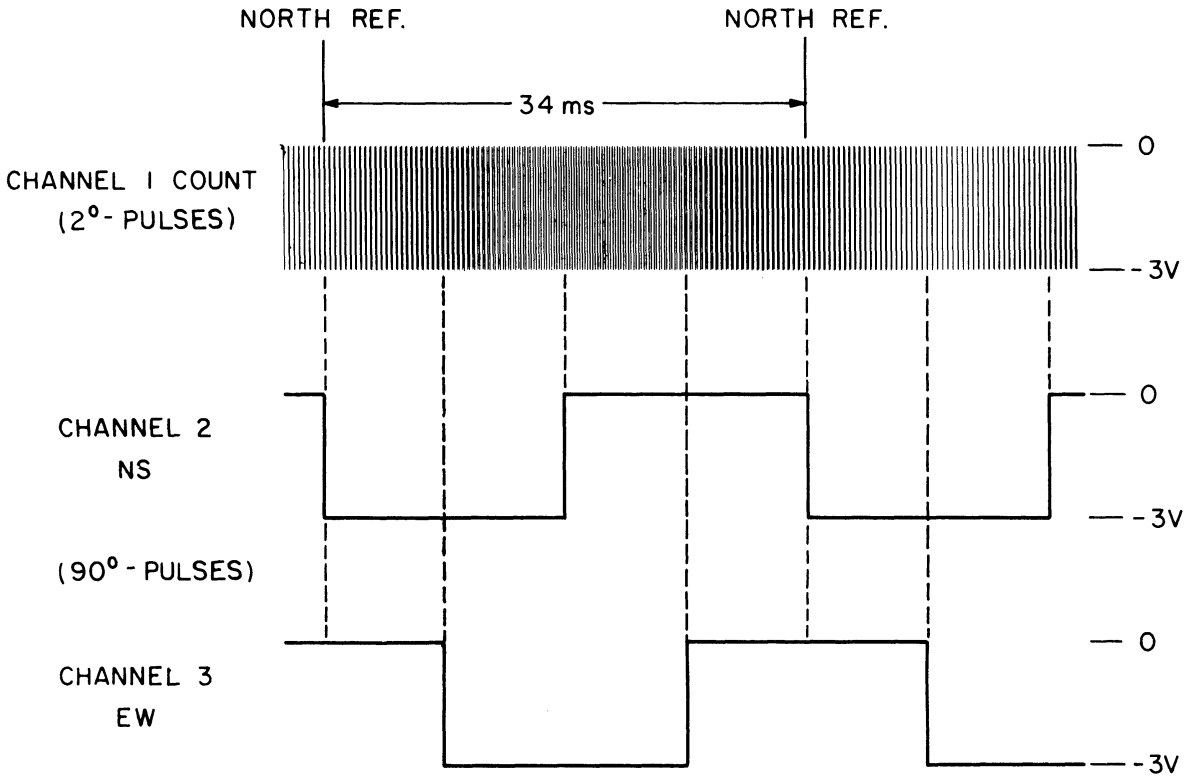

Fig. 12 Synchronizing Generator Waveforms

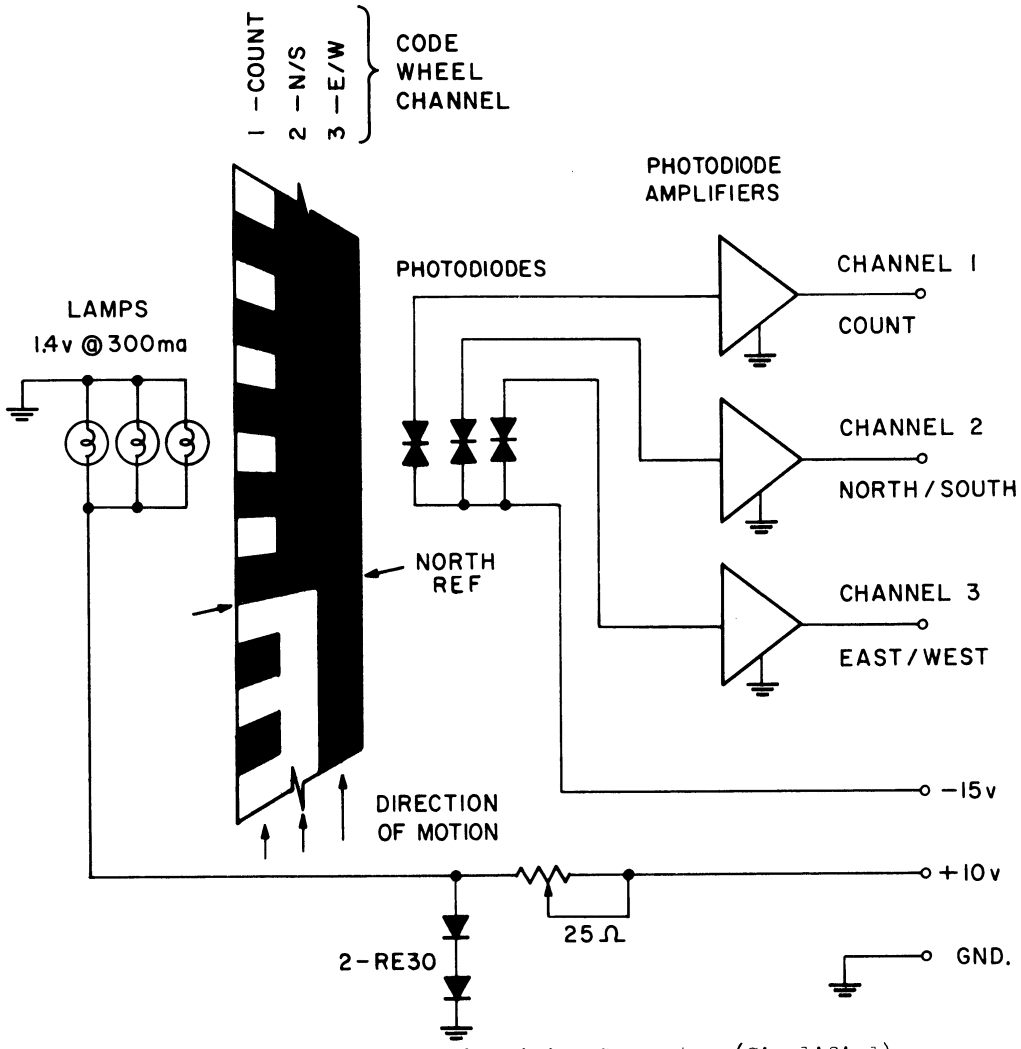

Fig. 13 Synchronizing Generator (Simplified)

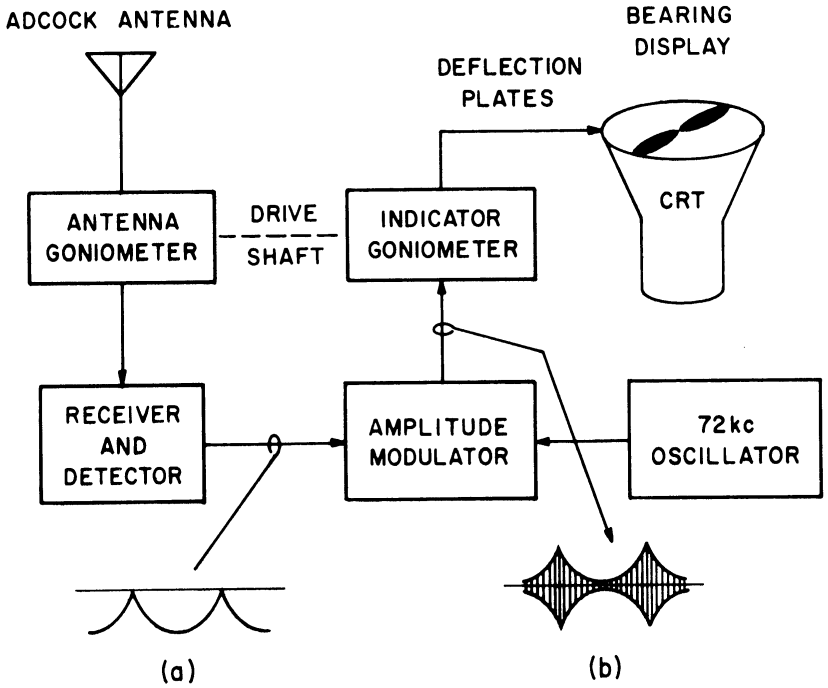

Fig. 14 Manual Sense Operation of AN/TRD-4A

have been chosen appropriate for 1-mcs operation, with zero volts corresponding to a logical "0" and -3 volts to a logical "1."

5. DISPLAY AND RECORDING SYSTEM

The MADFI display and recording system displays the amplitude and bearing of the incident signal on several types of readout devices. Instantaneous bearing indications are visible on the modified AN/TRD-4A cathode-ray display as the conventional propeller-shaped pattern. As an added convenience the automatic sense circuit blanks the anomalous half of the propeller associated with the 180^{o} ambiguity mentioned in Section 3.1. A permanent record of the cathode-ray display may be made by the pen recorder, which traces a polar-coordinate plot not only of the indicated bearing but of the bearing signal amplitude as well. A three-digit decimal display reading directly in degrees is included in the system as well as paper tape punch which records the decimal display indications. The decimal display and the paper tape punch are sampling-type systems which display and record bearings periodically at a preset rate. Such a system in conjunction with the processing system yields very low information rates for peripheral computer processing.

5.1 Cathode-Ray Display Operation

The cathode-ray display utilizes components of the prototype AN/TRD-4A system. Its principal modifications include the addition of the automatic sense circuit and provisions to convert the MADFI bearing signal to a compatible signal appropriate for the AN/TRD-4A cathode-ray display circuits.

The operation of the modified AN/TRD-4A cathode-ray display may be better understood by contrasting it with the operation of the unmodified display. Figure 14 is a block diagram of the unmodified AN/TRD-4A system. The cusped waveform (a) appearing at the receiver detector output is a full-wave rectified sine wave resulting from amplitude detection of a double-sideband suppressed-carrier wave. This wave, normal to the unmodified AN/TRD-4A operation, is connected to an amplitude modulator in such a fashion that its amplitude zeroes correspond to peaks in the output. The 72-kcs subcarrier frequency is used to facilitate passage of the wave through a second goniometer. The two resultant goniometer stator voltages deflect the cathode-ray tube to produce the conventional propeller pattern.

Figure 15 is a block diagram of the modified system with the addition of MADFI automatic sense circuitry. In this case, the receiver output is an amplitude-modulated wave with index less than unity, so that the detector output is a sine wave plus a d-c component. After removal of the d-c component by a high-pass filter, the resultant sine wave bearing signal is full-wave rectified to provide the normal cusped signal for the 72-kcs modulator.

If the remainder of the circuitry were unchanged, the propeller pattern would be identical with that described above. In the MADFI system, however, a blanking signal is generated in a balanced modulator by driving this modulator with wave (d), a 90^{o} phase-shifted version of the sine wave (a), and with the same 72-kcs subcarrier as the original modulator. This 72-kcs blanking signal, wave (e), is phased in such a manner as to blank one-half of the propeller pattern as shown.

5.2 Modifications and Additions to Cathode-Ray Display

Modifications to the AN/TRD-4A cathode-ray display are shown in Fig. 16. An amplifier was added to increase the blanking signal at the grid of the cathode-ray tube. The synchronizing signal which is routed to the automatic sense circuit is derived from the grid of the 72-kcs oscillator tube in the indicator chassis. The transformer and diodes and RC network shown are components of the full-wave rectifier and its associated phase equalization network. Although the transformer is operated well below saturation, considerable pattern distortion is observed with rapidly fluctuating incident signal amplitudes when the detector is patched via the patch panel directly to the cathode-ray display. The rapidly-changing d-c component generates low-frequency signals which cause saturation of the transformer. Since this patching condition is rarely used, a solution to this problem was deferred.

The automatic sense circuitry is contained in an external module located in the analog case. Its circuitry, shown in simplified form in Fig. 17, is that of a ring-diode balanced modulator preceded by a phase-shifting network and followed by a 72-kcs amplifier. Its performance is such that a discernible blanking action is visible on the cathode-ray tube even if the bearing signal is too low to form a recognizable propeller pattern.

The manual operation of the AN/TRD-4A indicator is left undisturbed, including the manual-sense circuitry. The MADFI operation is identical with manual operation except that the sense operation is automatic. The relay evident in Fig. 16 is part of the manual-automatic switching circuitry and is shown in the manual mode.

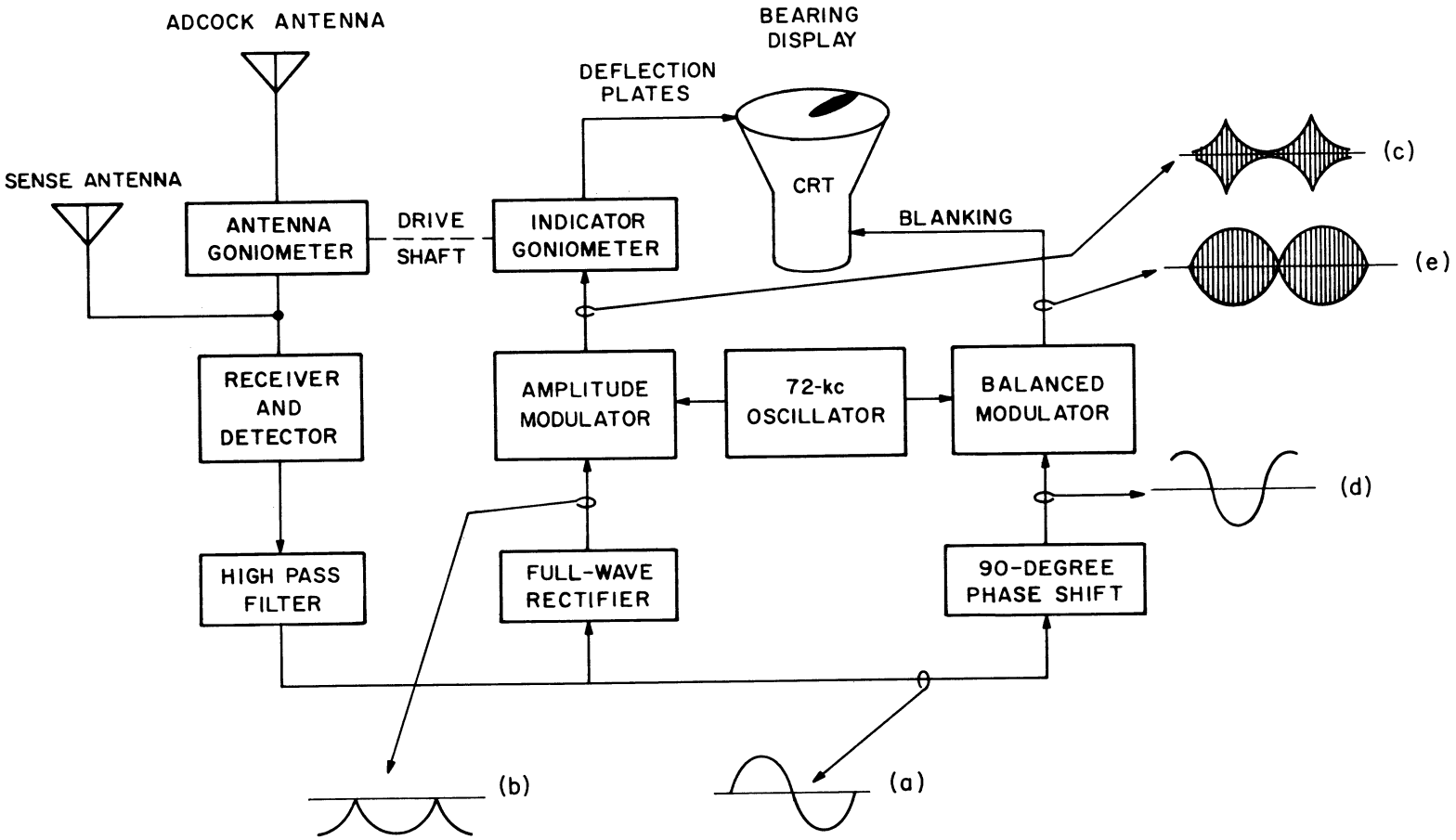

Fig. 15 Automatic Sense Operation of MADFI

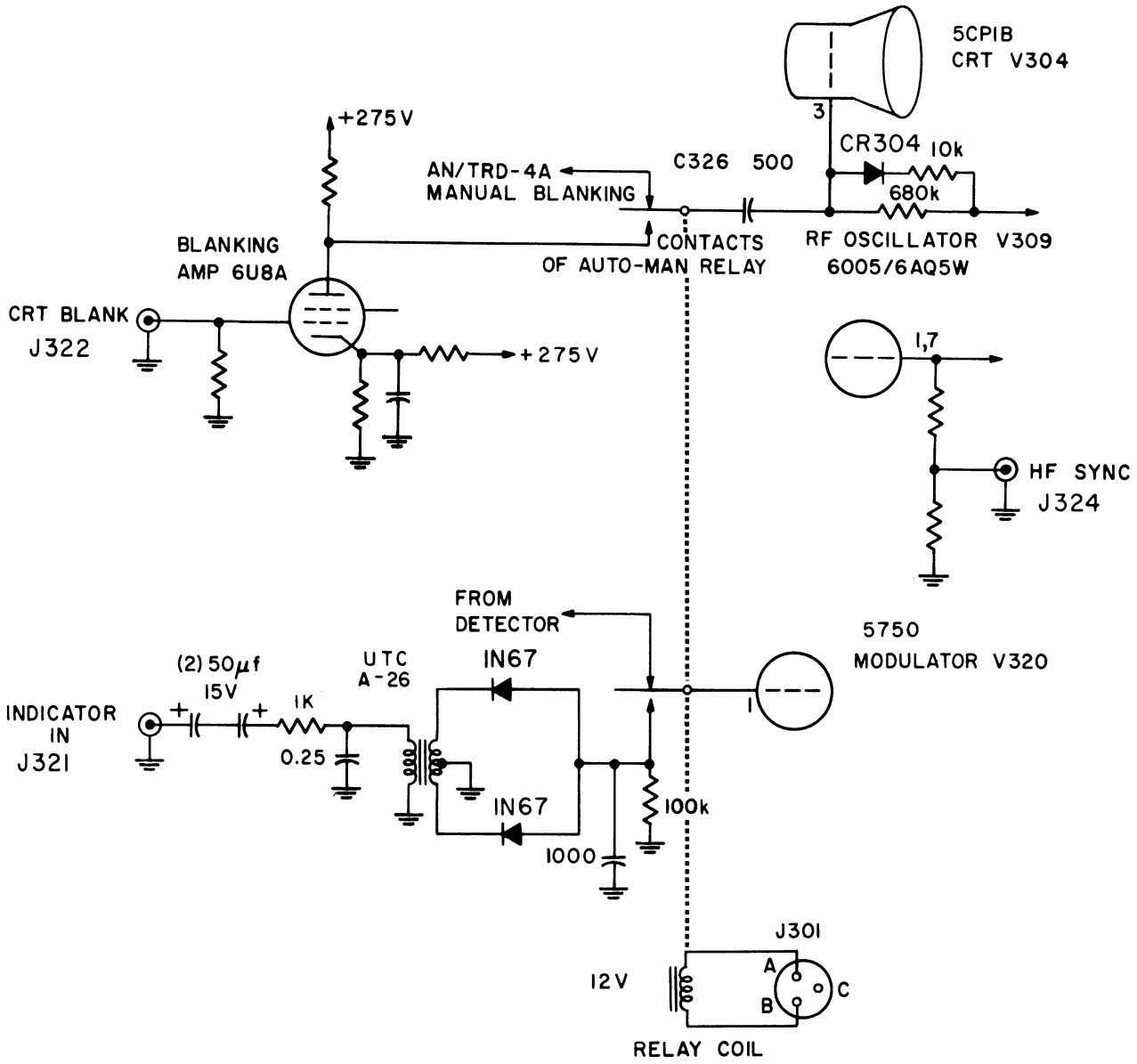

Fig. 16 AN/TRD-4A Indicator Modifications

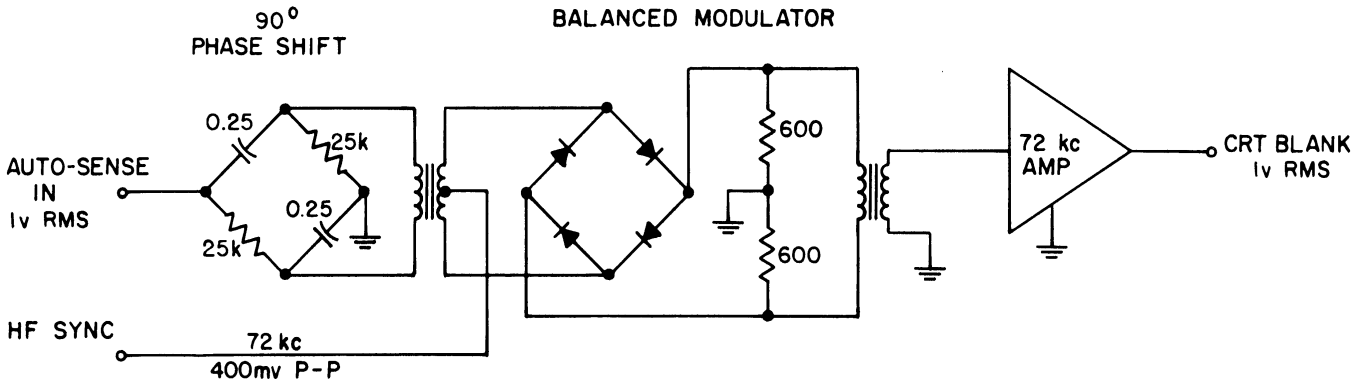

Fig. 17 Automatic Sense Circuit (Simplified)

5.3 Pen Recorder

The pen recorder used in the MADFI to record amplitude and bearing indications is a Moseley Model L X-Y Recorder. This recorder is connected to the bearing computer operational amplifier outputs so that the X-channel indicates the voltage e_{3a} at position (3a) on Fig. 10 and the Y-channel indicates the voltage e_{3b} at position (3b) on the same figure. Points are plotted on polar coordinate paper arranged on the pen recorder so that the Y-axis corresponds to an angle of zero degrees and the X-axis corresponds to an angle of 90^{o}. Inspection of Eq. (4.18) reveals that the amplitude A and bearing θ of the incoming signal are represented by the radial distance and angular argument respectively of points plotted in this manner.

The recorder is equipped with a 'pen pecker' which causes the pen to strike the paper periodically and produce a sequence of dots rather than scrawl continuously and produce a tangle of wavy lines. It is believed that 'scatter' plots produced in this manner over a time interval of a few minutes will provide considerable information as to the nature of the fading process.

5.4 Decimal Display

Digital readout of bearing indications is shown by a three-digit decimal display. The display contains large, easily read incandescent projection numerals and reads directly in degrees. Convenient binary-coded-decimal outputs are provided for either a peripheral paper punch or a digital telemetering link, making unattended operation at a remote field site convenient and attractive.

The circuitry used in the decimal display and shown in block diagram in Fig. 18 is basically that of an event counter which operates during that interval the goniometer shaft moves through the angular displacement φ corresponding to the incident signal bearing θ. The start-signal to the counter is generated by the synchronizing generator as the code wheel passes through an angular position established as a north reference. The stop-signal to the counter is generated at the time of each positive-going zero crossing of the bearing signal e_b from the bearing computer. During the interval between the start- and stop-signals, the counter totals the number of $1/2^{o}$-pulses produced by the synchronizing generator in conjunction with a circuit called the count multiplier. Several design innovations have been included in these circuits for reasons of accuracy and reliability and will be described in the following sections.

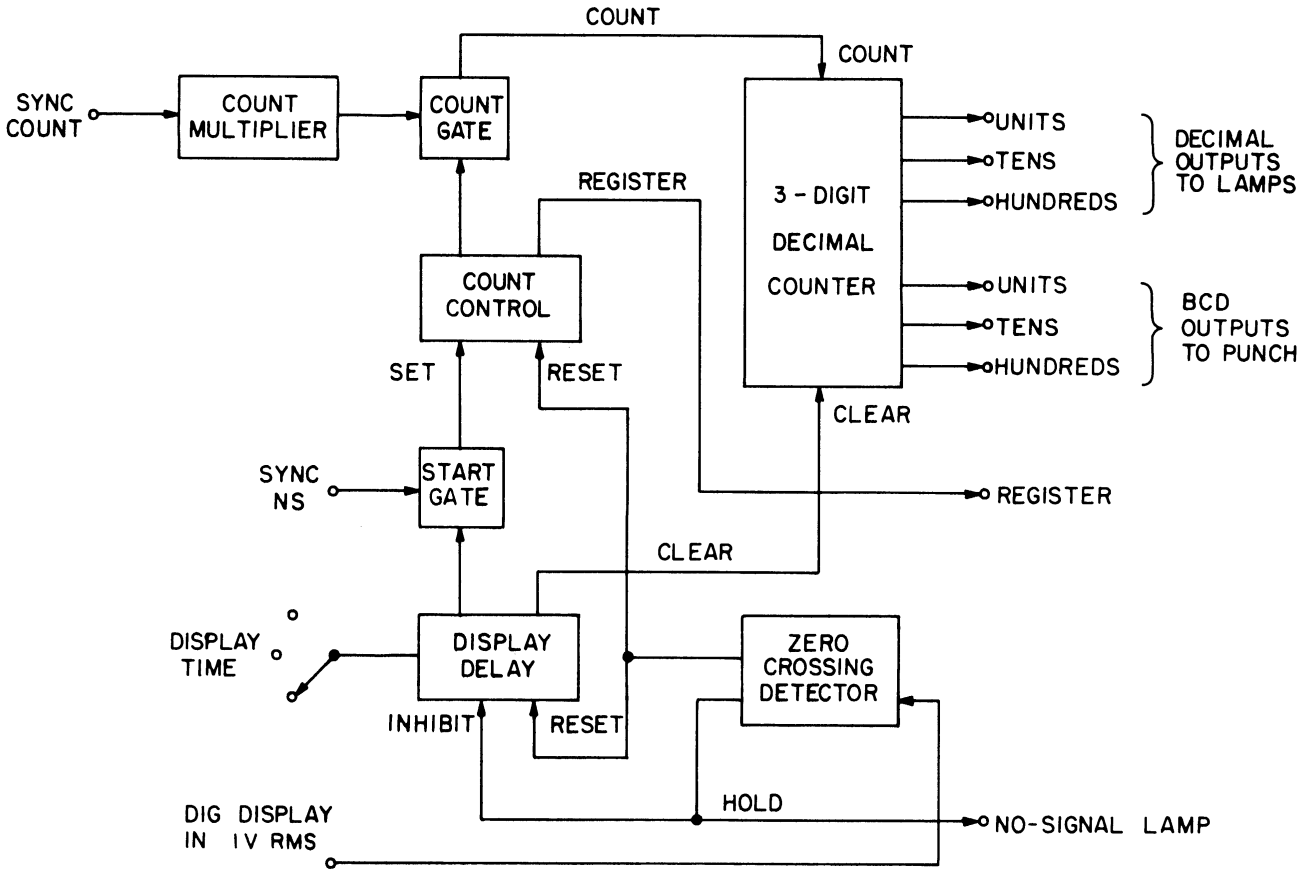

Fig. 18 Decimal Display (Simplified)

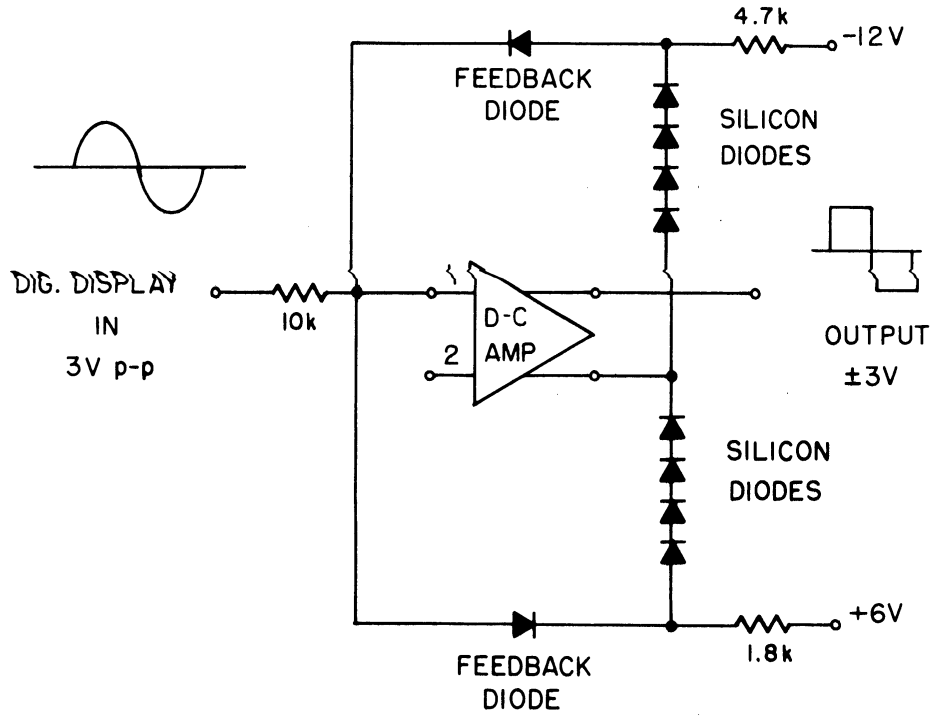

Fig. 19 Zero-Crossing Detector (Simplified)

5.4.1 Count-Control Circuitry

The count-control circuitry of the decimal-display consists of all the blocks in Figure 18 except the decimal counter and the zero-crossing detector. The count multiplier employs a blocking oscillator synchronized to the fourth harmonic of the 5.3-kcs count signal from the synchronizing generator. Since the count pulses occur once every 2^{o} of rotation of the code wheel, it is apparent that the pulses produced by the count multiplier occur every $1/2^{o}$ of rotation. The count-control and count-gate circuits gate the pulses produced by the count multiplier according to a start-signal produced by the synchronizing generator, a stop-signal produced by the zero-crossing detector, and an inhibit-signal produced by the display delay circuitry.

The inhibit-signal is generated by the display delay circuit, which controls the length of time a count is left on display before another count cycle is initiated. The circuit, controlled by a simple RC delay, establishes an enable condition to the start gate at some time during a revolution of the goniometer shaft. The next start-pulse to appear switches the count-control circuitry to the ON state. The following stop-pulse resets not only the count-control circuit, but the display delay circuit as well, and the delay begins timing the display interval. At the end of this interval, the enable condition is again established and the cycle repeats. The display interval may be adjusted by the operator, but a count may be initiated at any time by a reset control provided for that purpose.

Particular care was taken in the design of this circuitry to minimize false counts due to undesired coincidences of the various pulses. If in any case the counter is 'confused,' it is reset to zero and awaits the next start-pulse. This reset condition persists for only a fractional revolution and is generally unnoticeable.

5.4.2 Zero-Crossing Detector

The practice of finding the bearing estimation $\bar{\theta}$ of Eq. (4.5) by zero-crossing detection requires a highly precise zero-crossing detector. The design precision of the digital display was set to be $\pm 1/2^{o}$, which corresponds to three significant figures on the three-digit display. This precision corresponds to about one part in 700, which is also a voltage differential of one part in 700 since the slope of the bearing sine-wave signal at its zero crossings is unity.

Precisions such as this led to the approach chosen in the MADFI and illustrated in the circuit of Fig. 19, a circuit borrowed from analog computer technology. Each of the strings of four silicon diodes in this diagram provides a convenient voltage reference. When the voltage

at the output exceeds this voltage the feedback diodes conduct and the device gain approaches zero, whereas when the feedback diodes are not conducting the full gain of the d-c amplifier is active.

The circuit used in the MADFI includes a level detector which supplies a lock signal to the count-control circuitry in the event of insufficient bearing signal amplitude. The lock signal holds the decimal display at the last successfully completed count.

5.4.3 Binary-Coded Decimal Counter

The counter indicated in Fig. 18 is a three-digit Binary-Coded Decimal (BCD) type of conventional design. A feature of note is the automatic-rounding circuit, which rounds off the units digit according to whether the number of $1/2^{o}$-pulses passing the count gate is odd or even. Instead of the $\pm 1^{o}$-ambiguity present with conventional counters of this type, the reading is now accurate to the nearest half-degree. The technique consists of complementing the $1/2^{o}$-flip-flop of the counter with the register pulse and propagating any 'carries' generated.

The ten BCD outputs from the three decades—four each from the 'units' and 'tens' decades and two from the 'hundreds'—are connected by three BCD-decimal decoding matrices to driver transistors for the decimal-display lamps. Buffered outputs are also available to drive the paper tape punch.

5.5 Paper Tape Punch

The paper tape punch provides a means of saving bearing estimates produced by the system for later computer processing. With the present system the bearing is punched once for each count cycle of the decimal-display. No provision is made for recording any amplitude or time information. However, even records of this simpler type may be highly useful in evaluating various combinations of processing elements.

The tape punch, affectionately called the Michigan Automatic Generator of Indigenous Confetti (MAGIC), is adapted from a commercial tape transport through the addition of laboratory-constructed solenoid drivers and timing circuits and an integral d-c power supply. The unit is completely self-contained and may be driven from any source with compatible input signals.

The punch is capable of recording eight binary bits of information per line of tape at a rate of 60 lines per second. This rate is more than adequate to obtain one recording for each

revolution of the goniometer drive shaft should such a rapid rate be desired. Since ten channels are required to record the full three-digit number from the decimal-display, two lines of tape are required per count. At present no provision is made in the MADFI system to do this; only the low-order bits from the 'units' and 'tens' decades are recorded as one line of tape per count. A device to perform the desired multiplexing could be realized using, say, a multicontact pulsed relay. Also, the received amplitude information could be recorded through an analog-to-digital converter, but neither the complexity of currently available techniques nor the high cost of commercial units was considered justifiable under the present effort.

The diagram of Fig. 20 shows a logical diagram of the punch as well as the tape format. The inputs are connected to a set of lines in which a level of -3 volts corresponds to a punch and a level of zero to a no-punch. The inputs are normally gated off so that no-punch action is initiated except on the receipt of a register-pulse. The -3 volt register-pulse causes a 4.5-ms pulse to be produced which then routes the inputs through the solenoid drivers to the punch solenoids in the tape transport. Following the punch action, a sprocket hole is automatically punched and the tape advances one line.

A button is provided to punch sprocket holes and advance the tape without punching any input information. This button is used for loading and clearing the transport and preparing leaders, as well as for producing confetti for a multitude of uses.

6. FIELD MEASUREMENTS

Due to time limitations imposed on the present effort, very little quantitative information has been gathered concerning system performance. A site for the antenna array was chosen that is believed comparatively free from man-made noise. The site is a partially forested, gently rolling, hilly terrain about thirty miles northwest of Ann Arbor, Michigan. With the aid of a surveyor's theodolite, the antenna array was erected and surrounded with bearing-marker stakes every 15° at a radius of about 100 feet from its center. The target transmitter supplied with the AN/TRD-4A equipment was placed on each of these stakes in turn and the MADFI indicated-bearing recorded. Deviations between the actual and recorded bearings are summarized in Fig. 21 for frequencies of 6, 8, and 10 mcs. The deviations are evidently due in part to the influence of the shelter and, at the higher frequencies, to the octantal error.

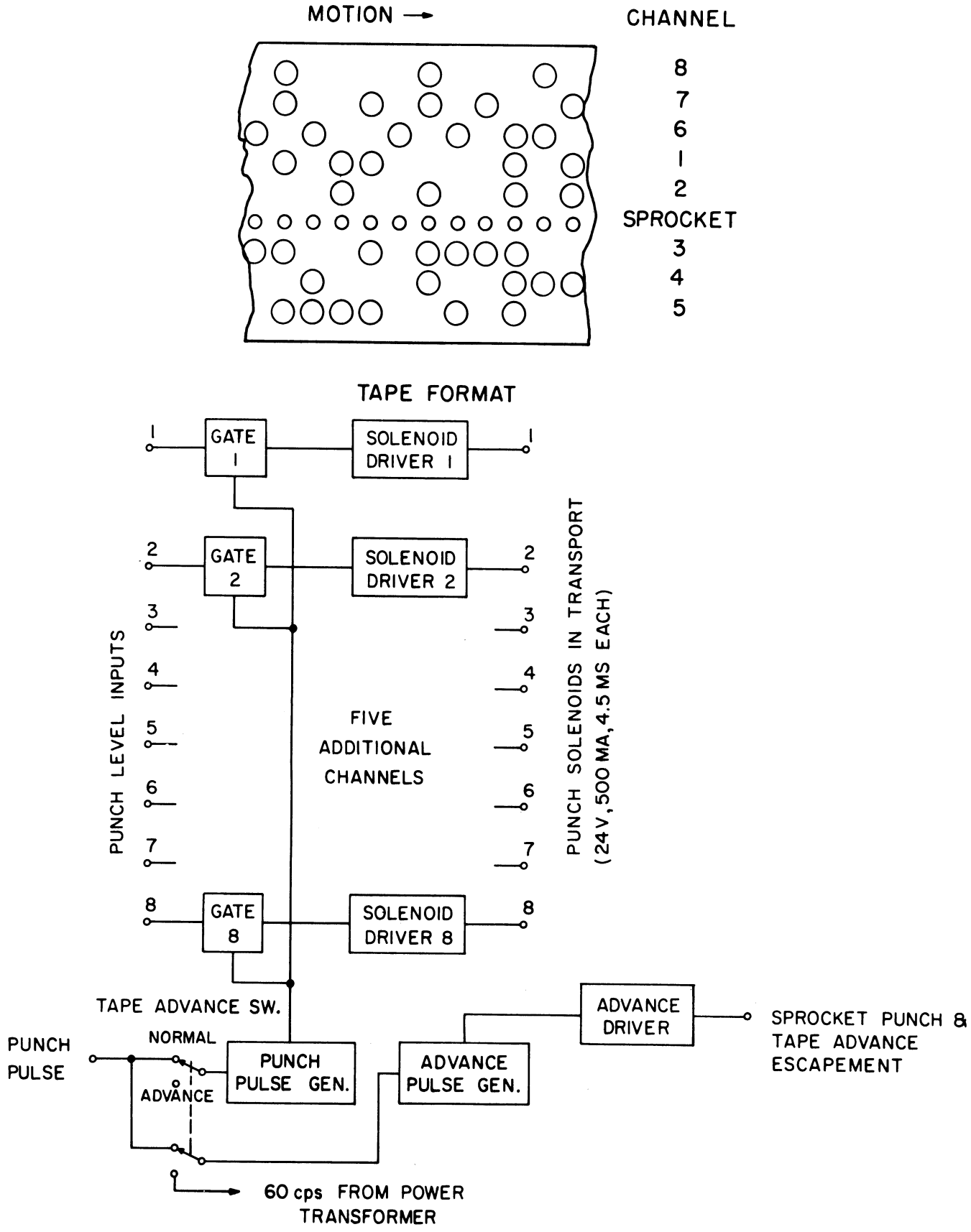

Fig. 20 Paper Tape Punch

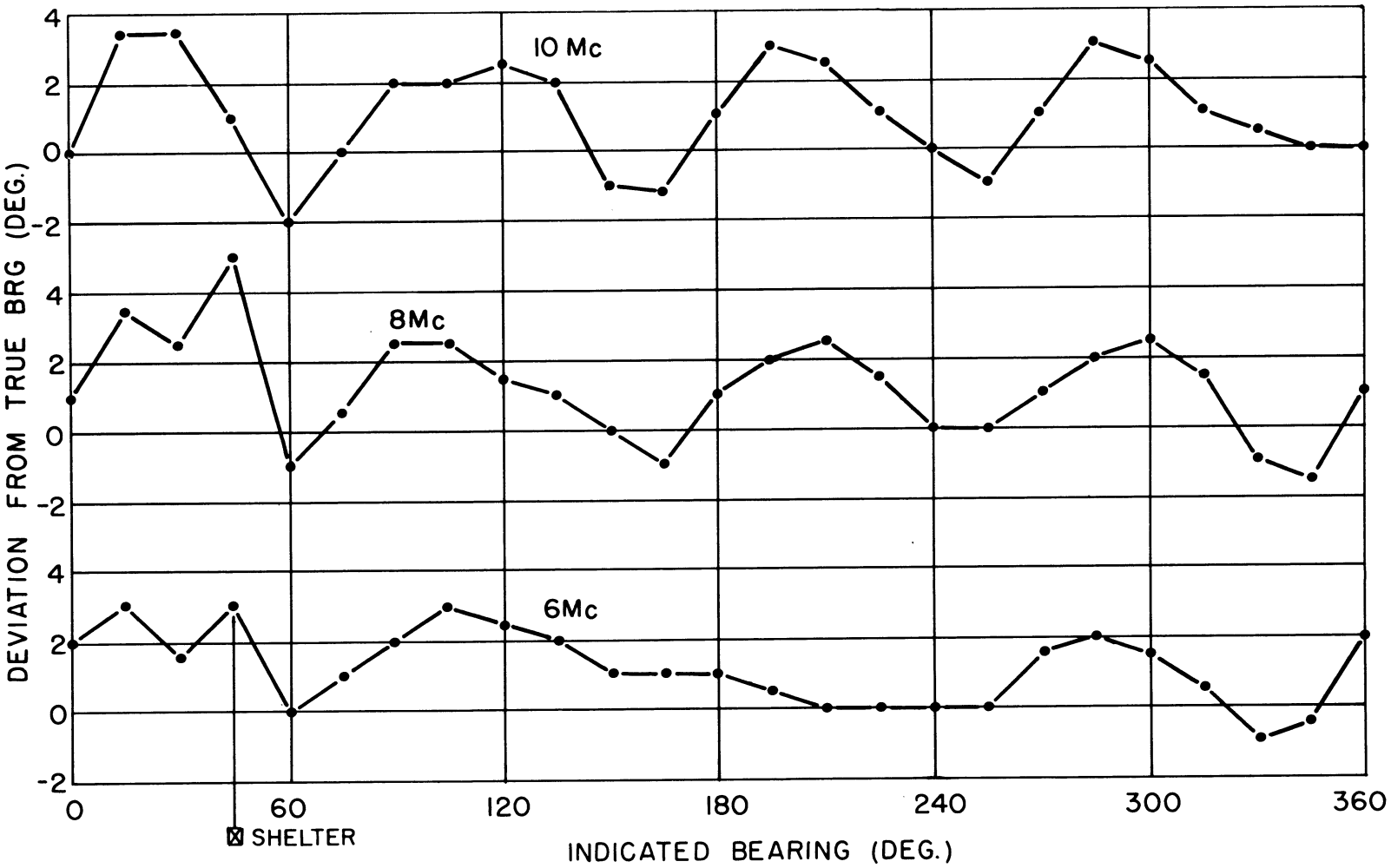

Fig. 21 MADFI Deviation--Indicated Bearing Curves

Qualitative data regarding the worth of the processing system components are difficult to collect since relevant data are largely statistical in nature. It is certain that, on a subjective basis, the appearance and stability of the cathode-ray display are vastly improved over that of the unmodified AN/TRD-4A. Stable bearings on single-sideband, hand- and machine-telegraph and even kineplex transmission are readily achieved. When the bearing of a station of known coordinates was compared to that indicated by the MADFI, agreement to within a couple of degrees was common even in the presence of multipath processes that caused the unmodified AN/TRD-4A indicated bearing to vary over a range of 180^{o}. However, to support these subjective observations quantitatively, it would be necessary to collect a large enough quantity of data for a thorough statistical analysis.

7. SUGGESTIONS FOR FURTHER RESEARCH

The MADFI system is intended as a research tool. As such it has application in studies of ionospheric phenomena and direction-finding techniques. However, some of the MADFI operating characteristics may need to be refined so as to inject the least amount of error into some specialized measurements. Thus, it is suggested that further research include some considerations of equipment improvement.

7.1 Collection of Bearing Statistics

Bearing statistics furnished by the MADFI equipment could well be used in studies of ionospheric phenomena related to radio transmission. Probably the most useful record of these would be the paper tape record, together with additional amplitude and time information. The bearing estimates could be read at high-speed directly from the tape by a general-purpose computer. Results of a large amount of data taken over several months could be processed in this manner to give statistical information concerning ionospheric dynamics and ray-retracing techniques. Of equal importance would be the quantitative information available concerning the evaluation of antennas, sites and direction-finding methods in general.

7.2 MADFI System Improvements

As a system, the MADFI has operating characteristics which are deemed undesirable under certain conditions. A few of these will be discussed in the following paragraphs together with suggested improvements. Some of the problems in the MADFI are directly related to those in the original AN/TRD-4A DF Set, and many in the areas of antennas, goniometers,

and receiver filtering have been discussed elsewhere (cf. References). It is believed that attention therefore should be concentrated on problems of the processing and display systems of the MADFI.

Throughout the MADFI effort, little attention was paid to the effects of nonuniform phase characteristics of the postdetection filtering components. The effects of this distortion are significant only in rapidly fluctuating multipath processes and in this connection may be worthy of further study.

The realization of the bearing computer has demonstrated the promising features of linearly-weighted time-averaging. Virtually no quantitative testing of this particular weighting scheme was possible on this project. Examination of this and various other weighting techniques for use in the bearing computer would be desirable, especially in connection with the problem of rapid and widely varying signal amplitudes. Some system of utilizing automatic gain control-circuitry in the receiver appears particularly attractive in view of the wide dynamic range associated with some multipath fading processes.

The operational amplifiers in the integrator circuit of Fig. 10 could be eliminated from the system by replacing their gain with the other active circuit components. Although the amplifiers were designed for maximum stability through the use of differential circuitry and silicon-type transistors, the small but measurable drift affects MADFI long-term accuracy.

As mentioned in Section 3.2.2, the comb filter might be improved through further study. The three-zero design was used as a result of an arbitrary choice made some time ago in the history of MADFI. Unquestionably, a method of eliminating the nonlinear iron-core inductors would be most desirable to implement. An estimate of bearing error due to residual harmonics at the filter output should be studied.

As mentioned above, the paper tape punch is not equipped to record the amplitude of the bearing signal. An obvious improvement in the recording system is to incorporate provisions for this. An analog-to-digital converter would be required along with a multiplex unit. Additional convenience would be gained by including a provision to record periodically the time of observation.

8. APPENDIX

OPERATION NOTES AND CIRCUIT INFORMATION

Most test points adjustments and indicators for setup and operation of the MADFI are readily accessible from the front of the equipment. Figures 22 and 23 show the logical diagram and cable interconnections, Figs. 24 through 28 show the equipment and connector placement within the racks, and Figs. 29 through 31 show the arrangement and labelling of the various controls. Figures 32 and 33 show the logical interconnection at the modules in the Analog and Digital racks. The remaining figures, 34 through 60, show the detailed circuit diagrams of the modules within the rack.

After the usual procedure is followed, the AN/TRD-4A is tuned and adjusted with the MADFI in the manual code. With the receiver RF gain control at minimum and MADFI in the automatic mode, the regulated power supply should be adjusted, and all d-c amplifiers zeroed. In the case of the operational amplifiers in the bearing computer, zero adjustments are made both with the INTEG RESET Button depressed and released. The balance control in the automatic sense module is adjusted for minimum 72-kc carrier at the output and the null controls of the comb filter adjusted for minimum goniometer-spin frequency harmonics at its output. The lamp current control (on the goniometer drive chassis) is adjusted for lamp brightness consistent with good pulse shape of the count (Channel 1) output. The narrowband filter gain is found by experiment. Sense phase adjustment is made using an oscilloscope connected to the R-390/URR IF output to obtain a good amplitude-modulated wave.

Using the RF gain control of the R-390/URR, the system gain is set at a point where the output meter reads one-half scale (50 μa) allowing for the integration time of the bearing computer. The input meter should not swing upward off-scale under any fading conditions. The narrowband filter gain may be used to increase the processing system gain if necessary. Integration and count times are chosen appropriately for the signal dynamics, and the AUTO SENSE and AUTO/MAN switches are used as desired.

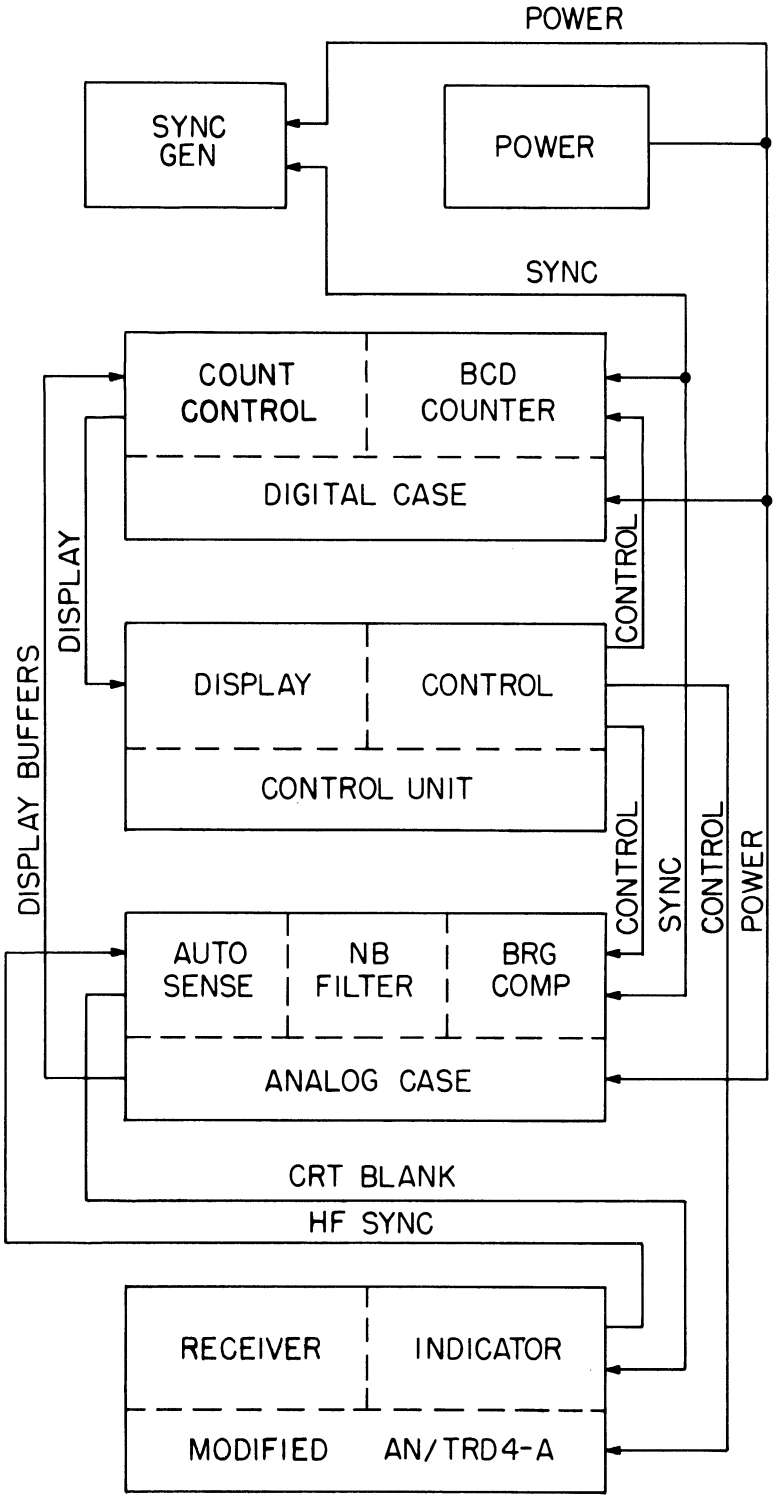

Fig. 22 System Logical Diagram

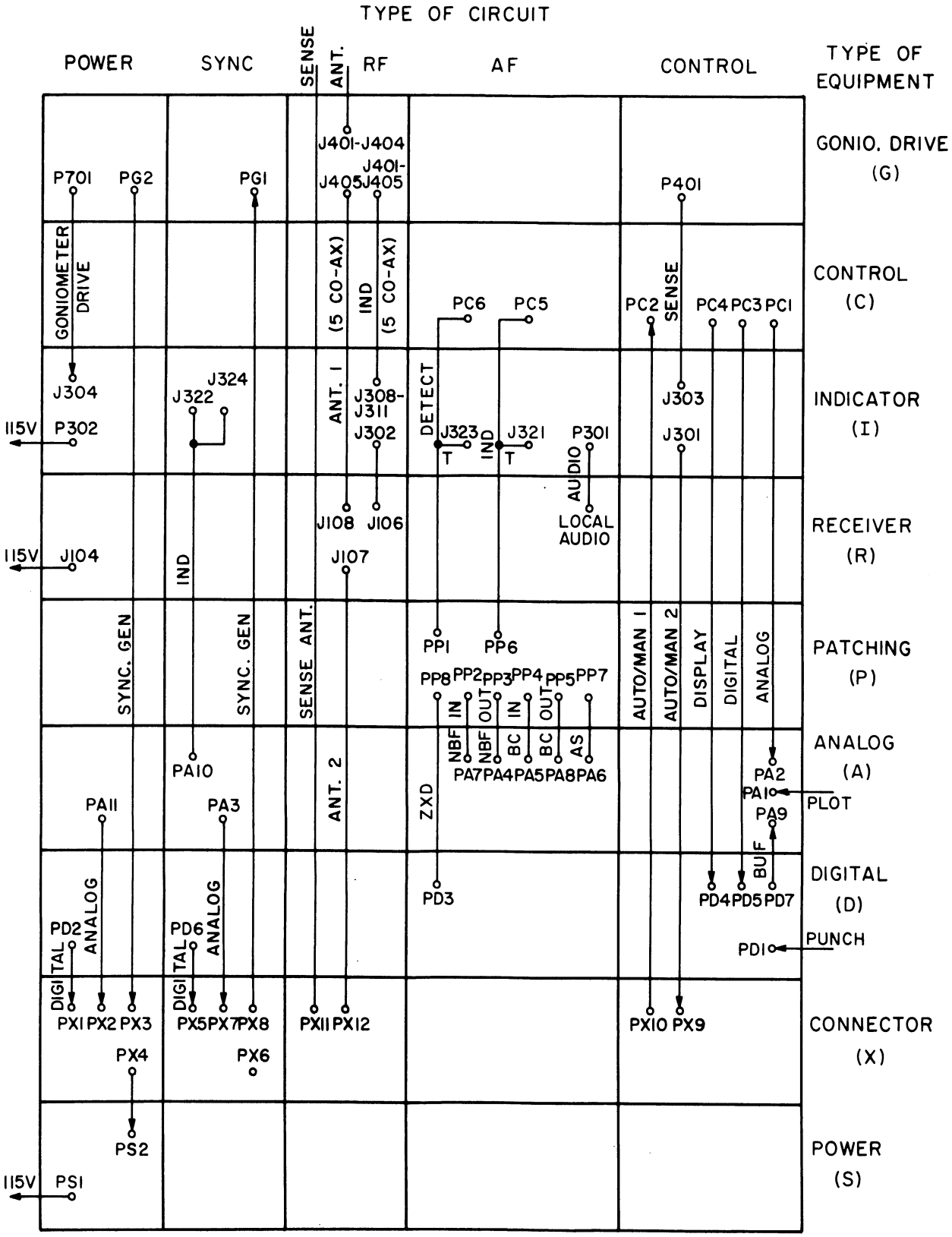

Fig. 23 System Connector Diagram

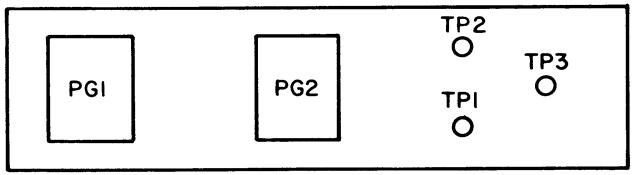

SYNC GENERATOR–REAR

Fig. 24 Synchronizing Generator Connector Placement

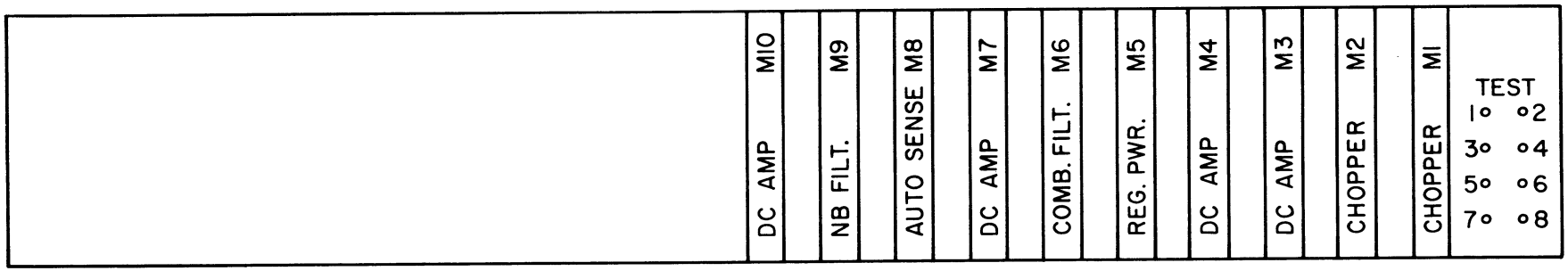

ANALOG CASE–FRONT

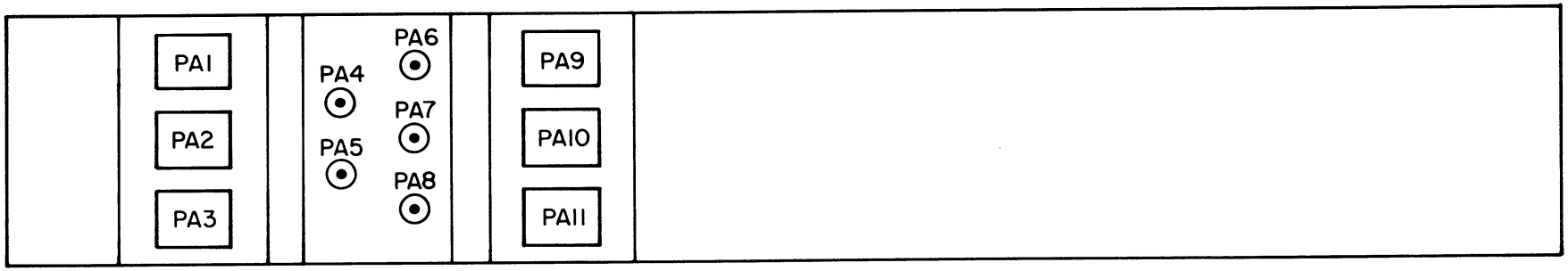

ANALOG CASE–REAR

Fig. 25 Analog Case Module and Connector Placement

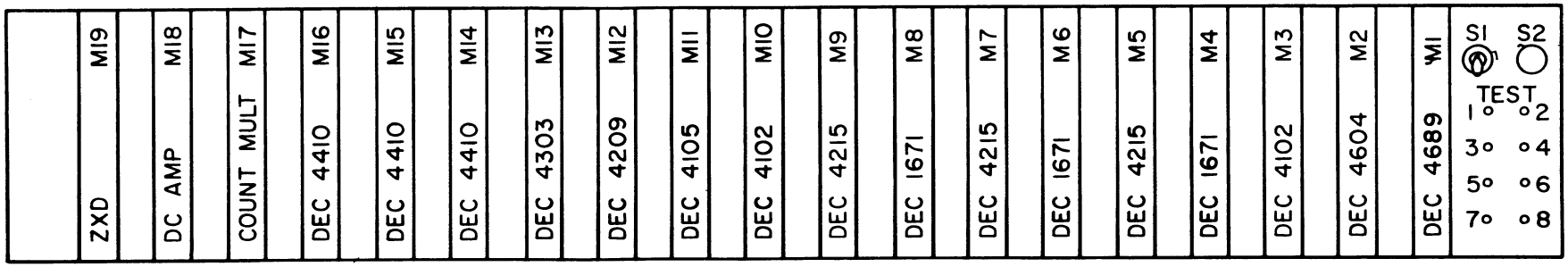

DIGITAL CASE-FRONT

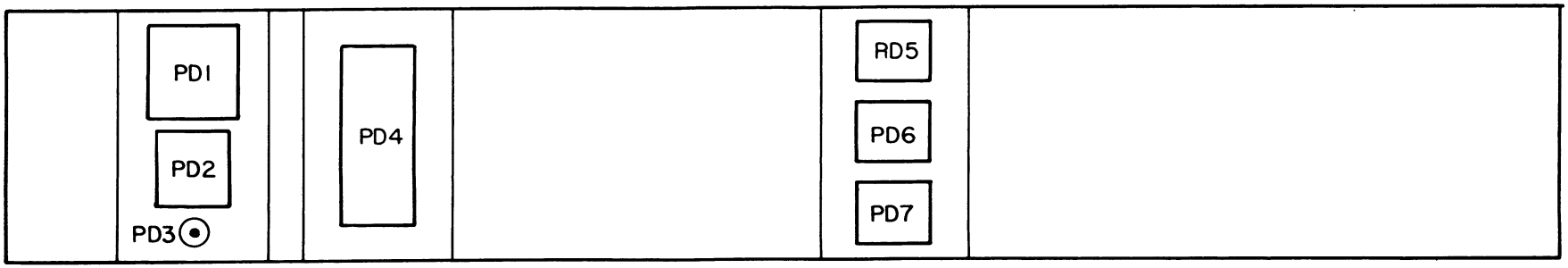

DIGITAL CASE-REAR

Fig. 26 Digital Case Module and Connector Placement

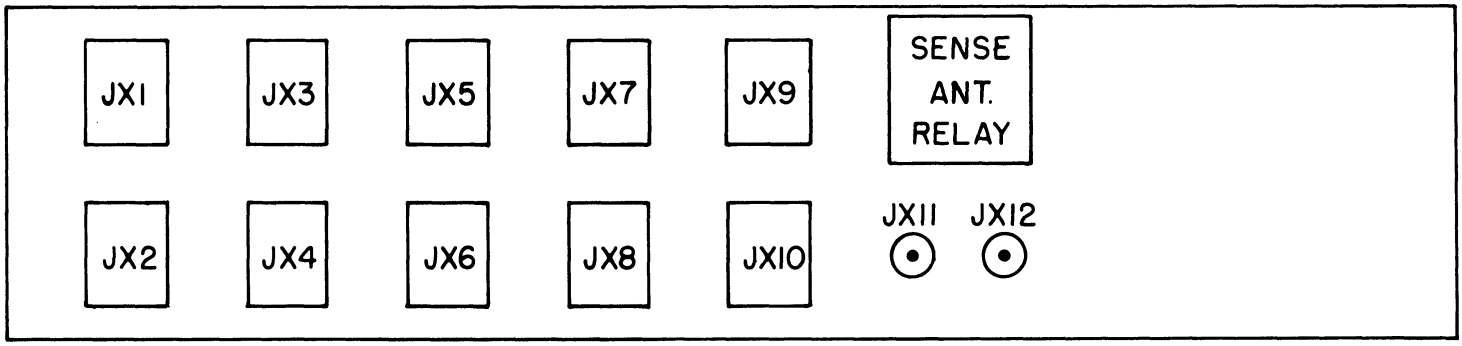

CONNECTOR PANEL-REAR

Fig. 27 Connector Panel Connector Placement

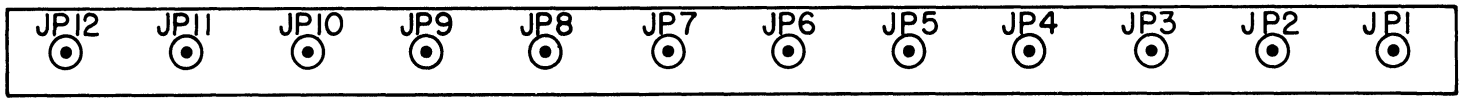

PATCHING PANEL-REAR

Fig. 28 Patching Panel Connector Placement

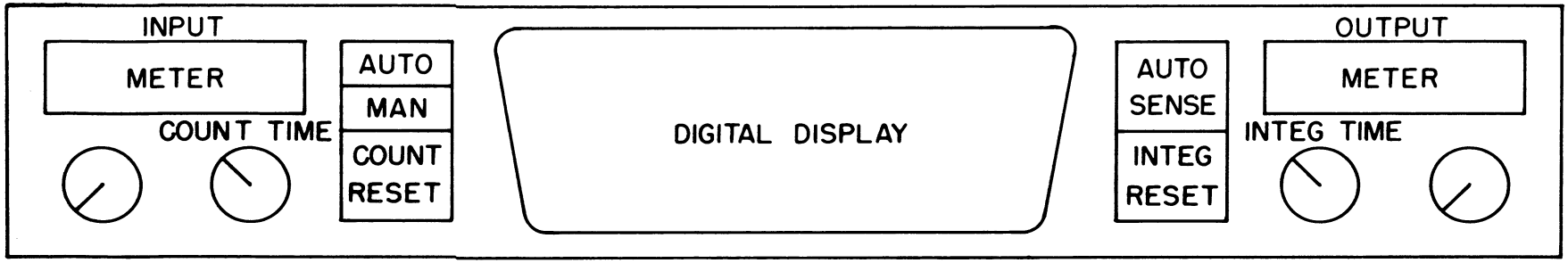

CONTROL UNIT-FRONT

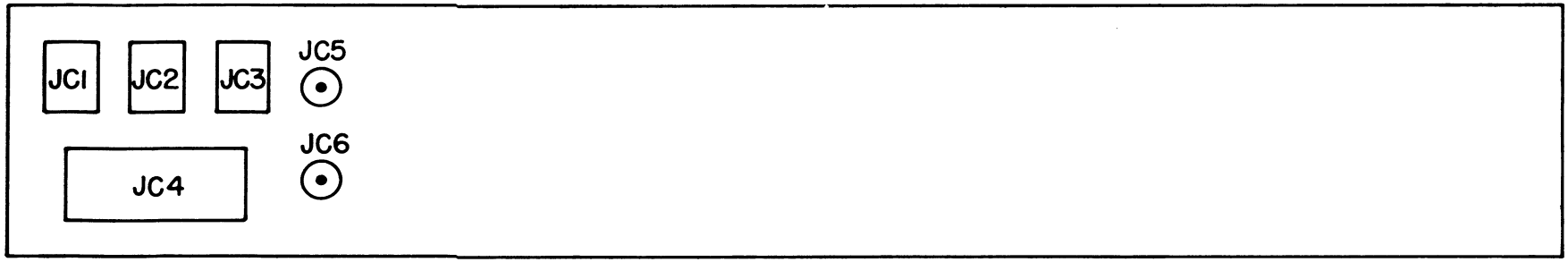

CONTROL UNIT-REAR

Fig. 29 Control Unit Control and Connector Placement

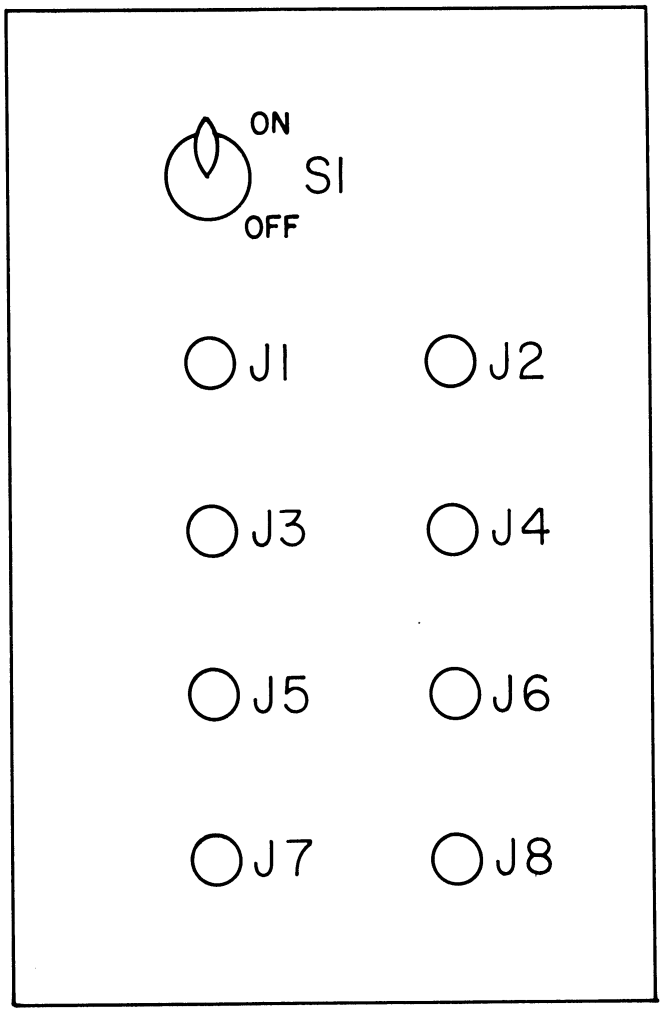

S1, J1, J2 } NOT USED

J3 - 72 kc AUTO SENSE
J4 - COMB FILTER OUTPUT
J5 - EW OUTPUT CHOPPER
J6 - NS OUTPUT CHOPPER
J7 - REGULATED +6 VDC
J8 - REGULATED -12 VDC

Fig. 30 Analog Case Test Panel

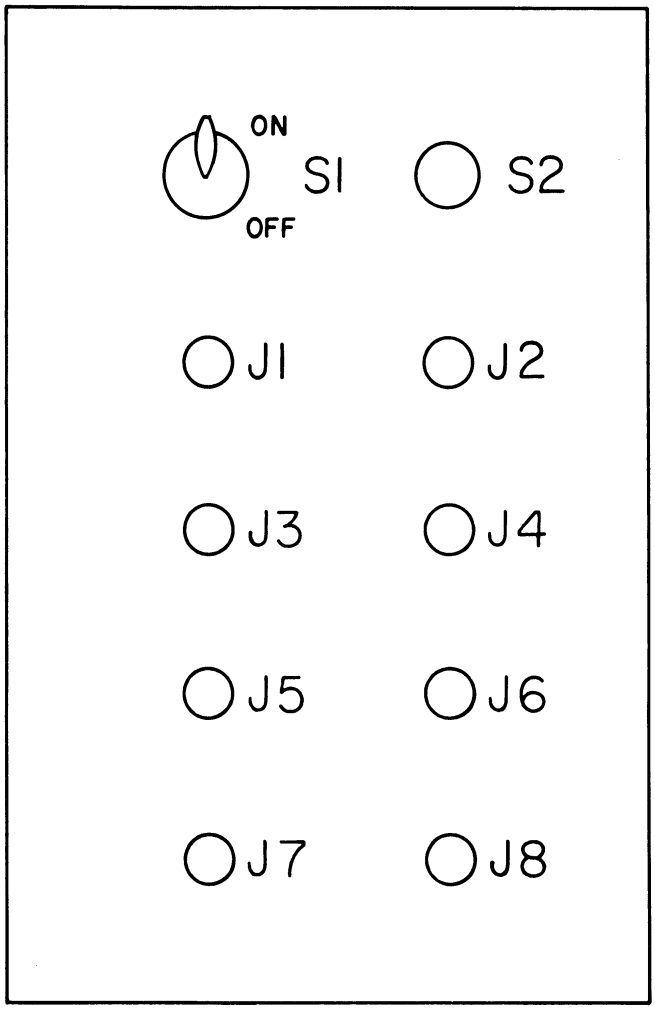

S1 { ON - TEST
OFF - NORMAL

S2 PUSH TO CLEAR

J1 - N-S SYNC
J2 - .5° CLCK
J3 - E-W SYNC
J4 - COUNT TIME
J5 - 2° CLCK SYNC
J6 - DELAY M.V. DISABLE
J7 - STOP PULSE
J8 - TEST PATCH

NOTE -
FOR TEST J8 IS PATCHED TO
J1 (0° OR 360°) OR J3 (90°)

Fig. 31 Digital Case Test Panel

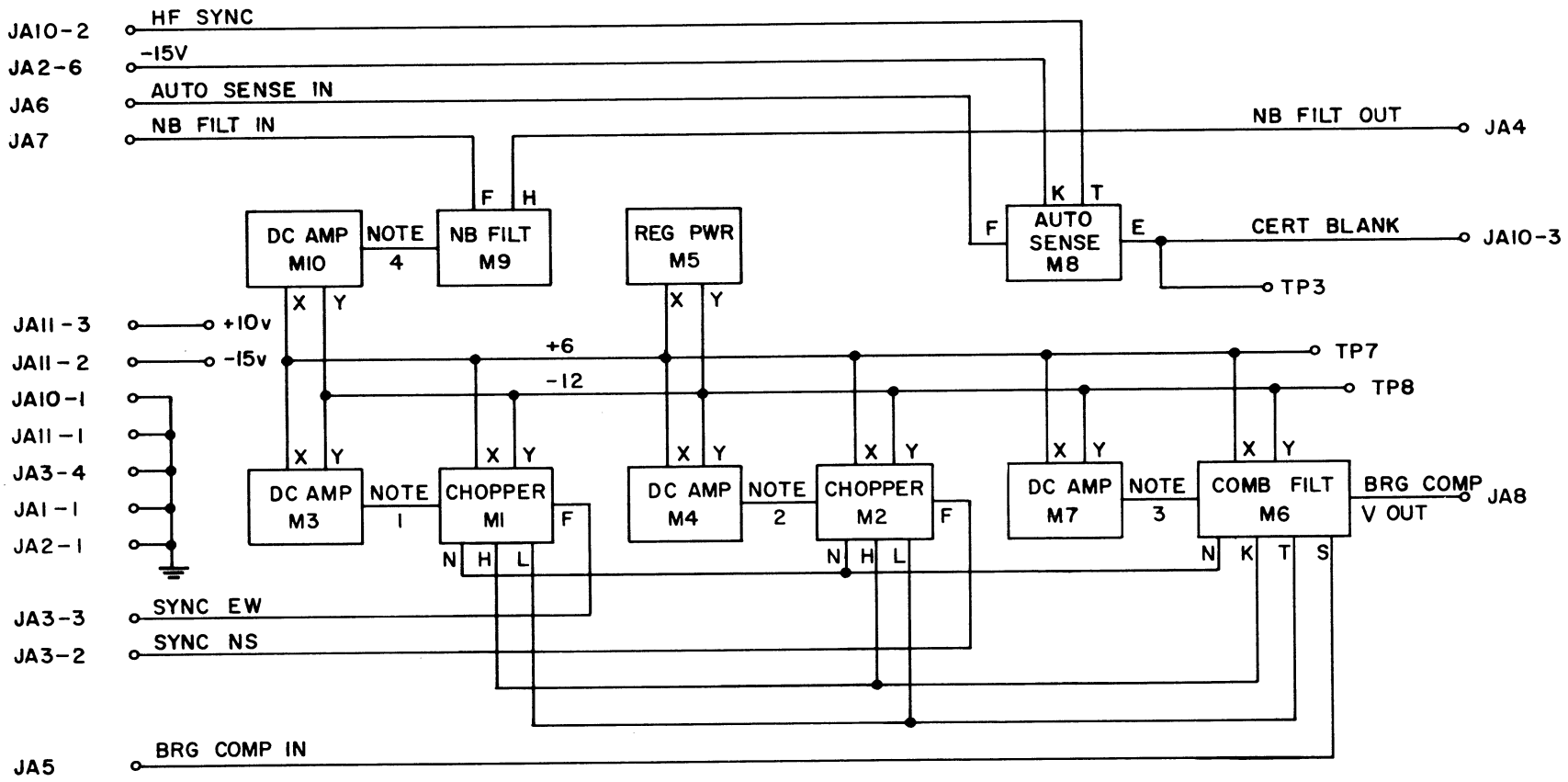

NOTE 1. SEE DETAIL A
NOTE 2. SEE DETAIL B
NOTE 3. SEE DETAIL C
NOTE 4. SEE DETAIL D

Fig. 32 Analog Case Logic

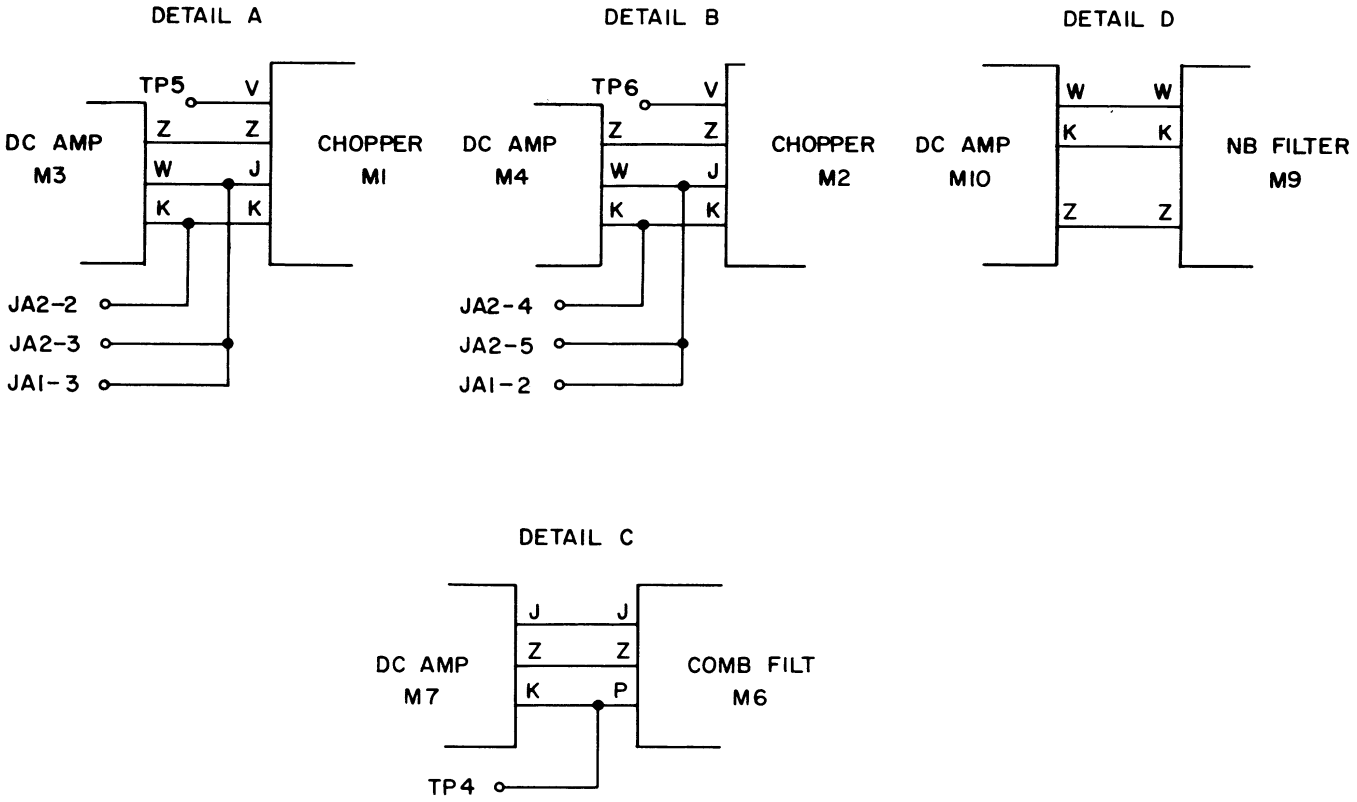

Fig 32 Analog Case Logic

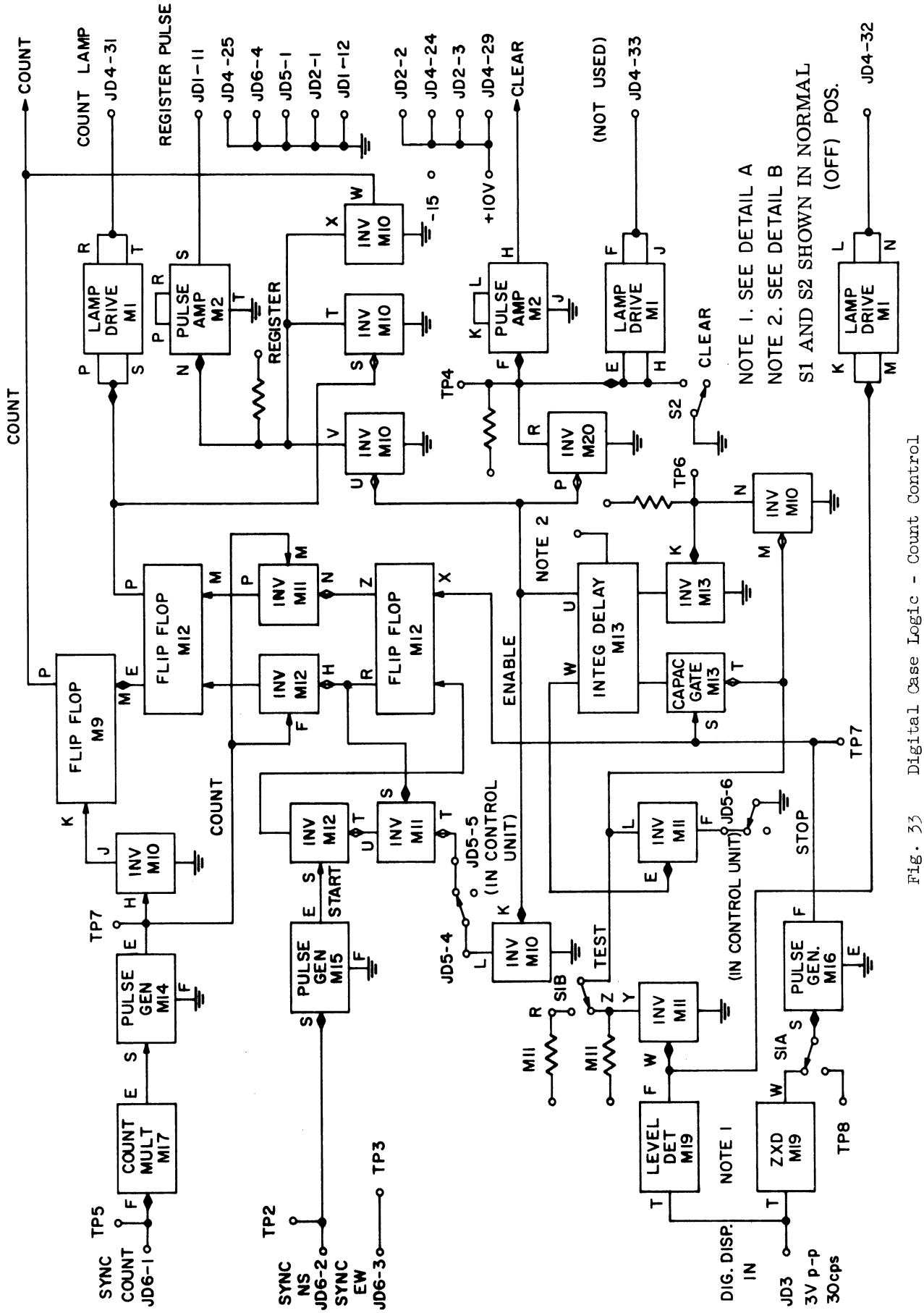

Fig. 33 Digital Case Logic - Count Control

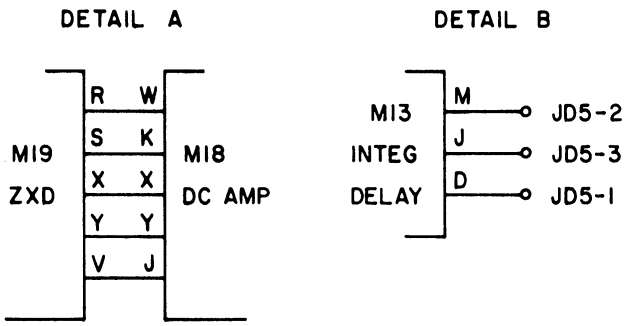

Fig. 33 Digital Case Logic - Count Control

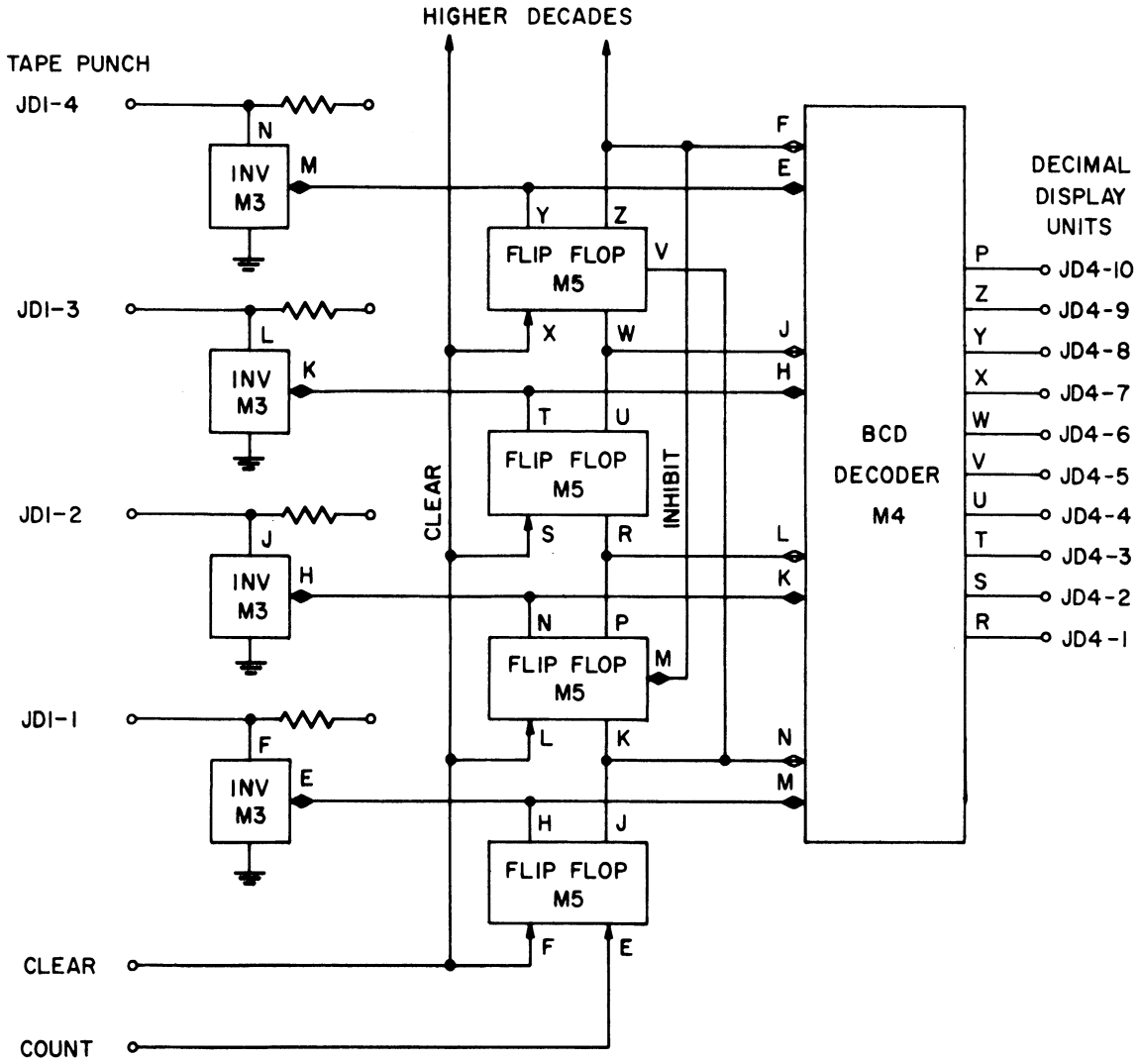

Fig. 34 Digital Case Logic - BCD Counter

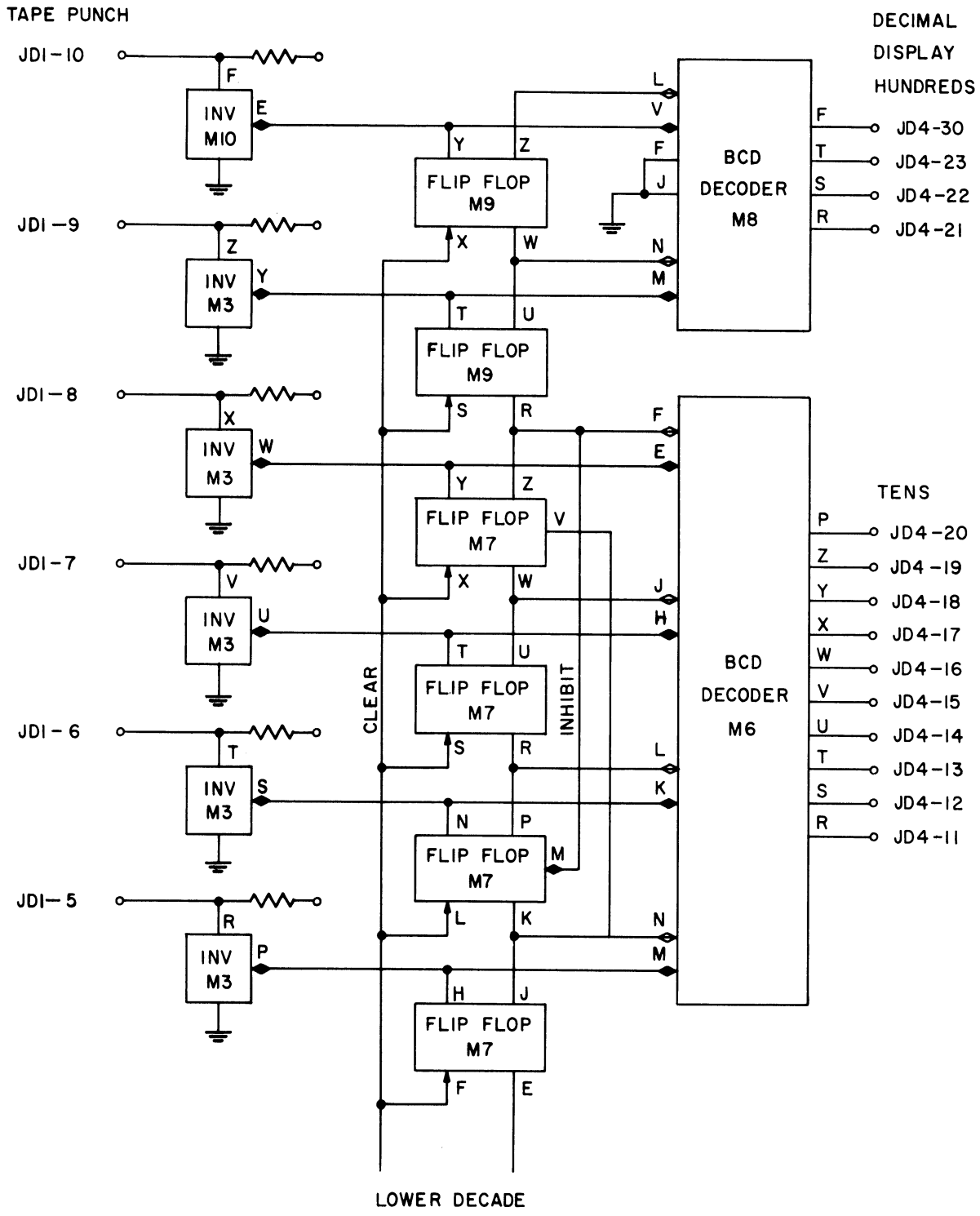

Fig. 34 Digital Case Logic - BCD Counter

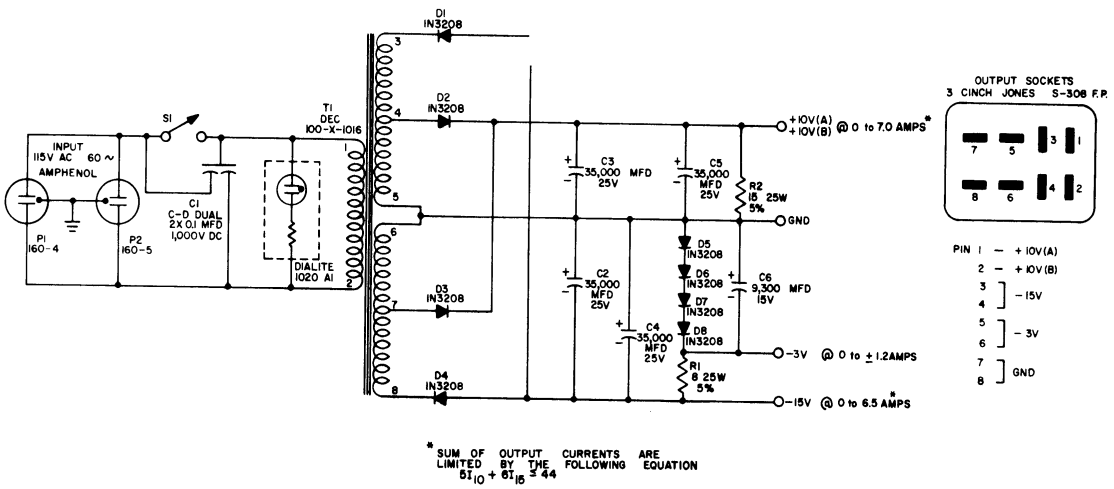

UNLESS OTHERWISE INDICATED
RESISTORS ARE 1/2W, 10%
CAPACITORS ARE MMFD

Fig. 35 POWER SUPPLY DEC722

RS-1671-3

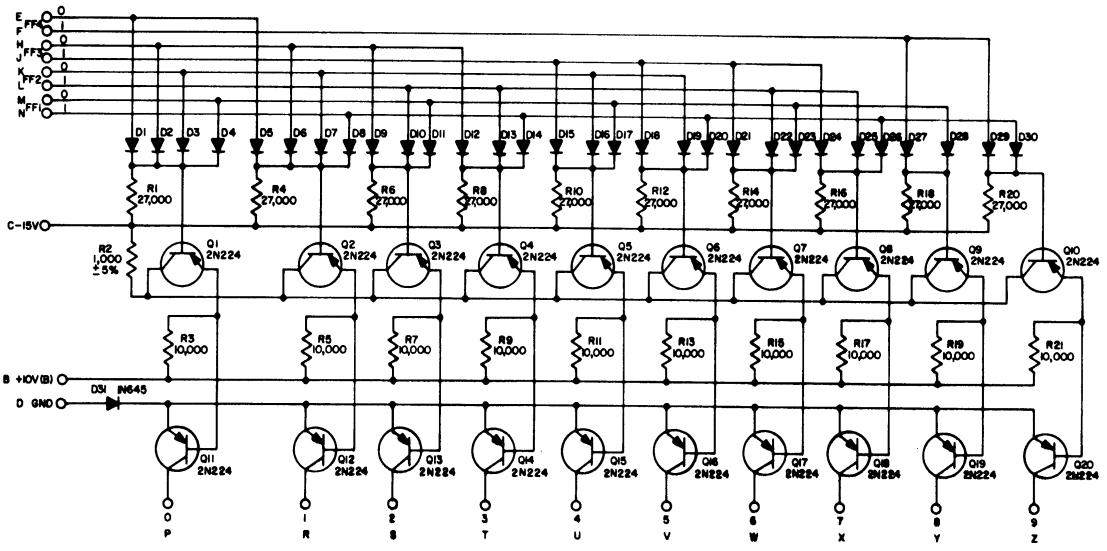

UNLESS OTHERWISE INDICATED
RESISTORS ARE 1/2W, 10%
DIODES ARE IN276

Fig. 36 B.C.D. LIGHT DRIVER DEC1671
(Digital Modules M4, M6, MB)

RS-4102

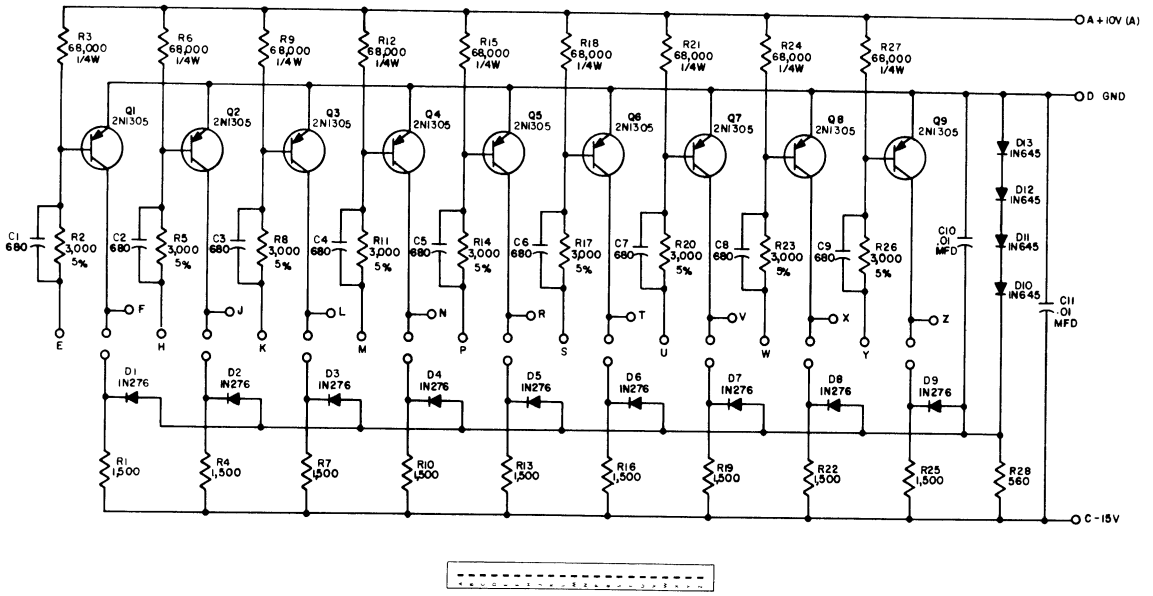

UNLESS OTHERWISE INDICATED
RESISTORS ARE 1/2 W 10%
CAPACITORS ARE MMFD

Fig. 37 INVERTER DEC4102
(Digital Modules M3, M10)

RS-4105-5

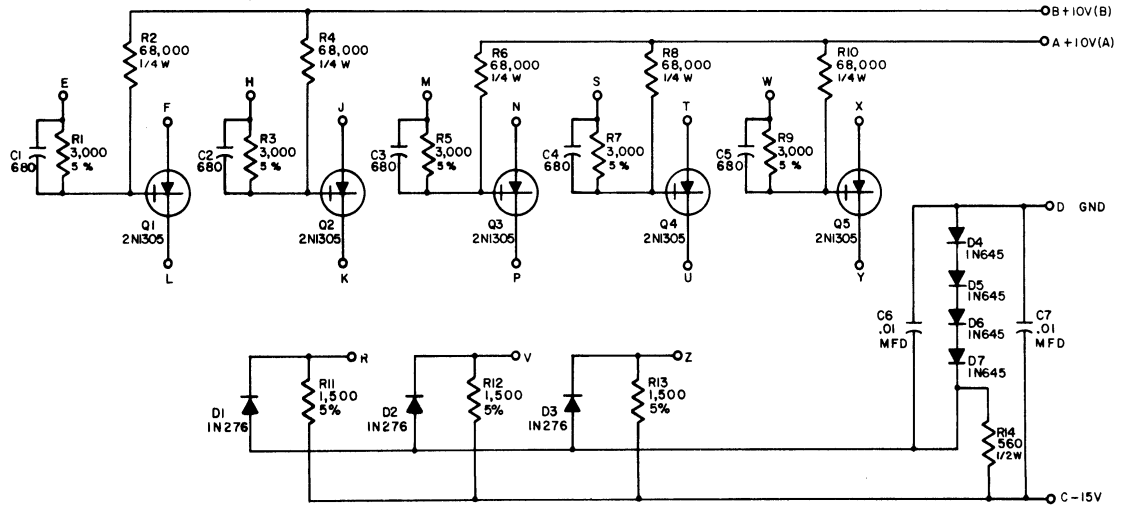

UNLESS OTHERWISE INDICATED:
RESISTORS ARE 1/4 W, 10%
CAPACITORS ARE MMFD.

Fig. 38 INVERTER DEC4105
(Digital Module M11)

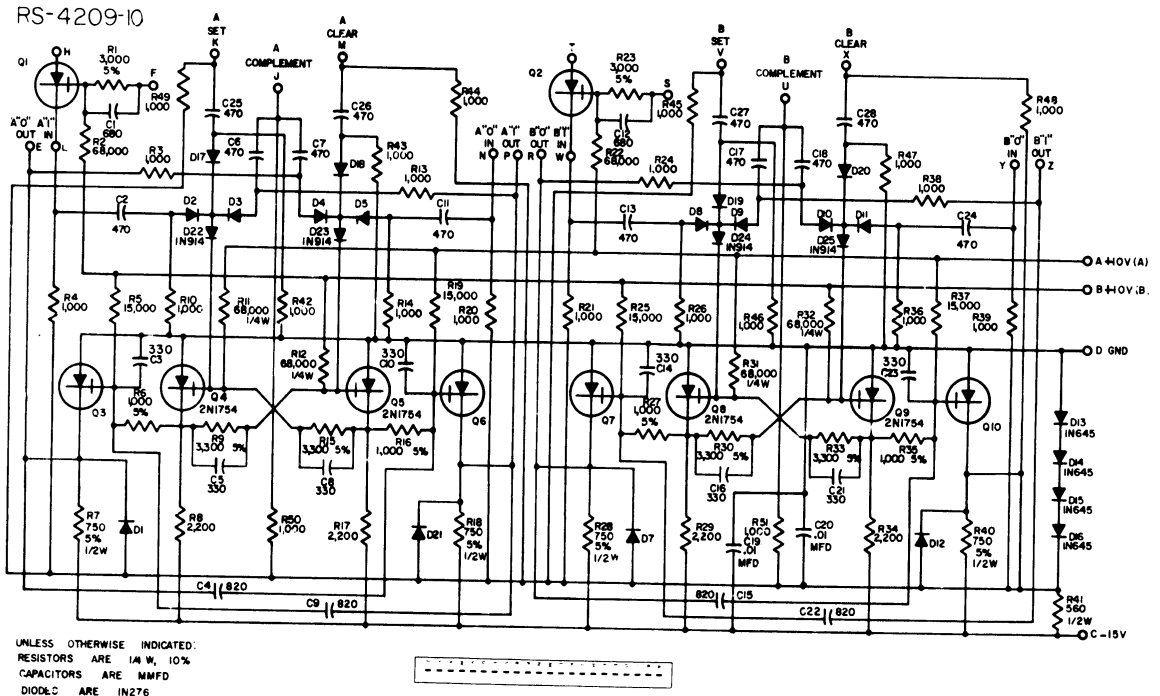

Fig. 39 DUAL FLIP-FLOP DEC4209
(Digital Module #M12)

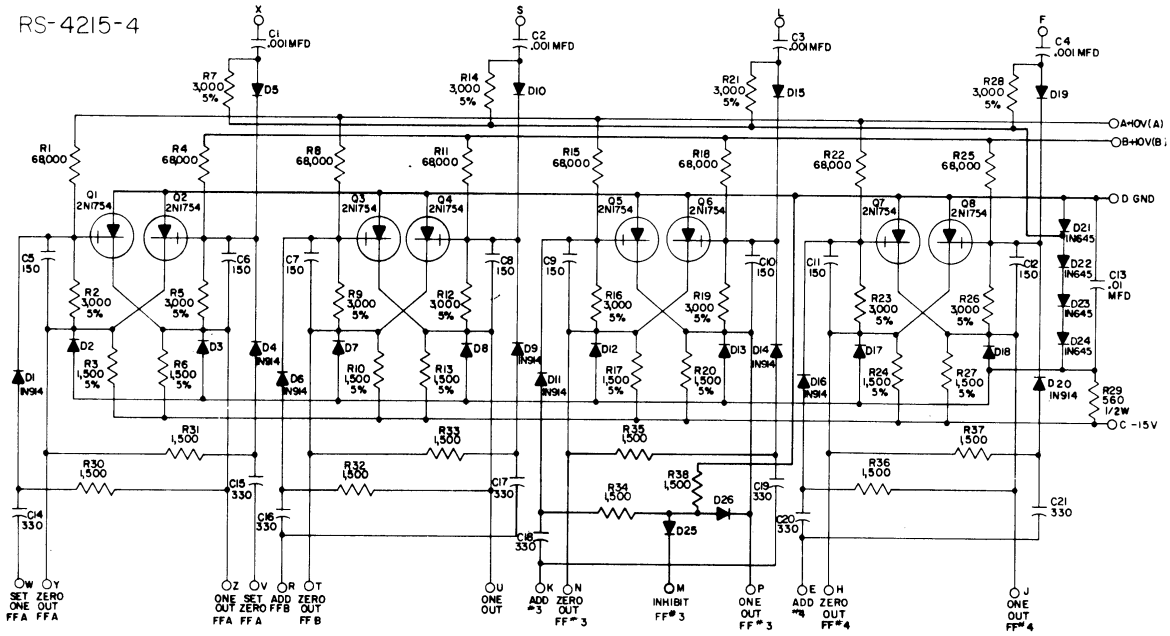

Fig. 40 4-BIT COUNTER DEC4215
(Digital Modules M5, M7, M9)

RS-4303-4

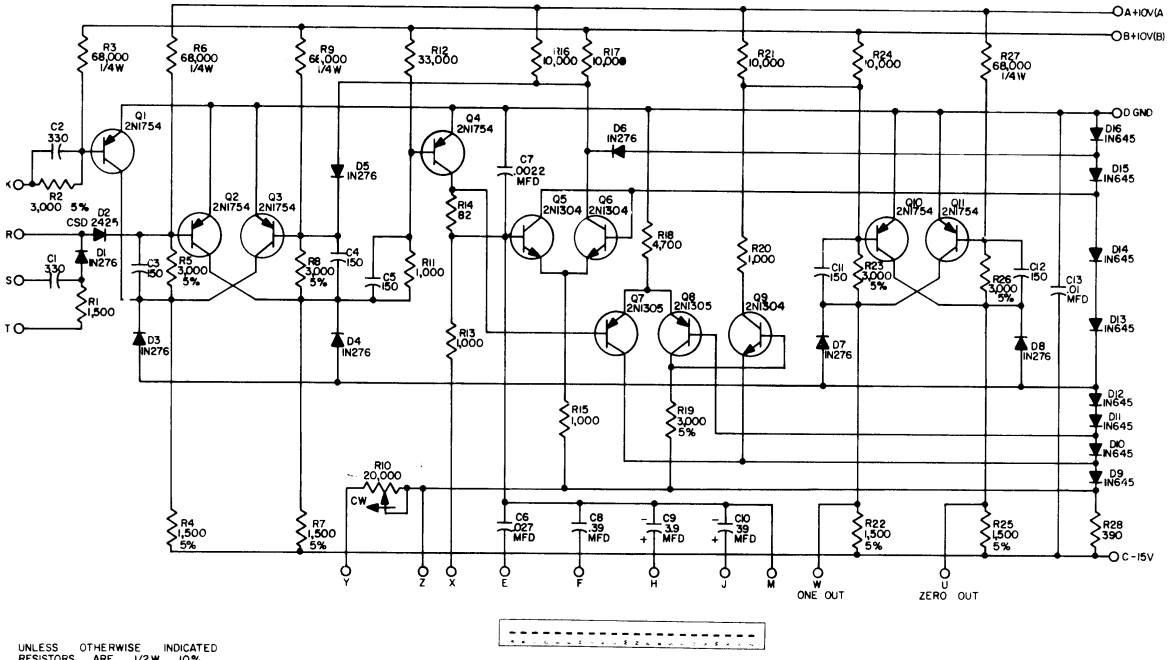

UNLESS OTHERWISE INDICATED
RESISTORS ARE 1/2W, 10%
CAPACITORS ARE MMFD

Fig. 41 INTEGRATING ONE-SHOT DEC4303
(Digital Module M13)

S-4410-11

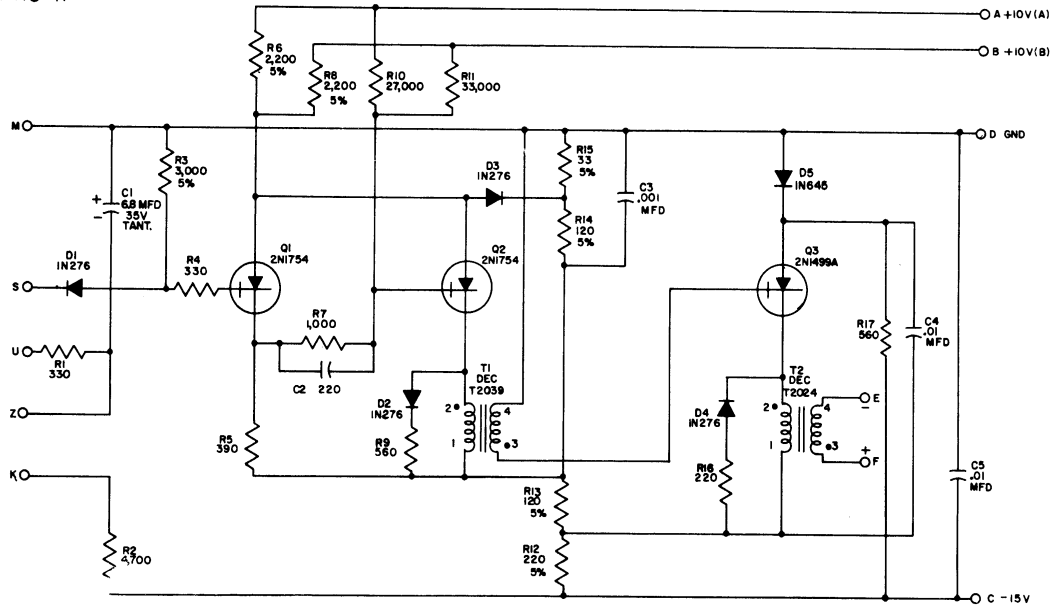

UNLESS OTHERWISE INDICATED
RESISTORS ARE 1/2W, 1%
CAPACITORS ARE MMFD

Fig. 42 PULSE GENERATOR DEC4410
(Digital Modules M14, M15, M16)

RS-4604-4

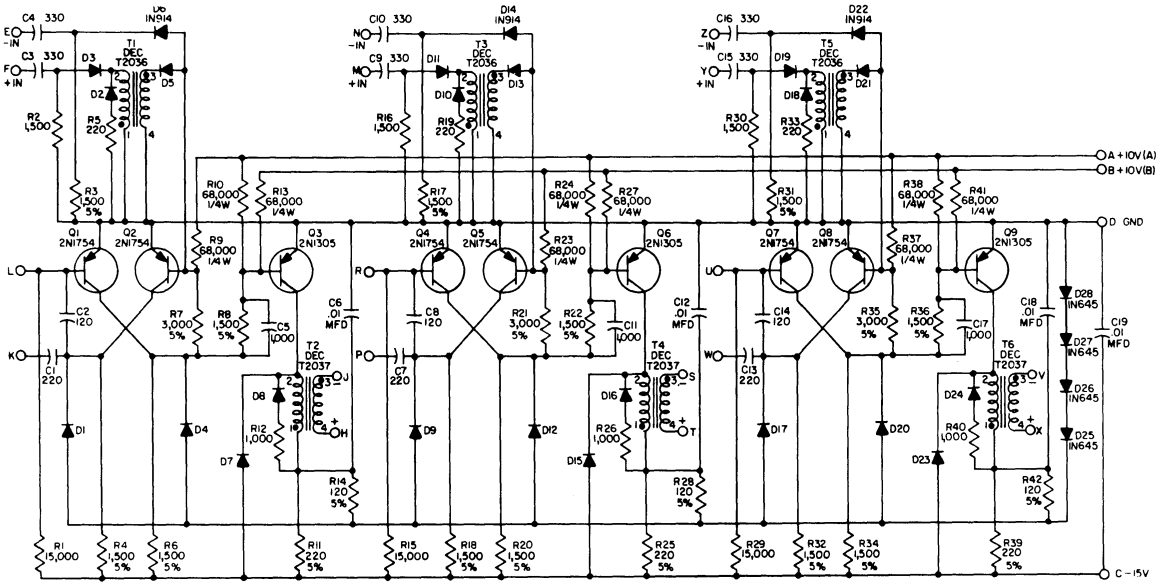

UNLESS OTHERWISE INDICATED
RESISTOR ARE 1/2W, 10%
CAPACITORS ARE MMFD
DIODES ARE IN276

Fig. 43 Pulse Amplifier Module - DEC4604
(Digital Module M2)

RS-4689-1

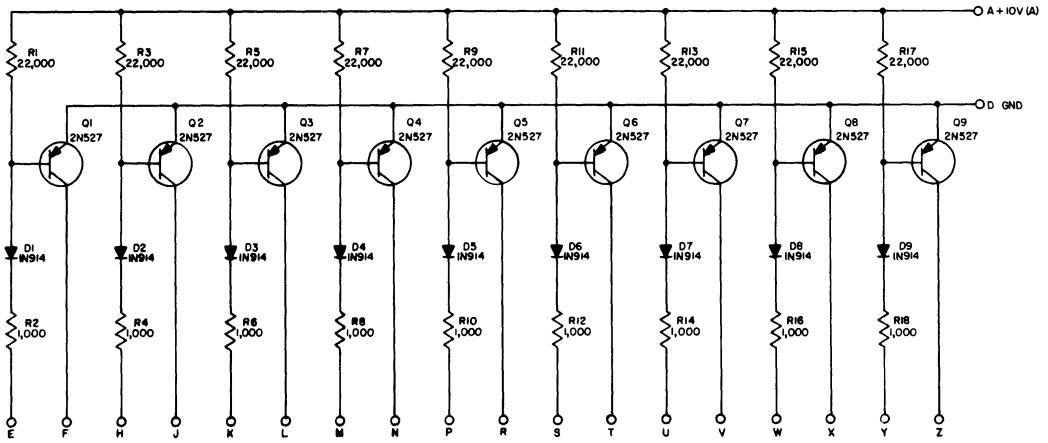

UNLESS OTHERWISE INDICATED
RESISTORS ARE 1/2W, 10%

Fig. 44 Indicator Driver Module - DEC4689
(Digital Module M1)

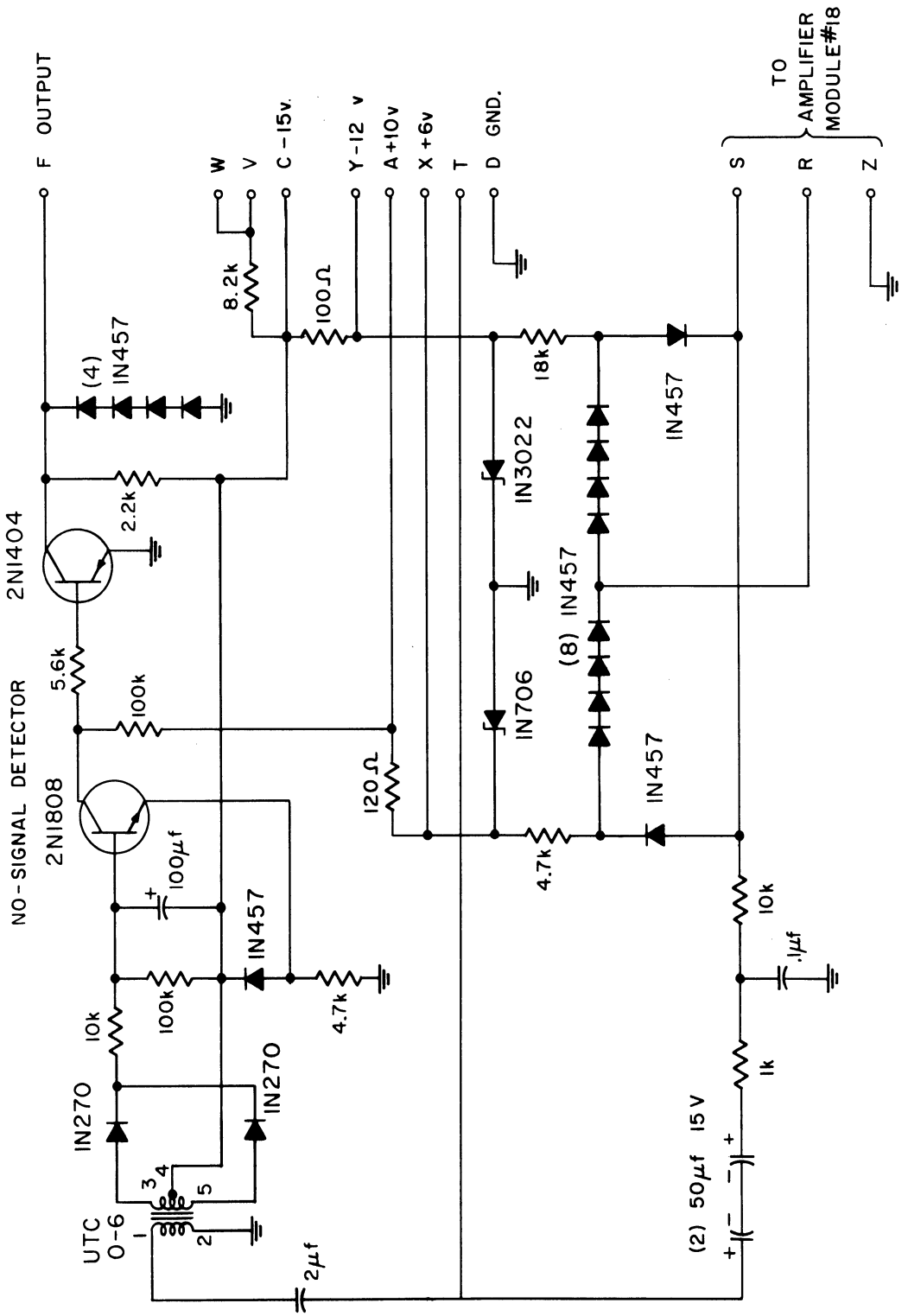

Fig. 45 Zero-Crossing Detector Module (Digital Module M19)

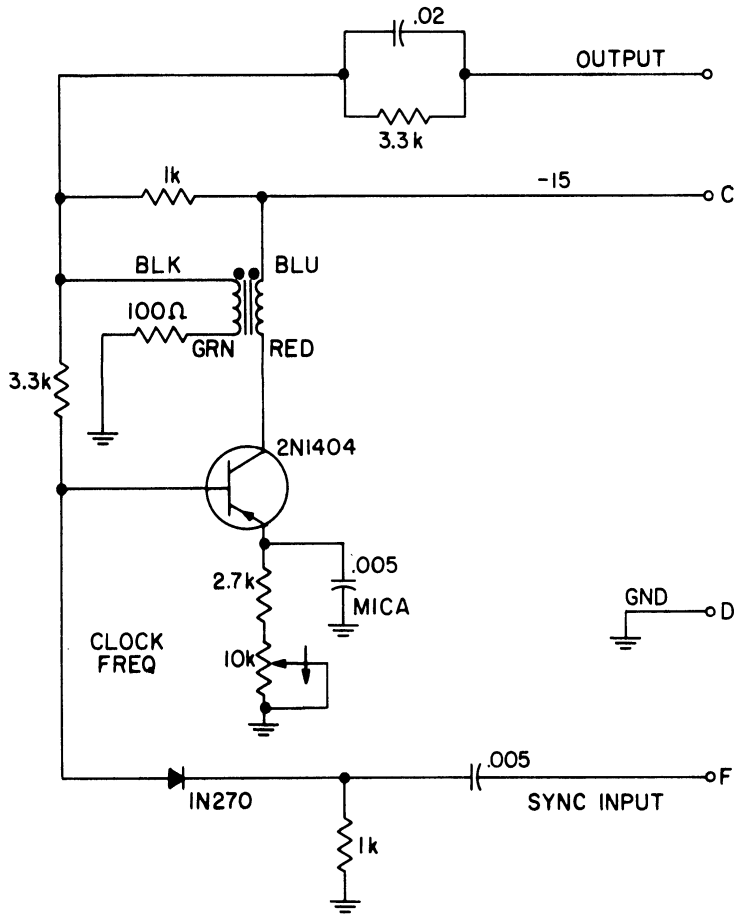

Fig. 46 Count Multiplier Module (Digital Module M17)

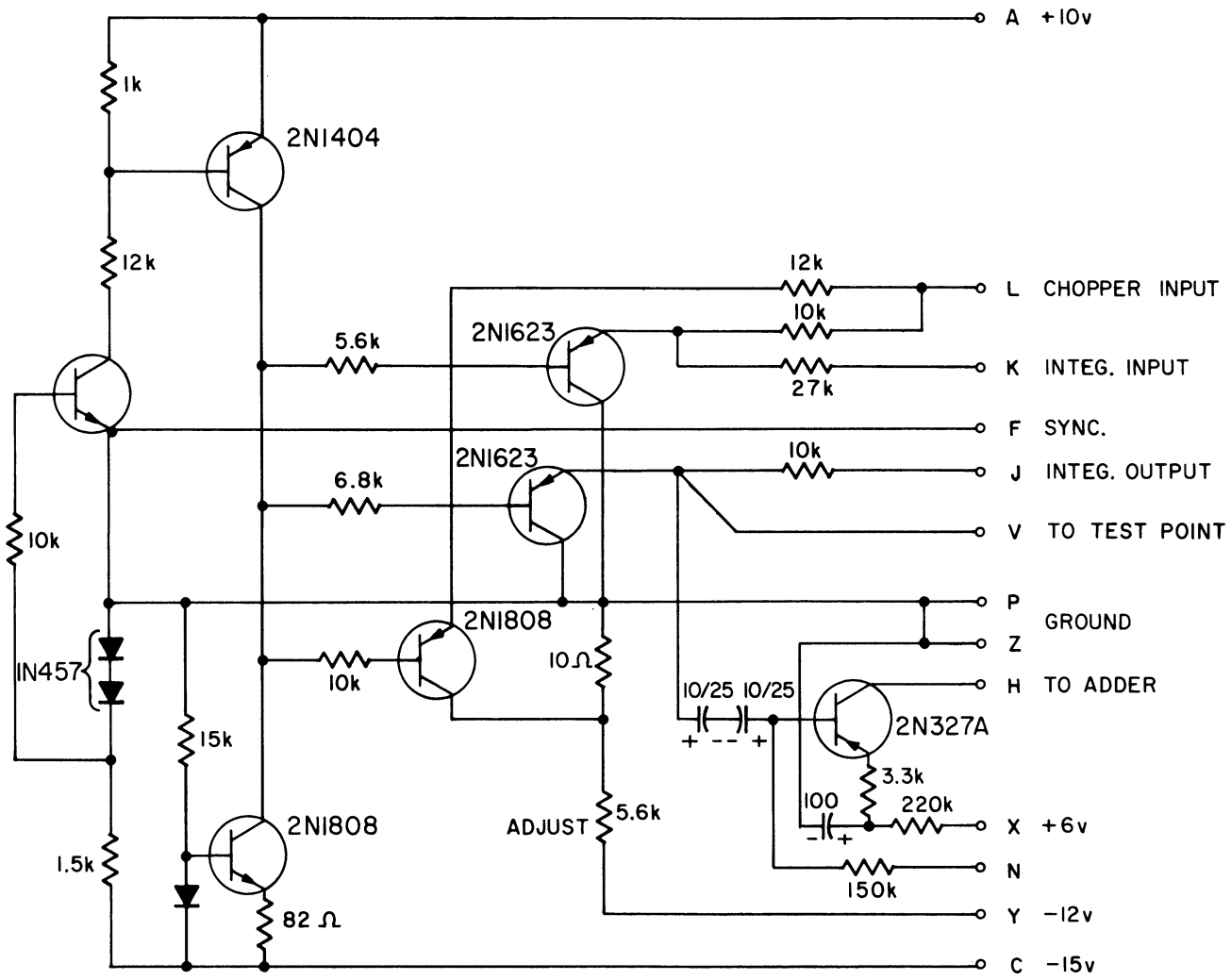

Fig. 47 Chopper Module (Analog Module M1, M2)

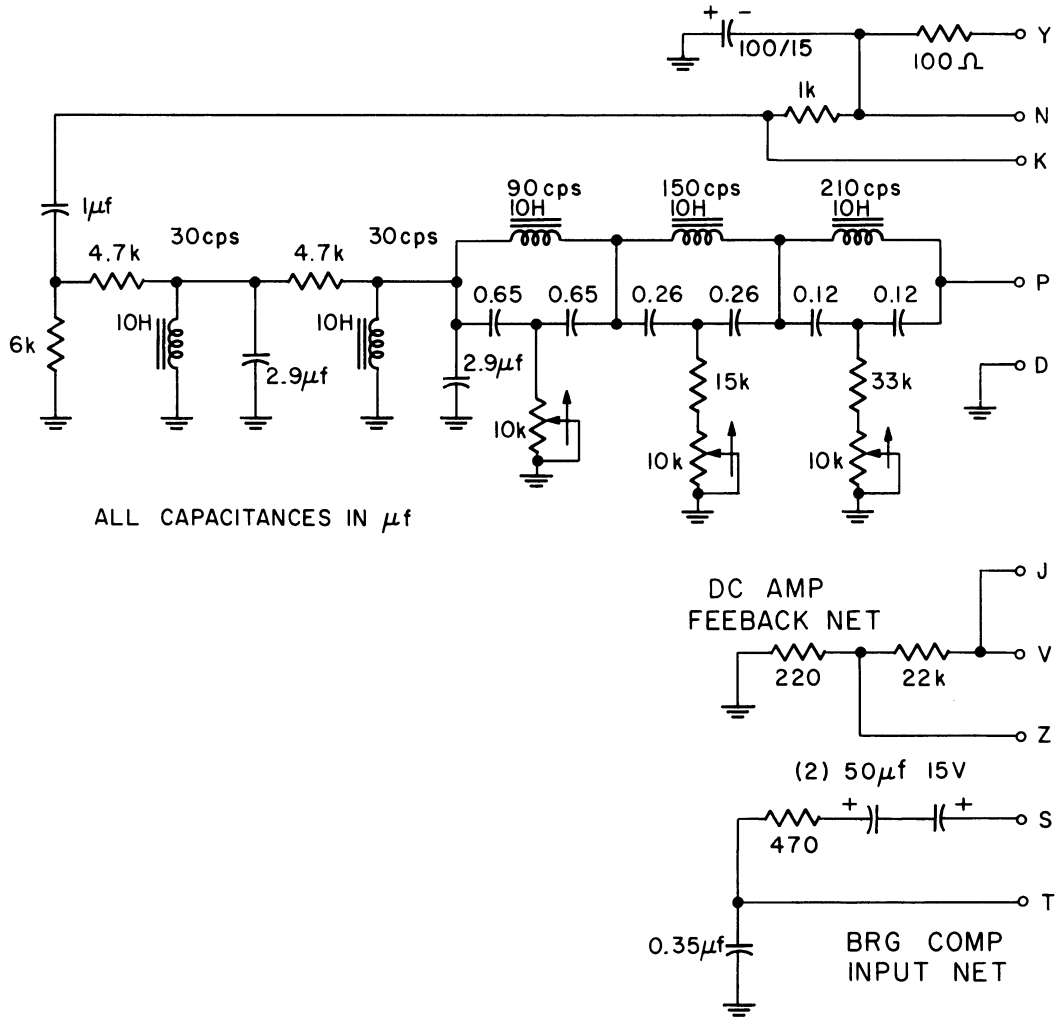

Fig. 48 Comb Filter Module (Analog Module M6)

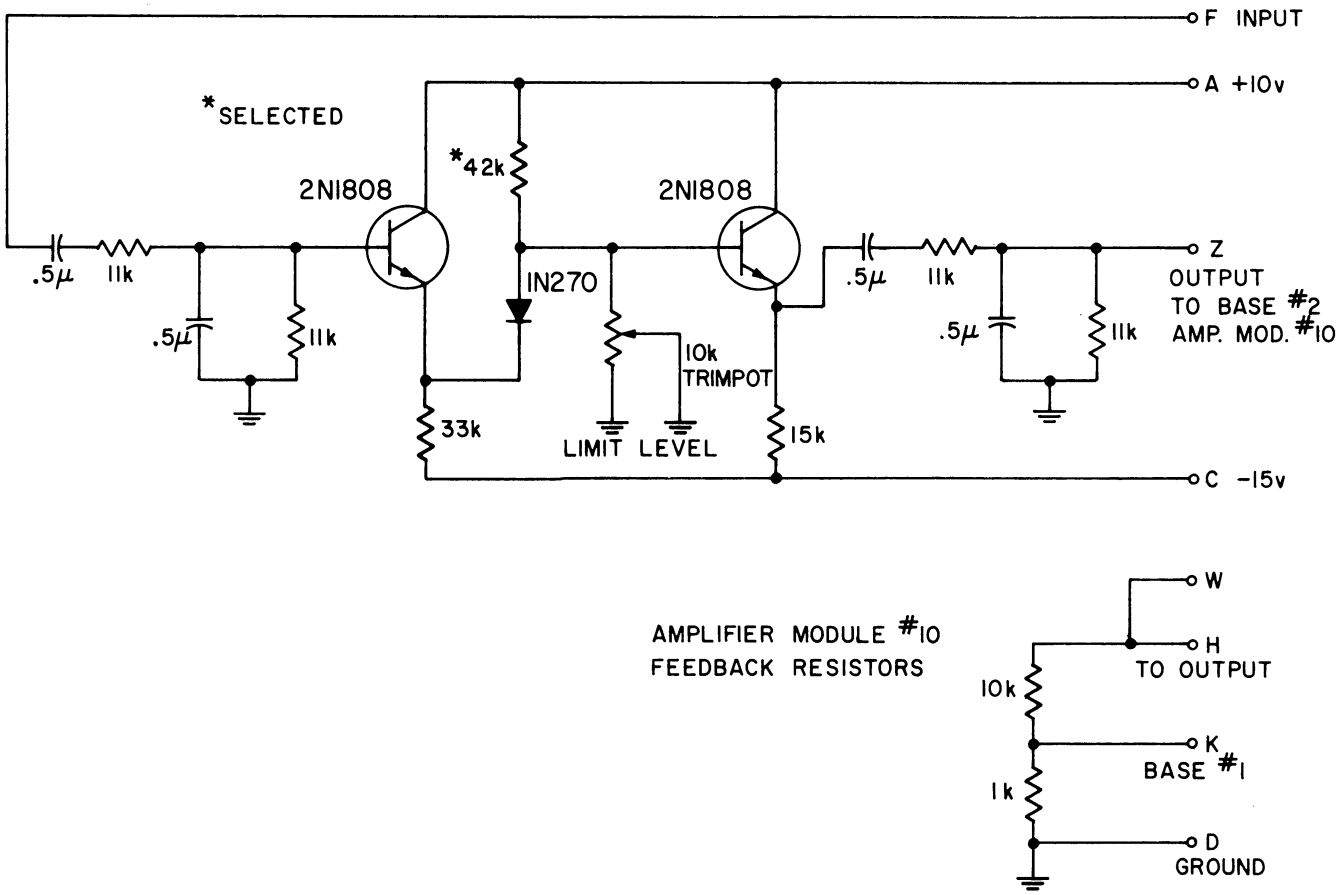

Fig. 49 Narrowband Filter Module (Analog Module M9)

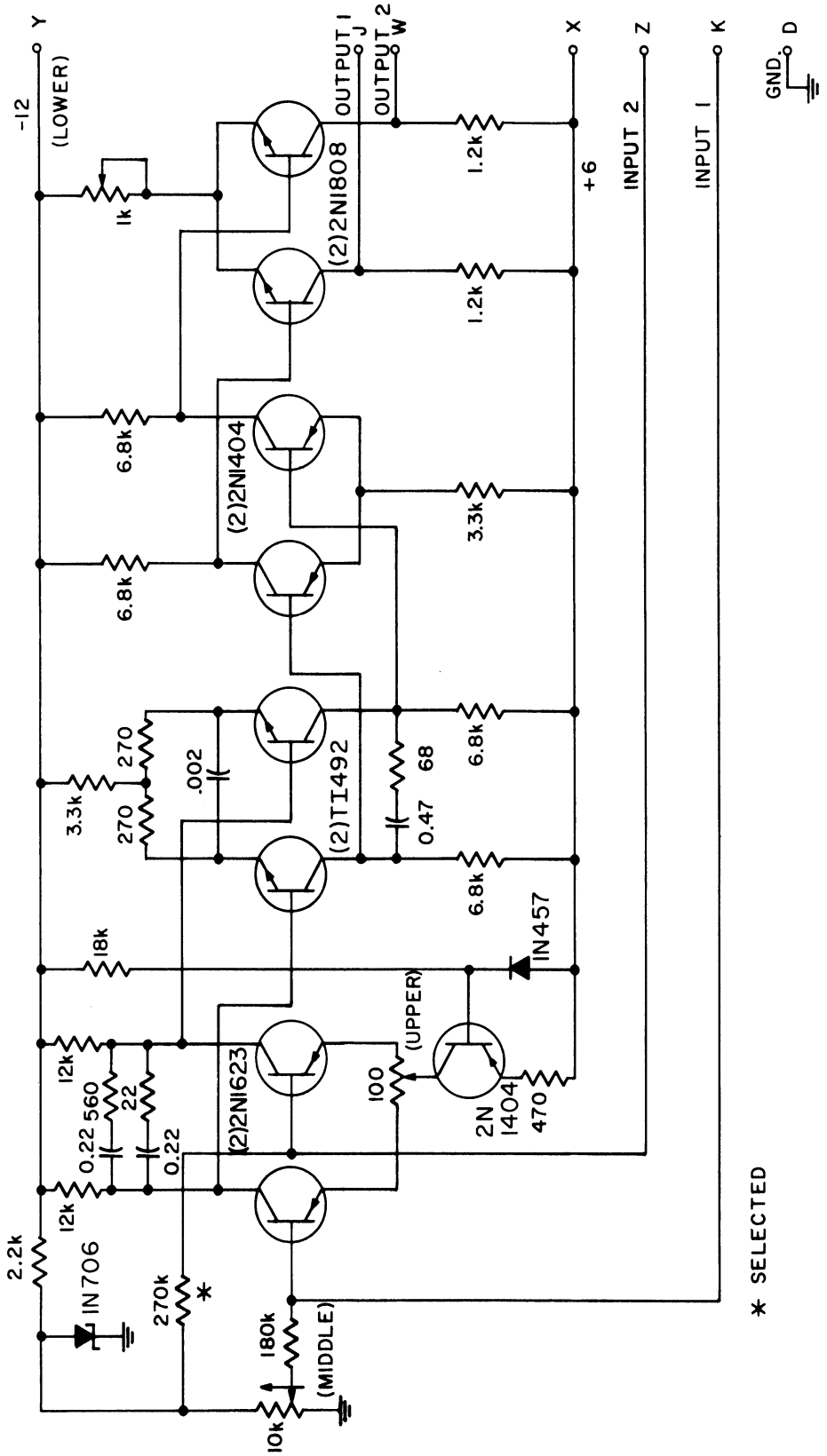

Fig. 50 DC Amplifier Module (Analog Modules M3, M4, M7, M10; Digital Module M18)

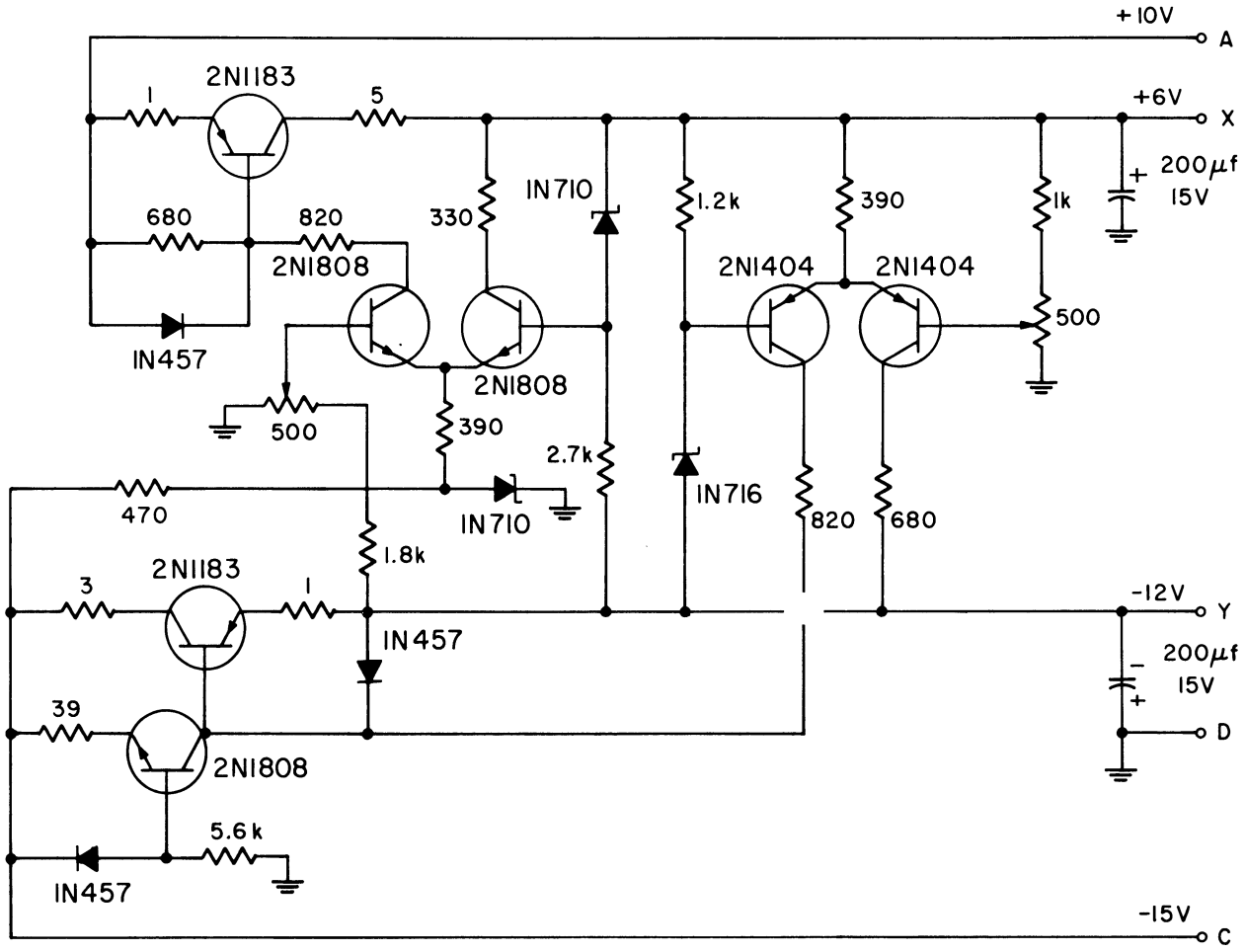

Fig. 51 Regulated Power Supply Module (Analog Module M5)

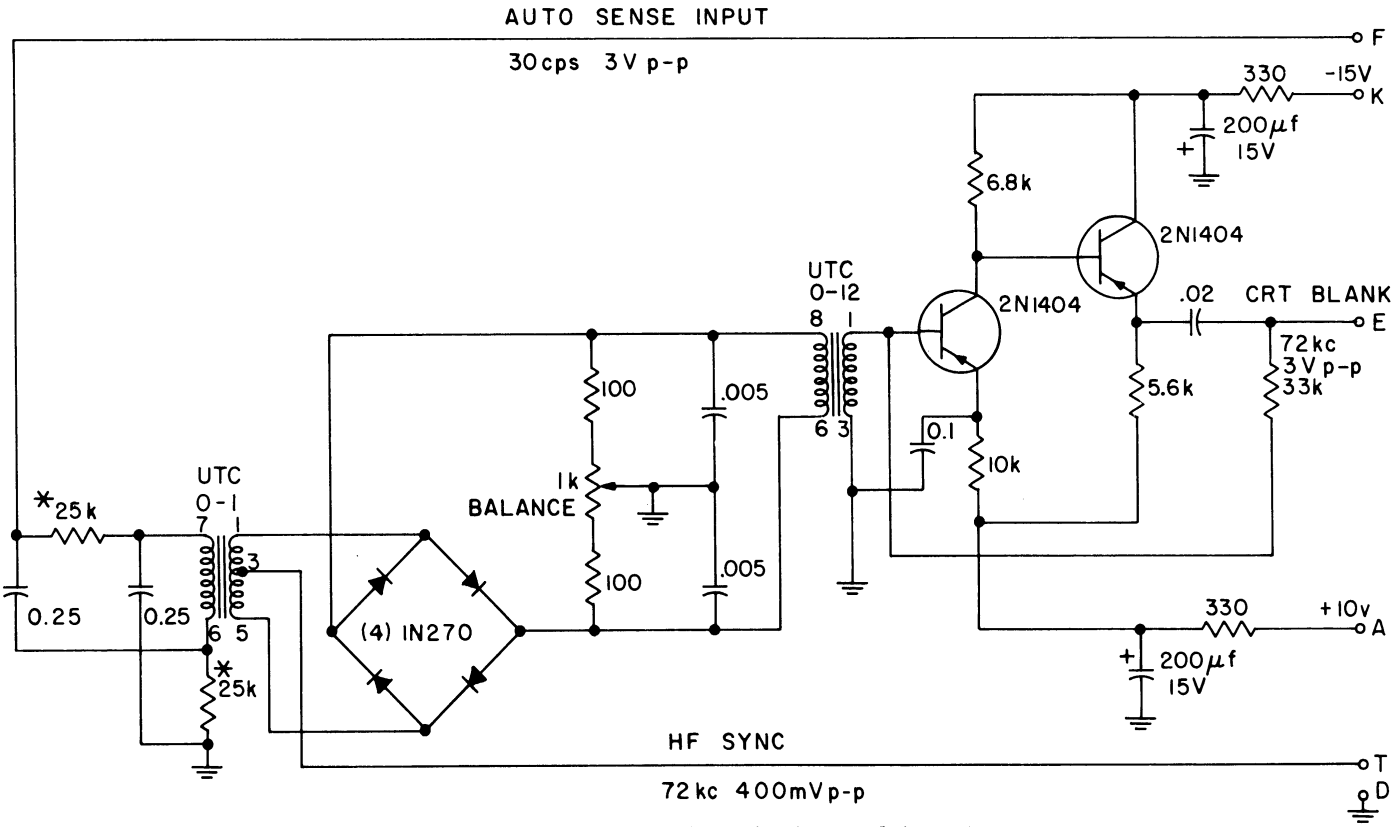

Fig. 52 Auto-Sense Module (Analog Module M8)

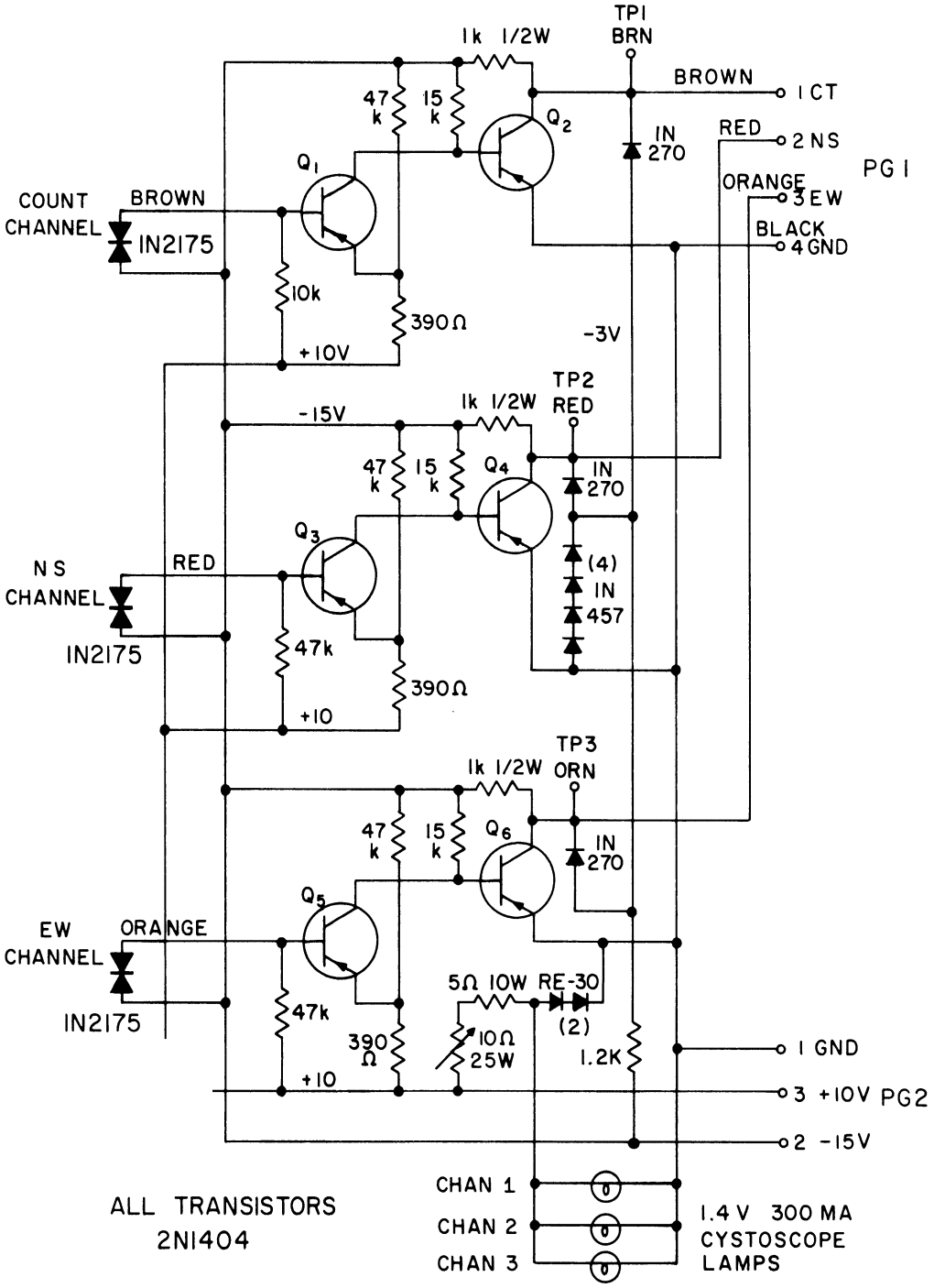

Fig. 53 Synchronizing Generator

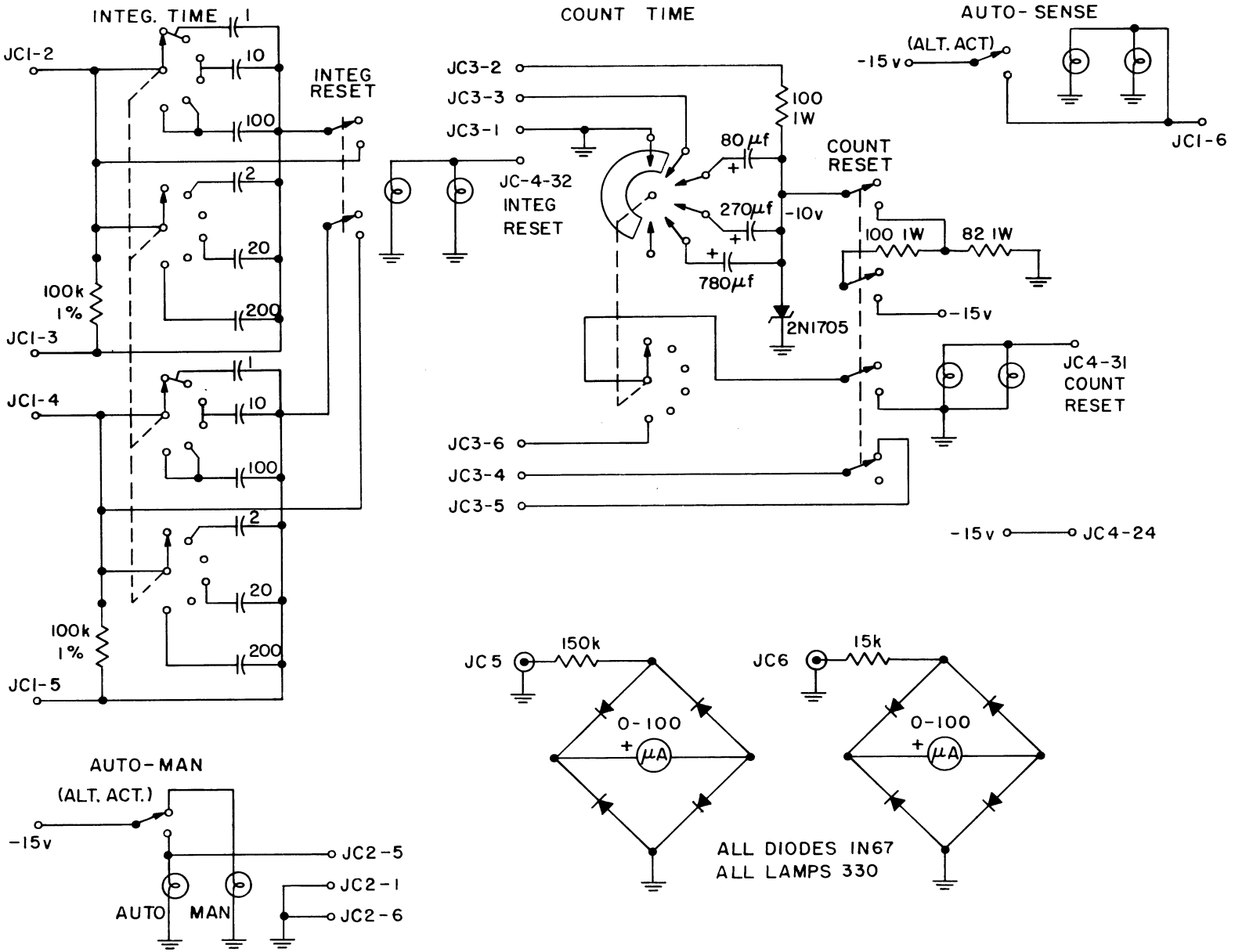

Fig. 54 Control Unit

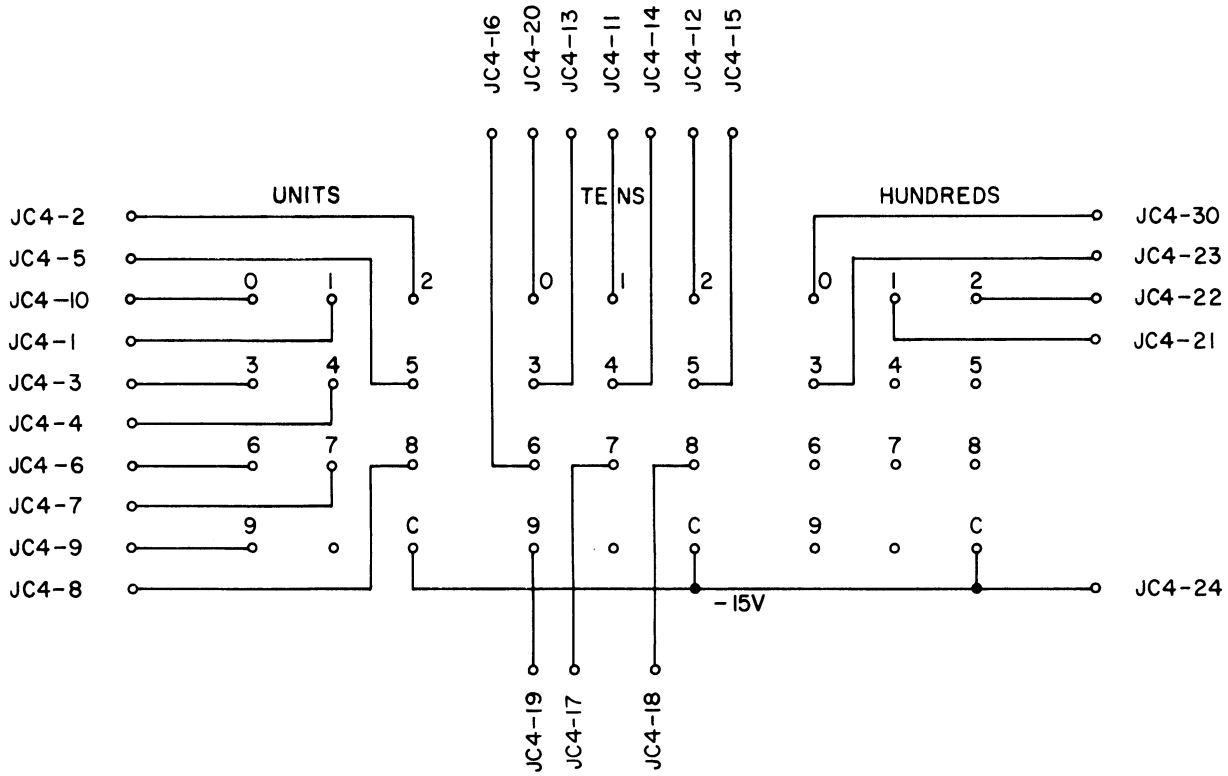

Fig. 55 Control Unit - Decimal Readout

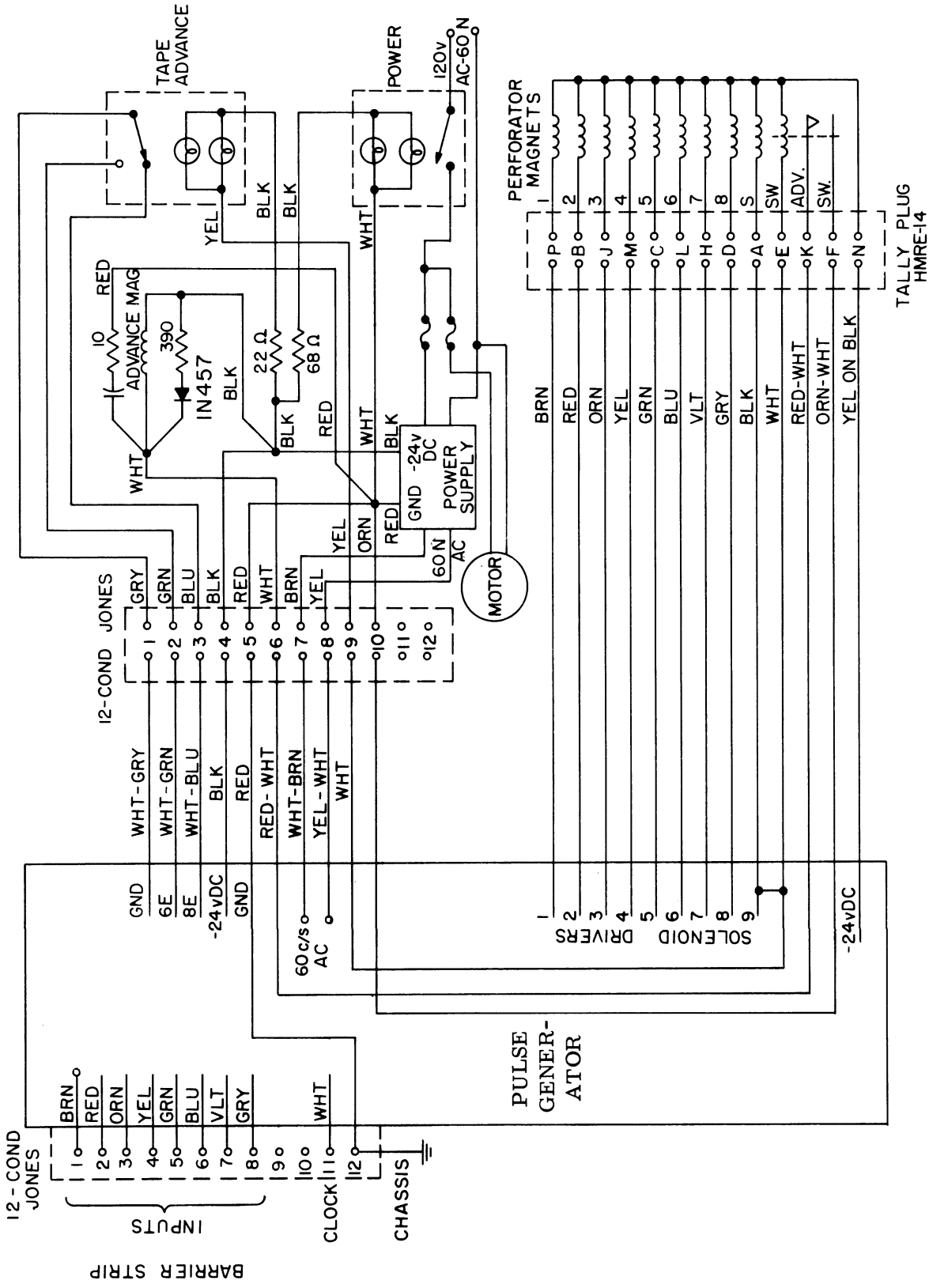

Fig. 56 Paper Tape Punch

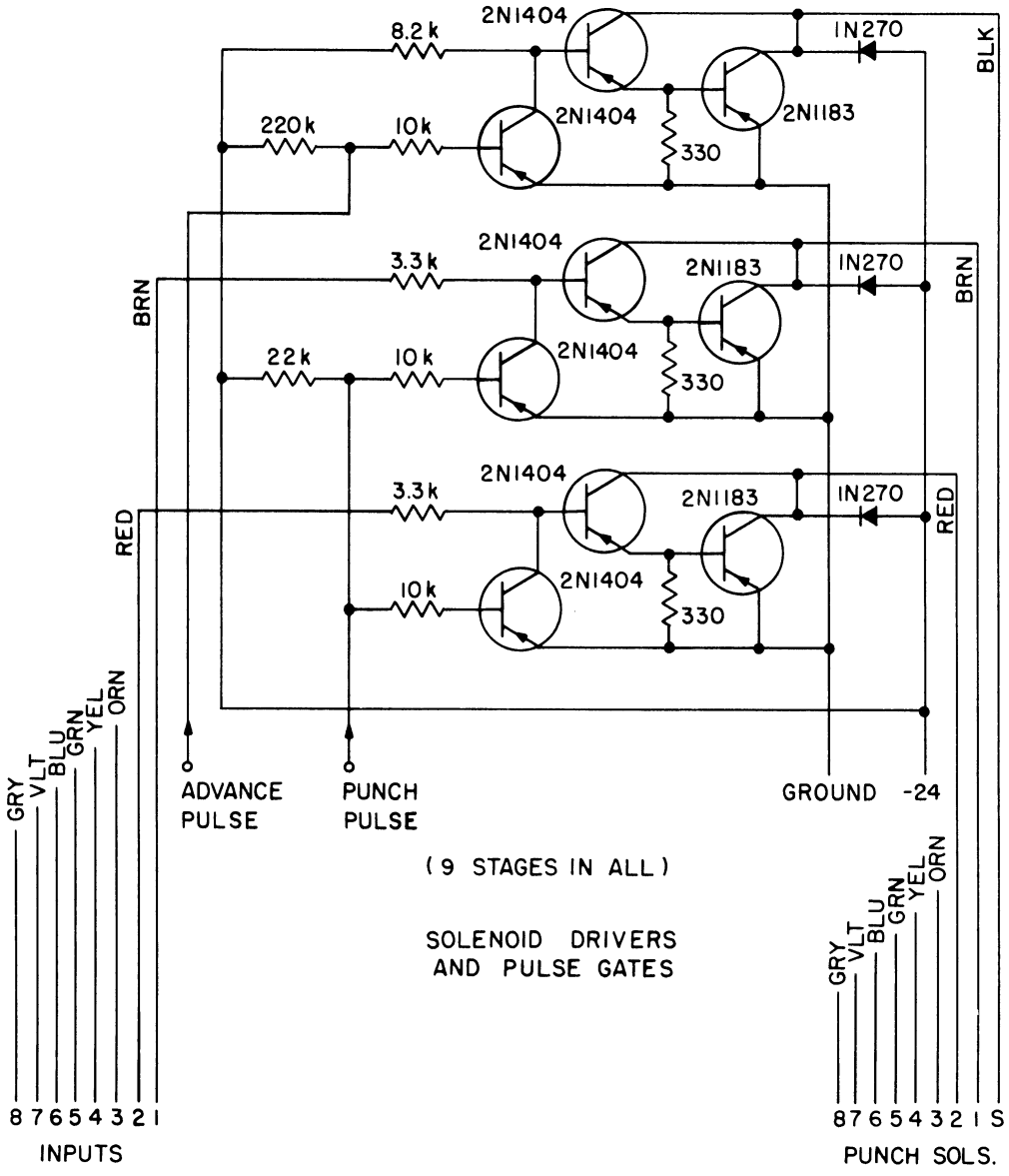

Fig. 57 Paper Tape Punch - Solenoid Drivers

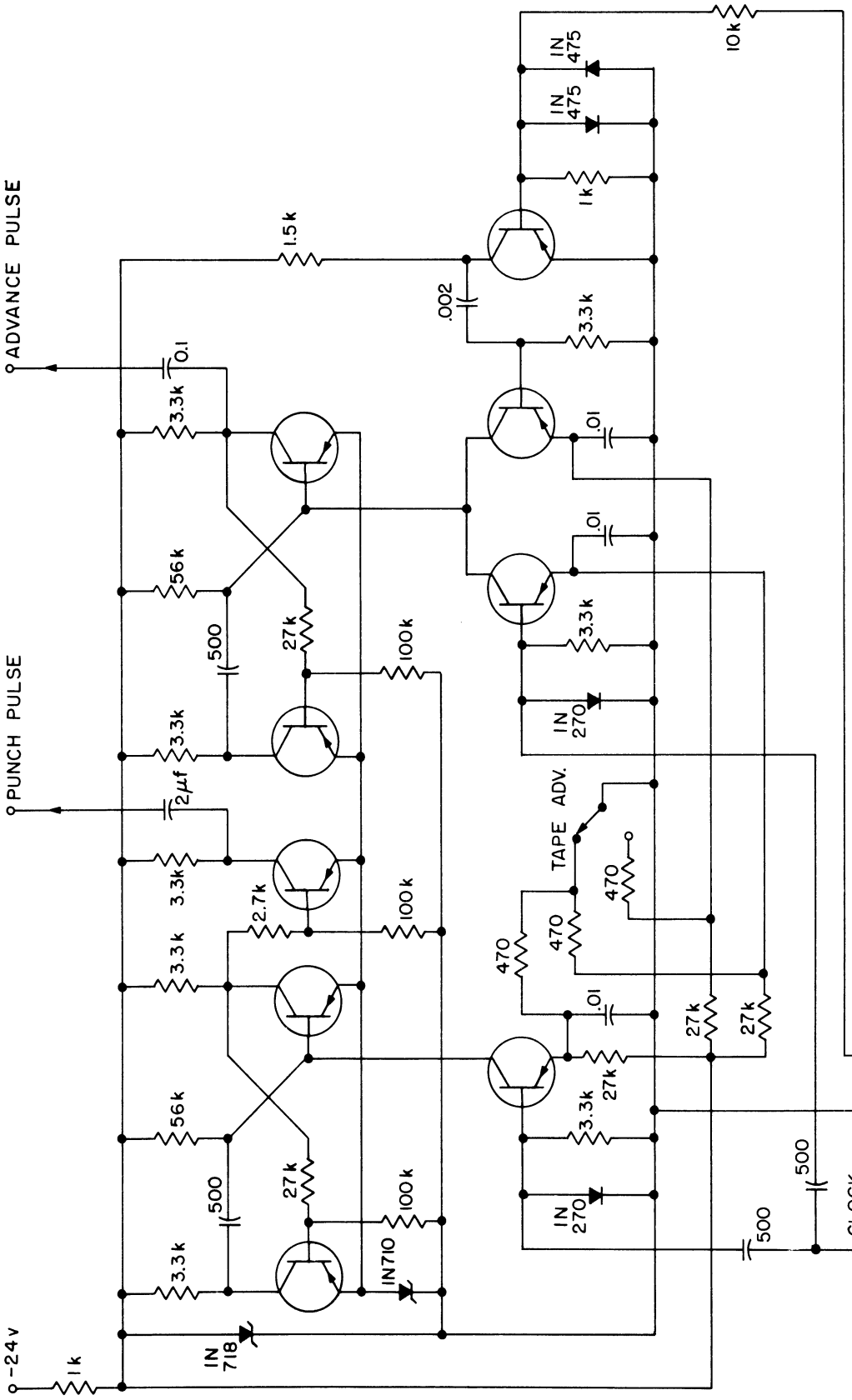

Fig. 58 Paper Tape Punch - Pulse Generators

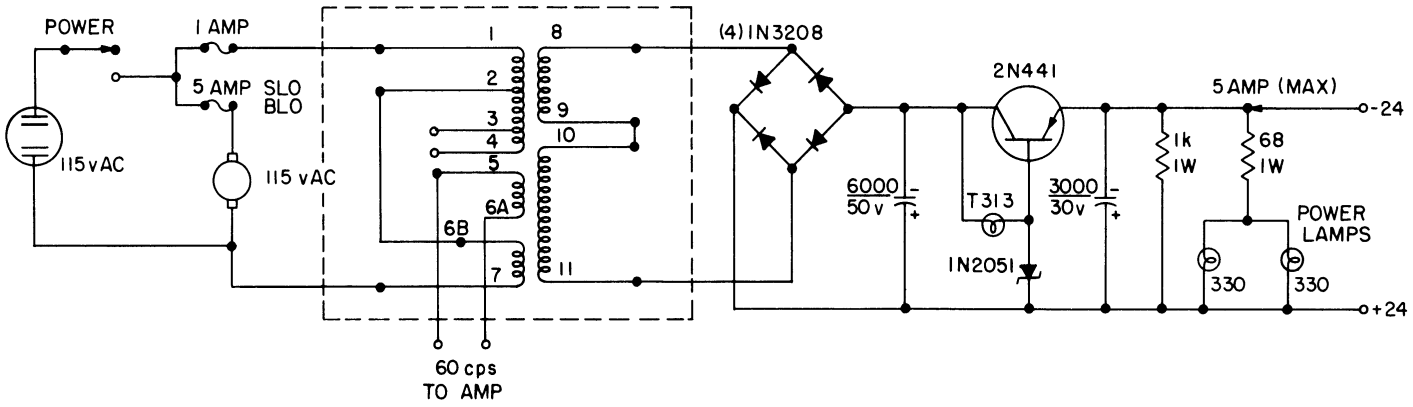

Fig. 59 Paper Tape Punch - Power Supply

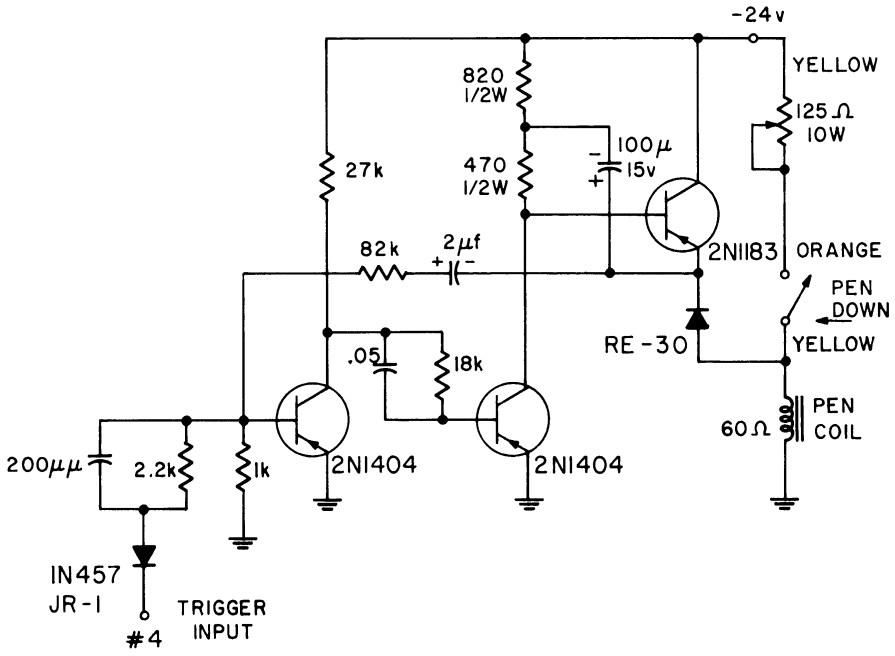

Fig. 60 X - Y Recorder Pen Pecker Amplifier

9. REFERENCES

1. E. M. Aupperle, T. W. Butler, Jr., and D. L. Mills, Remotely-Controlled Tactical Direction-Finding System, Cooley Electronics Laboratory Technical Report No. 124, The University of Michigan, Ann Arbor, 1961.

2. Busignies and M. Dishal, Some Relations Between Speed of Indication, Bandwidth and Signal-to-Random-Noise Ratio in Radio Navigation and Direction Finding, Proc. IRE, v. 37, pp. 473-488, 1949.

3. R. D. Carlsen, Amplitude, Phase and Time Delay Characteristics for the R390/URR AM Receiver, Cooley Electronics Laboratory Technical Memorandum No. 38, The University of Michigan, Ann Arbor, 1957.

4. C. E. Lindahl, A Linear Phase Bandpass Filter, Cooley Electronics Laboratory, Technical Memorandum No. 82, The University of Michigan, Ann Arbor, 1961.

5. C. E. Lindahl, Study of Input Circuitry of Direction Finder Set AN/TRD-4A, Cooley Electronics Laboratory Technical Memorandum No. 77, The University of Michigan, Ann Arbor, 1960.

6. C. E. Lindahl, System Study Covering an Antenna Suitable for a Spinning Goniometer Direction-Finding System, Cooley Electronics Laboratory Technical Report No. 125, The University of Michigan, Ann Arbor, 1961.

7. W. J. Lindsay and D. S. Heim, Considerations in the Automation of a Spinning-Goniometer Radio Direction Finder, Cooley Electronics Laboratory Technical Report No. 85, The University of Michigan, Ann Arbor, 1961.

8. Instruction Book for R-390/URR Radio Receiver, Department of the Army Technical Manual TM 11-856.

9. Instruction Book for AN/TRD-4A DF Set, Department of the Army Technical Manual TM 11-688.

DISTRIBUTION LIST

Copy No.	
1-2	Commanding Officer, U. S. Army Electronics Research and Development Laboratory, Fort Monmouth, New Jersey, ATTN: Senior Scientist, Electronic Warfare Division
3	Commanding General, U. S. Army Electronic Proving Ground, Fort Huachuca, Arizona, ATTN: Director, Electronic Warfare Department
4	Chief, Research and Development Division, Office of the Chief Signal Officer, Department of the Army, Washington 25, D. C., ATTN: SIGEB
5	Commanding Officer, Signal Corps Electronic Research Unit, 9560th USASRU, P. O. Box 205, Mountain View, California
6	U. S. Atomic Energy Commission, 1901 Constitution Avenue, N.W., Washington 25, D. C., ATTN: Chief Librarian
7	Director, Central Intelligence Agency, 2430 E Street, N.W., Washington 25, D. C., ATTN: OCD
8	U. S. Army Research Liaison Officer, MIT-Lincoln Laboratory, Lexington 73, Massachusetts
9-18	Defense Documentation Center, Cameron Station, Alexandria, Virginia
19	Commander, Air Research and Development Command, Andrews Air Force Base, Washington 25, D. C., ATTN: SCEC, Hq.
20	Directorate of Research and Development, USAF, Washington 25, D. C., ATTN: Electronic Division
21-22	Hqs., Aeronautical Systems Division, Air Force Command, Wright-Patterson Air Force Base, Ohio, ATTN: WWAD
23	Hqs., Aeronautical Systems Division, Air Force Command, Wright-Patterson Air Force Base, Ohio, ATTN: WCLGL-7
24	Air Force Liaison Office, Hexagon, Fort Monmouth, New Jersey
25	Commander, Air Force Cambridge Research Center, L. G. Hanscom Field, Bedford, Massachusetts, ATTN: CROTLR-2
26-27	Commander, Rome Air Development Center, Griffiss Air Force Base, New York, ATTN: RCSSLD - For retransmittal to - Ohio State University Research Foundation
28	Commander, Air Proving Ground Center, ATTN: Adj/Technical Report Branch, Eglin Air Force Base, Florida
29	Chief, Bureau of Naval Weapons, Code RRR-E, Department of the Navy, Washington 25, D. C.
30	Chief of Naval Operations, EW Systems Branch, OP-35, Department of the Navy, Washington 25, D. C.
31	Chief, Bureau of Ships, Code 691C, Department of the Navy, Washington 25, D. C.
32	Chief, Bureau of Ships, Code 684, Department of the Navy, Washington 25, D. C.

Copy No.

33 Chief, Bureau of Naval Weapons, Code RAAV-33, Department of the Navy, Washington 25, D. C.

34 Commander, Naval Ordnance Test Station, Inyokern, China Lake, California, ATTN: Test Director - Code 30

35 Director, Naval Research Laboratory, Countermeasures Branch, Code 5430, Washington 25, D. C.

36 Director, Naval Research Laboratory, Washington 25, D. C., ATTN: Code 2021

37 Director, Air University Library, Maxwell Air Force Base, Alabama, ATTN: CR-4987

38 Commanding Officer - Director, U. S. Naval Electronics Laboratory, San Diego 52, California

39 Office of the Chief of Ordnance, Department of the Army, Washington 25, D. C., ATTN: ORDTU

40 Commanding Officer, U. S. Naval Ordnance Laboratory, Silver Spring 19, Maryland

41-42 Chief, U. S. Army Security Agency, Arlington Hall Station, Arlington 12, Virginia, ATTN: IADEV

43 President, U. S. Army Defense Board, Headquarters, Fort Bliss, Texas

44 President, U. S. Army Airborne and Electronics Board, Fort Bragg, North Carolina

45 U. S. Army Antiaircraft Artillery and Guided Missile School, Fort Bliss, Texas

46 Commander, USAF Security Service, San Antonio, Texas, ATTN: CLR

47 Chief, Naval Research, Department of the Navy, Washington 25, D. C., ATTN: Code 931

48 Commanding Officer, 52d U. S. Army Security Agency, Special Operations Command, Fort Huachuca, Arizona

49 President, U. S. Army Security Agency Board, Arlington Hall Station, Arlington 12, Virginia

50 The Research Analysis Corporation, 6935 Arlington Rd., Bethesda 14, Maryland, ATTN: Librarian

51 Carlyle Barton Laboratory, The Johns Hopkins University, Charles and 34th Streets, Baltimore 18, Maryland

52 Stanford Electronics Laboratories, Stanford University, Stanford, California, ATTN: Applied Electronics Laboratory Document Library

53 HRB - Singer, Inc., Science Park, State College, Pennsylvania, ATTN: R. A. Evans, Manager, Technical Information Center

54 ITT Laboratories, 500 Washington Avenue, Nutley 10, New Jersey, ATTN: Mr. L. A. DeRosa, Div. R-15 Lab.

55 Director, USAF Project Rand, via Air Force Liaison Office, The Rand Corporation, 1700 Main Street, Santa Monica, California

Copy No.

56 Stanford Electronics Laboratories, Stanford University, Stanford, California, ATTN: Dr. R. C. Cumming

57 Stanford Research Institute, Menlo Park, California

58-59 Commanding Officer, U. S. Army Signal Missile Support Agency, White Sands Missile Range, New Mexico, ATTN: SIGWS-EW and SIGWS-FC

60 Commanding Officer, U. S. Naval Air Development Center, Johnsville, Pennsylvania, ATTN: Naval Air Development Center Library

61 Commanding Officer, U. S. Army Electronics Research and Development Laboratory, Fort Monmouth, New Jersey, ATTN: U. S. Marine Corps Liaison Office, Code AO-C

62 Director, Fort Monmouth Office, Communications-Electronics Combat Development Agency, Bldg. 410, Fort Monmouth, New Jersey

63-71 Commanding Officer, U. S. Army Electronics Research and Development Laboratory, Fort Monmouth, New Jersey

ATTN: 1 Copy — Director of Research
1 Copy — Technical Documents Center ADT/E
1 Copy — Chief, Special Devices Branch, Electronic Warfare Div.
1 Copy — Chief, Advanced Techniques Branch, Electronic Warfare Div.
1 Copy — Chief, Jamming and Deception Branch, Electronic Warfare Div.
1 Copy — File Unit No. 2, Mail and Records, Electronic Warfare Div.
3 Cpys — Chief, Security Division (For retransmittal to - EJSM)

72 Director, National Security Agency, Fort George G. Meade, Maryland, ATTN: TEC

73 Dr. B. F. Barton, Director, Cooley Electronics Laboratory, The University of Michigan, Ann Arbor, Michigan

74-97 Cooley Electronics Laboratory Project File, The University of Michigan, Ann Arbor, Michigan

98 Project File, The University of Michigan Office of Research Administration, Ann Arbor, Michigan

99 Bureau of Naval Weapons Representative, Lockheed Missiles and Space Co., P. O. Box 504, Sunnyvale, California - For forwarding to - Lockheed Aircraft Corp.

100 Lockheed Aircraft Corp., Technical Information Center, 3251 Hanover Street, Palo Alto, California

Above distribution is effected by Electronic Warfare Division, Surveillance Department, USAELRDL, Evans Area, Belmar, New Jersey. For further information contact Mr. I. O. Myers, Senior Scientist, Telephone 5961262

ERRATA SHEET FOR

TECHNICAL REPORT NO. 137

COOLEY ELECTRONICS LABORATORY

Page

16 Equation (4.6a) should read

$$e_{3a} = 1/2 \int_0^T A \cos \theta \, dt + 1/2 \int_0^T A \cos (2\omega_g t - \theta) \, dt ,$$

20 In Eq. (4.13) the term $R_2^1 C$ should read $\frac{1}{R_2 C}$.

21 Line 10 should read

$$+ \sin (\omega_g \tau - \theta) \sin (2k + 1) \omega_g \tau \, dt ,$$

23 In line 15, replace "Section 5.2" with "Section 5.4".

32 In line 25, replace "Eq. (4.5)" with "Eq. (4.4)".

38 In line 19, replace "Section 3.2.2" with "Section 4.3.2".